THE UNIVERSITY OF MANITOBA

FACULTY OF GRDUATE STUDIES

*****

Design and Prototype of a Robotic System for Remote Palpation and Ultrasound Imaging

BY

FARSHID NAJAFI

A Thesis/Practicum submitted to the Faculty of Graduate Studies of The University of Manitoba in partial fulfillment of the requirements of the degree of

MASTER OF SCIENCE

May, 2004

THE UNIVERSITY OF MANITOBA

FACULTY OF GRADUATE STUDIES

*****

COPYRIGHT PERMISSION

Design and Prototype of a Robotic System for Remote Palpation and Ultrasound Imaging

BY

Farshid Najafi

A Thesis/Practicum submitted to the Faculty of Graduate Studies of The University of

Manitoba in partial fulfillment of the requirement of the degree

Of

MASTER OF SCIENCE

To My Mother, Leila Khalaj Hedayati

And Father Najaf Najafi.

Abstract

Accurate assessments of the abdomen and interpretations of abdominal pain are difficult, particularly for an inexperienced clinician or nurse. These difficulties are amplified for remote patients who have less access to clinical experts. The goal of this project, of which this thesis forms a part, is to develop an appropriate robotic system capable of performing palpation/ultrasound imaging by an expert at the remote site. Specifically, this thesis presents the design, development and evaluation of a novel four-degree-of-freedom hand-controller with a force reflecting capability and a novel four-degree-of-freedom wrist mechanism to assist the physician in performing abdominal examinations such as palpation and ultrasound imaging from a remote site.

A compact desktop four degree-of freedom spherical parallel hand-controller has been designed with backdrivability, a large and singularity-free workspace and a large force reflecting capability. The structure is light and rigid and the actuators are all placed on the ground, providing independent control of each degree of freedom. All degrees of freedom are kinematically decoupled from each other. The operator is able to control the position and orientation of a remote wrist holding an ultrasound or a palpating probe and receive the interaction forces between the patient at the remote site and the probe in return. A simplified version of this design with three degrees of freedom has been fabricated and exhibits the abovementioned unique features.

A compact, spherical, parallel, modular, robotic wrist with four degrees-of-freedom has also been designed, having similar unique characteristics as in the hand-controller. The wrist has two exchangeable modules to provide standard clinical motions for palpation and ultrasound. A simplified prototype of the design with three degrees-of-freedom has been constructed that exhibits all of the novel design specifications.

Both systems are interfaced to a computer and simple control schemes have been applied for controlling them. When operated together, both mechanisms are kinematically similar. This property simplifies control algorithms, increases force transparency and generates a user-friendly robotic system for tele-medicine applications.

Acknowledgements

My most sincere and heartfelt thanks goes to my advisor, Dr. N. Sepehri, whose encouragements and supports have made this thesis possible. I feel tremendously fortunate to have had opportunity and freedom to embark on this project.

I also wish to sincerely thank Dr. Ray Pastuma, head of the paediatric surgery at the University of Manitoba and medical director of Manitoba Tele-Health, who played a major role in initiating this project, when he told us, "we can see and talk to patients in remote sites, but as a surgeon I need to feel and touch those patients".

Sincere thanks also goes to Dr. Wayne Boyce and Dr. Sarah Muttit past and present directors of Manitoba Tele-Health for their continued support.

On this project, I have had this opportunity to work with Reza Ghorbani, and Mark Karpenko, Ph.D. students in Experimental Robotics and Tele-Operation Laboratory of the Department of Mechanical and Manufacturing Engineering during computer interfacing and software development for both hand-controller and the robotic wrist. I learned a lot about computer interfacing by working alongside Reza and Mark.

I also wish to thank Mr. Al. Lohse and Mr. Irwin Penner the support staff. They contributed significantly during mechanical fabrication of the system.

Mr. Pooya Sekhavat has always been my best friend since my arrival to Canada. He has been a very supportive and helpful friend during my life here.

No words describe my heartfelt thanks to my mother (Leila Khalaj Hedayati) and father (Najaf Najafi) for a lifetime of supports and encouragements, which have made me who I am today. I will never forget their exceptional and unlimited supports during my study at Mofid High school and Sharif University of Technology (Tehran-Iran).

My brother, Dr. Farid Najafi, whose supports and guidance gave me this opportunity to continue my postgraduate studies here. He has always been both a friend and brother for me. He is now Assistant Professor at Department of Mechanical Engineering K.N.T. University (Tehran-Iran).

Finally, I wish to acknowledge the support of The Institute of Robotics and Intelligent systems (IRIS) Network Center of Excellence, Manitoba Tele-Health Network and the University of Manitoba.

Table of Contents

List of Figures and Tables

Chapter 1

Introduction

1.1. Preliminary Remarks

Health care is a critical social issue today. While much emphasis is given to the need for quality health care for all citizens, the high costs of medical care under the current system make health care a difficult challenge. The most advanced equipment and highly trained professionals are generally located in large urban hospitals in order to ensure the cost-effective use of these expensive resources. However, uniform health coverage requires that high-quality care be readily available to all citizens, including those people living in smaller cities and rural areas. Under the current system, providing access to medical specialists for patients in sparsely populated areas often results in inconvenience and/or inefficient use of resources.

Most commonly, a patient seeking care travels to see a medical specialist at the urban hospitals. These trips require hours of travel time for a relatively short examination, and thus are neither convenient nor efficient. A different approach is to have the physician travel to remote clinics as a circuit rider. Health Canada estimates that travel associated with health care for First Nation people in remote communities amounts to $200 million per year, including health staff[1].

On the other hand, in emergency cases, immediate medical care is also an issue. There is a wide variety of examples of emergency cases such as in ambulances after accidents or in ships navigating at seas, or in airplanes, or even in space for astronauts. Recent studies show that early and specialized pre-hospital patient examinations (for example during patient transfer) contribute to the patient's survival. A quick look at statistical data clearly points out that more than 60% of people lost their lives in accidents before being admitted to any health care institution. Thus, injuries-monitoring and examination are critical in all emergency cases (Kyriacou, 2001).

---

[1] http://strategis.ic.gc.ca/epic/internet/inlsg-pdsv.nsf/vwGeneratedInterE/Home.

A wide variety of a patient's vital parameters such as blood pressure, temperature, heart, and respiration rates can be measured by a nurse. But accurate assessment of the abdomen and interpretation of abdominal pain are difficult, particularly for the inexperienced clinician or nurse. Errors and uncertainty can lead to delays in diagnosis, morbidity and even death, as in appendicitis. These difficulties are amplified for remote patients who may have less time and less access to expert clinical care. Abdominal examination includes palpation and ultrasound imaging. In ultrasound diagnosis the clinician performs the examination by moving the echo-graphic probe over the patient's body to acquire bi-dimensional images. She/he may perform her/his diagnosis from static measurements performed on the images and/or from a dynamical analysis on the organs, for instance, by pressing the probe on the body, which requires specialized skills and remains a frequent reason for the patient's or physician's transfer. Palpation is a physical examination performed by a physician on a patient's abdomen at a regular physical exam or when a patient is experiencing pain or discomfort in the abdomen. The aim of this procedure is to study the patient's abdominal reaction to some forces exerted by the physician's hand. Accurate palpation must be done by the expert clinician, which is also a major reason for the patient's transfer.

Tele-medicine is a promising approach for addressing some of the issues associated with the problem of distance between the patient and clinician. Tele-medicine offers the advantage of cost saving, availability of expertise, remote accessibility, and timeliness. Tele-medicine includes tele-medical diagnostics and analytical services. Tele-medical diagnosis has so far been implemented as mainly consultation. It includes the ability to observe, talk and listen to remote patients or to read x-rays or ultrasound images from a remote medical center or to listen to local physicians as they examine the patient. Tele-medicine could also use tele-robotic techniques. Tele-robotics enables us to manipulate in remote sites by employing a combination of robots, communication systems and controllers. A typical tele-robotics system for medical diagnosis consists of a physician side, a communication system and a patient side (see Fig. 1.1).

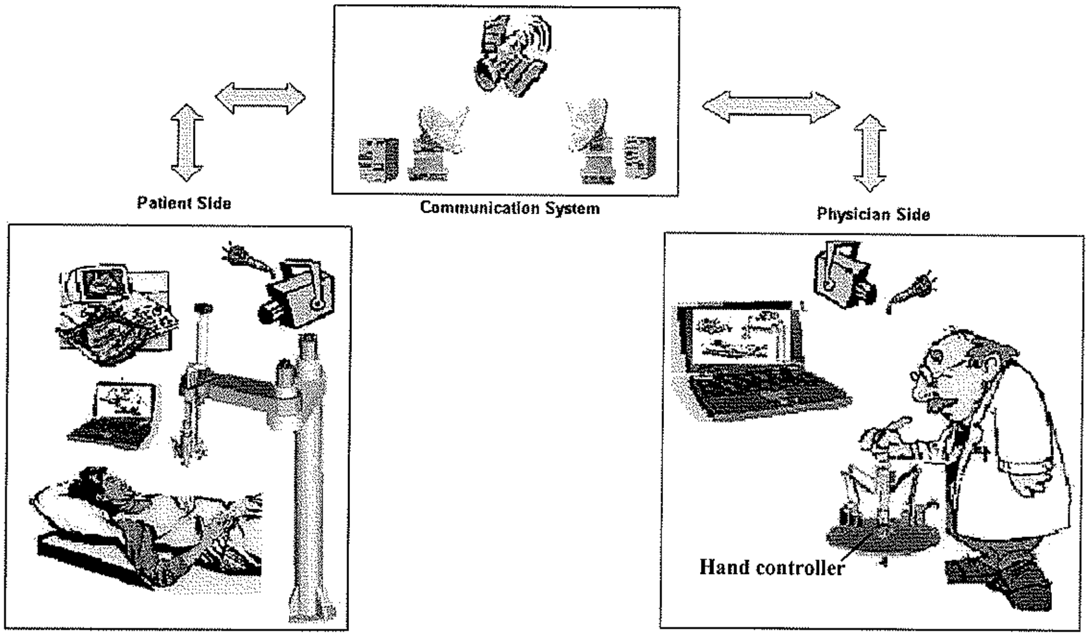

Fig. 1.1: Master-slave tele-medical diagnosis system.

The physician side includes an expert doctor, hand-controller, microphone, TV and camera system. The communication system includes servers and satellite links. The patient side consists of a patient, a nurse, a robotic arm, medical equipment such as ultrasound or even surgical instruments, a TV, a microphone and a camera system. The physician and the patient can see and talk to each other through their microphone and camera systems. The physician is also able to control the remote robotic arm by means of his hand controller to touch the patient and get some medical images such as ultrasound or X-ray.

1.2. Literature Survey of Machine-Mediated Palpation and Ultrasound Imaging

Sublett et al. (1995) presented the design and implementation of a digital image capture and distribution system that supports remote ultrasound examinations. They did not use any tele-robotics techniques in their work. All the work was accomplished with cooperation between a remote technician manipulating an ultrasound probe on the patient and a radiologist at the remote site.

Degoulange et al. (1998) designed and constructed a complete articulated robot base on serial configuration for moving an ultrasound probe on the patient's skin with a given force. They applied different techniques to make a safe robot. In their design, all the robot's joints should be simultaneously in motion, which may decrease the safety level of the robot during interaction with the patient. Due to its serial configuration, all the electric actuators are floating, which makes the robot heavier compared with a non-floating actuation system.

Salcudean et al.(see US patent 6,425,865); Zhu et al. (2000) developed an ultrasound robot in order to reduce joint fatigue of the ultrasound technicians. They used a pantograph to generate a conical motion around a fixed point on the patient using a serial configuration and floating actuators. They balanced the whole manipulator by adding counterbalance weights. Adding counterbalance weights increases the overall weight of the system, which in turn increases the impact force between the patient and the robot in unwanted situations. In providing palpation motion for abdominal ultrasound, the whole manipulator should be moved up and down, which is not desirable from the safety aspect (see Fig. 1.2).

Masuda et al. (2001) designed and constructed a complete robot for tele-echography. The whole mechanism sits over the patient's body during examination. For orienting the probe about a fixed point on the abdomen, all joints should move in a coordinated manner. There is no reasonable access to the patient in emergency cases. Masuda et al. (2001) controlled the robot from a remote site by ordinary joysticks with no force feedback (see Fig. 1.3).

Mitsubishi et al. (2001) developed a remote ultrasound diagnostic system consisting of circular guides connected in a serial configuration and embedded with gears of high ratio. The system is heavy and bulky. They also developed a six degree-of-freedom force reflecting hand-controller with a kinematical configuration different from that of the ultrasound robot. An impedance control mode was used in their system.

The European TER project described in Gonzales et al. (2001), shows the development of a robotic system, which uses parallel configuration based on pneumatic artificial muscles. This system uses the compliance in the pneumatic actuators to simulate the compliant behavior of a human hand. The system appears to be bulky with limited workspace and entirely embraces the patient in a way that there is no reasonable access to the patient in emergency cases.

The European OTELO project described in Delgore et al. (2002), developed a four degree-of -freedom manipulator. The system is able to orient an ultrasound probe around a fixed point on the patient's abdomen. All the actuators are floating and can come close to the patient's body during an examination. The manipulator also has a singular configuration exactly at the middle of its workspace, which destroys ultrasound pictures in that orientation. Delgore et al. use a Phantom haptic device as their force reflecting hand-controller. These two manipulators have different kinematical configurations (see Fig. 1.4).

Kato and Koganezawa (1988) developed a clinical test for automatic breast palpation. They used a Cartesian-type industrial robot as a positioning stand for a detecting head with four pressure sensors to detect very small breast abnormalities. No tele-operation technique for performing examinations from a remote site was developed.

Dario and Bergamasco (1988) developed an anthropomorphic finger incorporating force and position sensors to detect and measure pulses. Their robotic finger is not suitable for deep abdominal palpation. Howe et al. (1995) studied different tactile sensors and displays to assist the surgeon's fingers in measuring and sensing small tissues during remote surgery in order to localize small abnormalities such as tumors. The tactile sensors are not suitable for deep palpation.

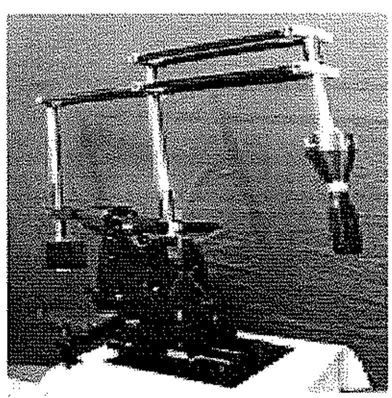

Fig. 1.2: The UBC ultrasound robot (Zhu et al., 2000).

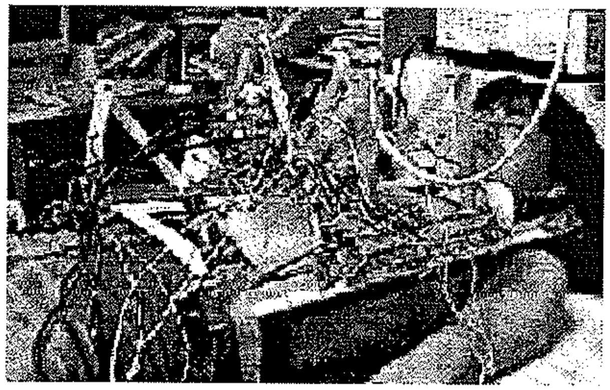

Fig. 1.3: Ehime University (Japan) ultrasound robot (Masuda et al., 2001)

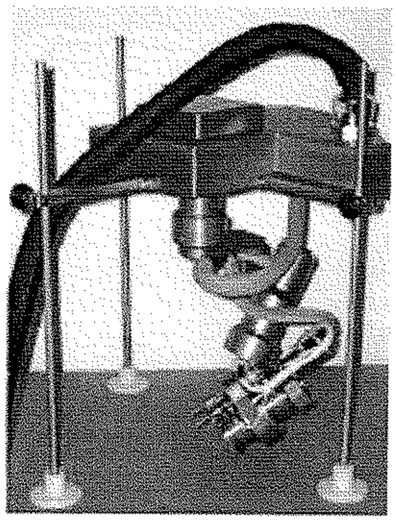

Fig. 1.4: European (OTELO project) ultrasound robot (Delgore et al., 2002).

1.3. Objectives and Scope of this Thesis

The concept of remote control in the medical field for diagnosis and/or other operations to be performed by a doctor on a remote patient is gaining more and more acceptance as it may be used to overcome serious problems of availability, particularly in areas with low population that are insufficient to locally support a doctor having specific expertise. Presently, there is no system that permits distant clinical palpation. This includes abdominal examination as well as ultrasonic diagnosis, which require expert assessment and are frequent reasons for patient's transfer. The objective of this thesis is to develop a tele-robotic system to enable a physician from a remote site to perform remote ultrasound and palpation (see Fig. 1.2). The proposed system includes a hand-controller and a robotic wrist. The hand-controller is designed with four degrees-of-freedom to meet requirements of hand-controllers and haptic devices. In order to evaluate the design performance, a simplified version of the hand-controller with three degrees-of-freedom is prototyped. The robotic wrist is designed with four degrees-of-freedom to meet design requirements and safety aspects of medical robots. A simplified version of the wrist with three degrees-of-freedom has been fabricated. Both systems are designed to have similar kinematic chains as well as being suitable for performing palpation and ultrasound imaging tasks. Both systems are interfaced to a computer to be operated in master-slave mode. By doing so, the physician is able to control the orientation of the robotic wrist from a remote site.

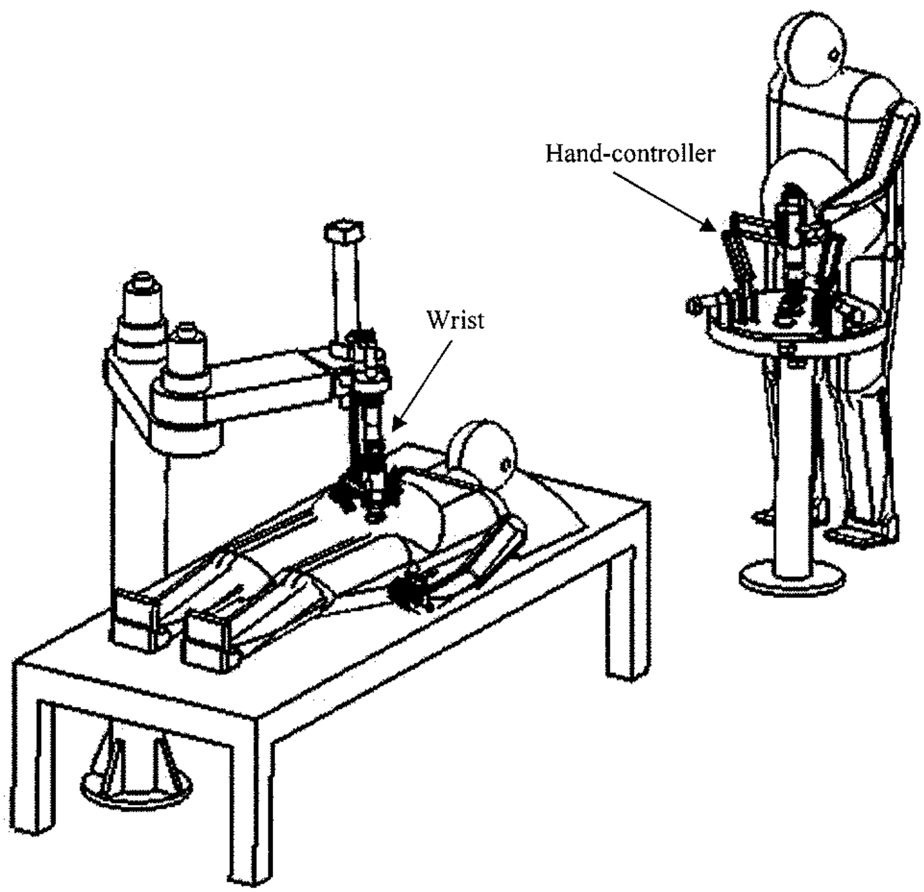

Fig. 1.5: Proposed system for remote palpation/ultrasound imaging.

The remainder of this thesis describes the approach taken to achieve the abovementioned objectives. Chapter 2 presents a brief description of requirements for palpation and ultrasound imaging. This chapter also introduces the concept of 3-D ultrasound. Chapter 3 investigates the design of tele-operators from the systematic point of view. This chapter studies three major categories in tele-operation control systems. It also introduces the concept of bilateral tele-robotic systems, which is the ultimate goal of this project. Chapter 4 describes requirements for designing force reflecting hand-controllers. This chapter also describes the embodiment design of a four degrees-of-freedom hand-controller in order to assist physicians in controlling a remote robotic wrist performing medical examinations such as ultrasound imaging and palpation. Chapter 5 describes requirements for designing robotic wrists. This chapter also describes the embodiment design of the four degrees-of-freedom robotic wrist to enable the physicians to perform medical examinations such as ultrasound and palpation on a patient. Chapter 6 presents the kinematic analysis of the hand-controller and the wrist, which includes forward and inverse kinematic analysis. Chapter 7 presents the prototyped hand-controller and the wrist with their workspaces at different configuration. Chapter 8 presents the computer interfacing of the wrist and the hand-controller. Typical results of the whole system in operation are also presented. Concluding remarks describing the contribution of this thesis are given in chapter 10.

Chapter 2

Ultrasound/Palpation Task Descriptions

This chapter describes basic ultrasound and palpation examination procedures. Acquisition techniques for ultrasound imaging including linear, pitch, yaw, roll and combined scanning are described first. Next, the concept of 3-D ultrasound and its relation with tele-operation is discussed. The concept of the abdominal palpation is also reviewed.

2.1. Ultrasound Imaging Technique

2.1.1. Definition

In medicine, ultrasound or sonography, refer to a technique that uses sound waves to study and treat hard-to-reach body areas. In scanning with ultrasound, high-frequency sound waves are transmitted to the areas of interest and the returning echoes are recorded. The waves are produced by a transducer containing a piezoelectric substance such as a quartz-crystal oscillator, which converts high-frequency electric current into vibrating ultrasonic waves. The technique is now widely used in every branch of medicine.

2.1.2. Acquisition Techniques

Acquisition techniques basically produce 2-D images, which are noisy due to respiration, and the physician or patient's involuntary motions. The physician, based on his/her experience and knowledge, manipulates the transducer on the patient's organ and mentally transforms the 2-D images into a 3-D tissue structure and makes the diagnosis. In free hand acquisition, the operator holds the transducer and manipulates it in a special manner over the anatomy to be viewed. This manipulation technique consists of linear, pitch, yaw and spinning scanning fashions (Fenster and Downey, 1996). The images are acquired with arbitrary position and orientation under the operator's control. This technique offers special advantages because the physician can select optimal views and orientations and accommodates complex patient surfaces due to his/her hand –eye coordination skills. Free hand acquisition must be considered in the design of any master-slave system to allow the physician to move his/her hand in a most natural way to capture optimal images.

In linear scanning, the transducer is moved in a linear fashion, perpendicular to the patient's skin. The transducer can also be tilted to allow for 3-D color doppler imaging (see Fig. 2.1). This technique is used for vascular imaging and echocardialogy. The range of the motion depends on the length of the anatomy to be investigated. The maximum velocity recorded by Zhu and Salcudean (2000) during manual carotid artery examination was 0.2 m/s and the average velocity wase very small, of the order of 5 mm/s.

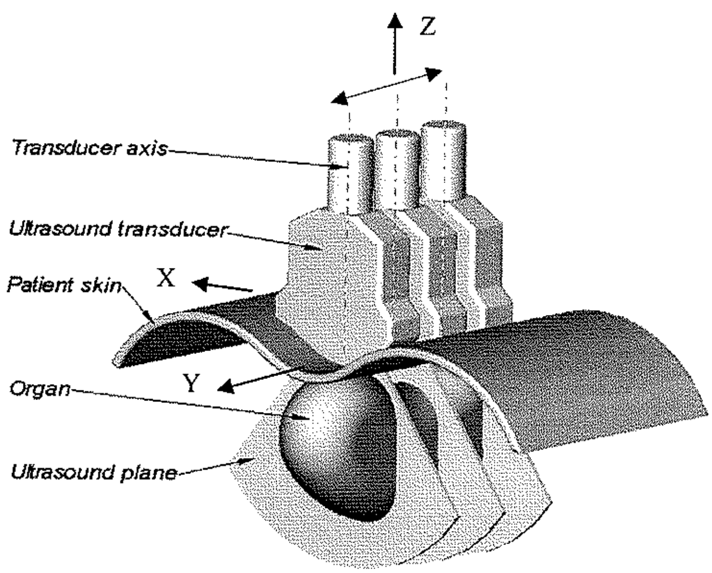

Fig. 2.1: Linear scanning.

In pitch scanning, the transducer is rotated about the X axis (see Fig. 2.2). It results in an angular sweep, providing a fan of the ultrasound planes. In this technique, the transducer is pivoted on a point on the patient's skin, and the physician moves the transducer in a circular motion around the pivot point. The maximum inclination of the probe axis is $\pm 45^{\circ}$. In most existing studies, the inclination angle was reported to be approximately $\pm 25°$. The maximum velocity recorded by Zhu and Salcudean (2000) during manual carotid artery examination is 260 deg/s and the average velocity was reported to be, of the order of 3 deg/s. The maximum skin deformation along the probe axis is 3 cm (Guerin et al. 2003). In yaw scanning, the transducer is rotated about the Y axis (see Fig. 2.3). This results in an angular sweep that provides a fan of the ultrasound planes.

In roll scanning, the transducer is rotated about its central Z axis (see Fig. 2.4). The acquired images sweep out in a conical volume. In roll scanning, the acquired planes intersect in the centerline of the volume along the axis of rotation. In addition, to angular steps between

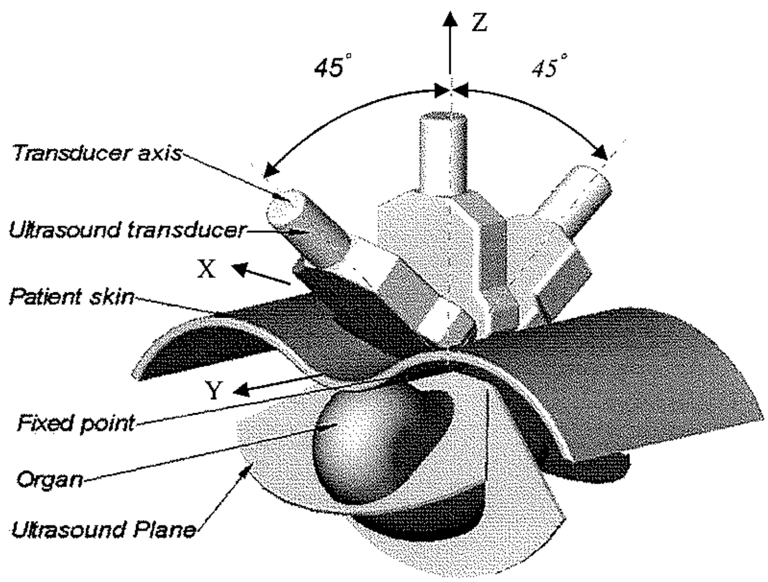

Fig. 2.2: Pitch scanning.

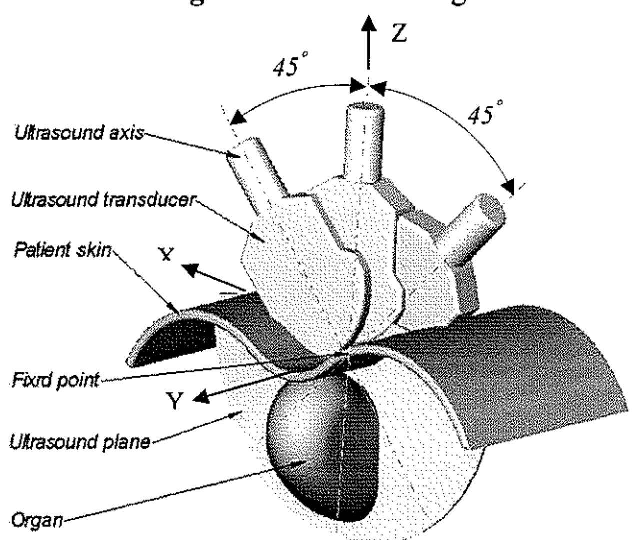

Fig. 2.3: Yaw scanning.

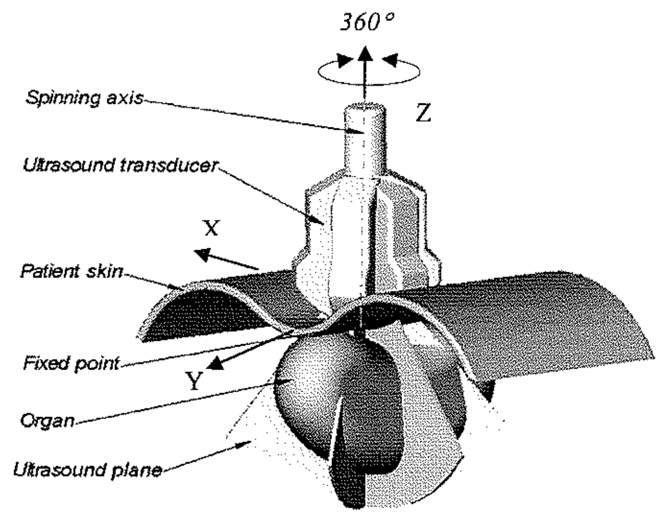

Fig. 2.4: Roll scanning.

the planes, the tilt or the offset from the rotation axis must be measured and corrected by special means to avoid significant artifacts around the center of the image.

2.1.3. 3-D Ultrasound Imaging

The goal of 3-D ultrasound imaging is to provide an imaging technique to allow the physician to view the anatomy in 3-D. Fig. 2.5 shows a block diagram of 3-D ultrasound system. The first stage refers to the imaging acquisition hardware used to manipulate the transducer. It could be a combination of a physician and a tele-robotic system. The second stage refers to the manner in which the 2-D ultrasound images are recorded. The third stage refers to the reconstruction technique used to obtain the 3-D images, which requires the position and orientation of the transducer at each acquired 2-D image. In this stage, the 2-D acquired images are put together in a specific manner to generate a 3-D image, and the fourth block refers to the display technique used to visualize the 3-D images (Fenster and Downey, 1996). 3-D ultrasound has many applications in kidney, liver, fetus, breast, heart, tumor, and eye examinations.

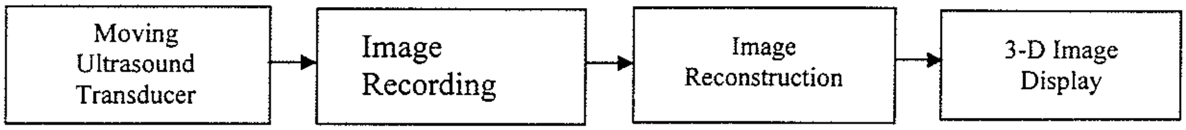

Fig. 2.5: 3-D ultrasound imaging technique.

2.2. Abdominal Palpation

Palpation is a physical examination performed by a physician on a patient's abdomen at a regular physical exam or when a patient is experiencing pain or discomfort in the abdomen. The aim of this procedure is to study the patient's abdominal reaction to some forces exerted by the physician's hand. The palpation examination begins with a light palpation of the abdomen. The physician presses lightly around the abdomen, using the same amount of forces in all regions, beginning in the least tender region. The light palpation is followed by a deep palpation, again moving from the least tender region to the tenderest region. The physician presses on the abdomen using much more force for the deep palpation and observes the displacement of the abdomen as well as the reaction of the patient. During the palpation process, there are two key aspects that the physician tries to observe: tenderness and muscle guarding.

Tenderness can be referred to as the pain-to-pressure ratio of certain regions of the abdomen. The reason that the physician begins the palpation exam in the least tender region of the abdomen is that a comparison can be made between the pain-to-pressure in a healthy region and the pain-to-pressure ratio in the tender region. The variable in each case is the patient's threshold for pain. Every person is different and so the physician is left to decide, relatively, how much pain the patient is feeling compared to a healthy region of the abdomen. If the tenderness of certain regions of the abdomen can be quantified, the physician would have a much better idea of what is causing the tenderness. Muscle guarding is a measure of the abdominal wall compliance, characterized by tightened and is a body's natural reaction. This type of behavior in the abdomen can give the physician an indication as to the cause of abdominal pains. Quantifying the muscle's deformation or the compliance of the abdomen wall can allow physicians to diagnose abdominal problems much easier. The muscles tighten around an injured part of the body as a protective reaction. The muscle tightening or spasm is involuntary.

Chapter 3

Tele-Operation Systems

This chapter investigates the design of tele-operators from the system point of view and shows the most suitable approach for the remote tasks in hand. Section 3.1 reviews the building block of typical tele-operation systems. Section 3.2 introduces three major categories in tele-operation control systems and compares the advantages and disadvantages of each approach. Section 3.3 introduces the concept of bilateral tele-operation.

3.1. Tele-Operation Subsystems

A tele-operator is a general-purpose, dexterous, cybernetic machine. A tele-operator always has an operator in the control loop. A tele-operator is a class of the man-machine system, which has the ability to project man's innate dexterity not only across the distance but through physical barriers (Johnsen, 1971).

With reference to Fig. 3.1, a tele-operation system consists of the following subsystems. The manipulation mechanism carries out dexterous activities ordered by a human operator. A control subsystem or control mechanism enables the operator to generate the manipulator's control commands. A sensory subsystem permits the operator to see, feel and hear what the manipulator is doing in the remote environment. A computer receives the incoming information, processes and displays it. A communication subsystem may consist of hard wire, internet or mechanical links.

3.2. Tele-Operation Control Systems

In terms of control, remote manipulators may be classified into push button, joystick, and master-slave controlled types. Each type may use a large variety of control mechanisms.

In a simple pushbutton control, the operator controls the arm by hitting respective keys or pushbuttons arranged on a pendant, panel, or gun-grip. Toggles or other kinds of switches may be used instead of pushbuttons. Each actuator or degree of freedom in a manipulator has a respective pushbutton on the pendant (see Fig. 3.2) (Popov, 1987).

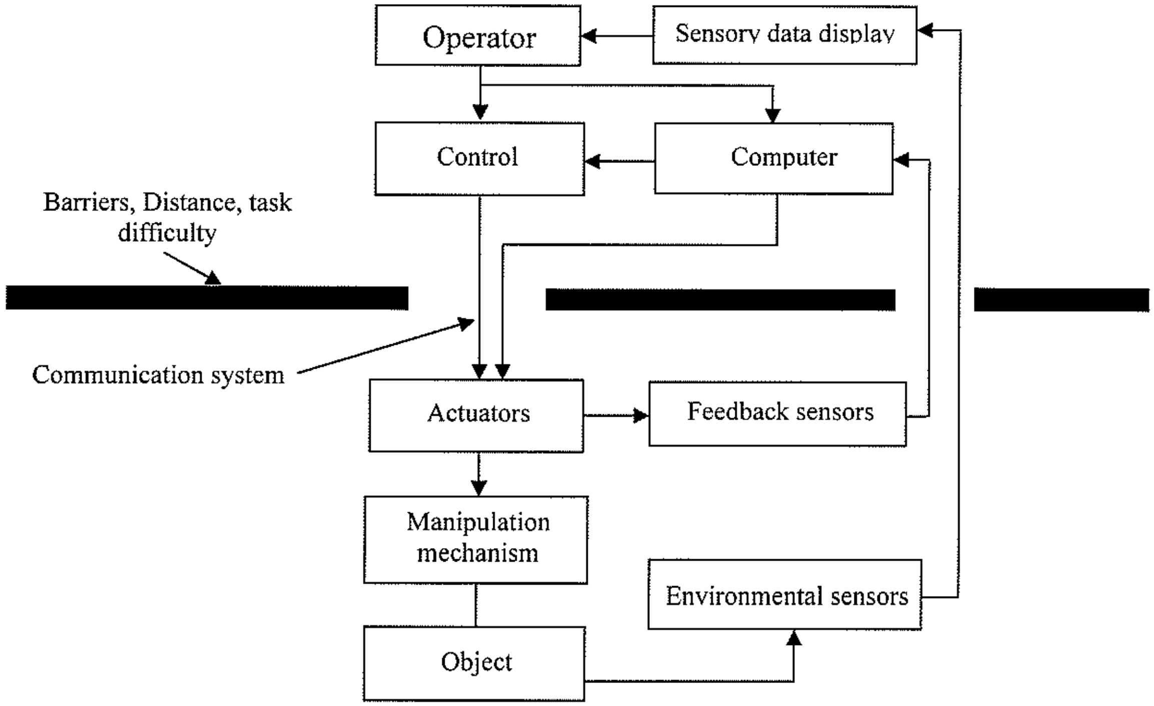

Fig. 3.1: Tele-operation block diagram.

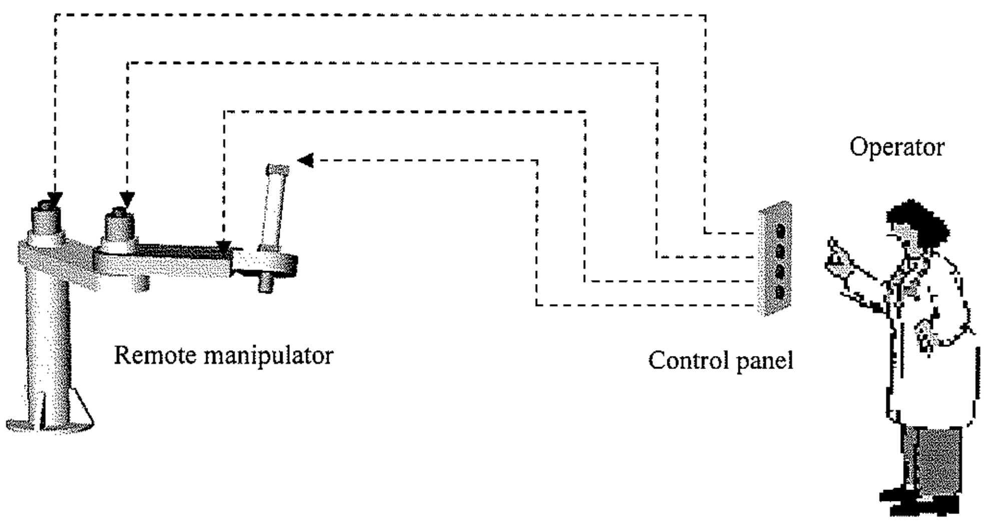

Fig. 3.2: Tele-operation in push button control mode.

A push button control style can be best applied to material-handling robots, which usually operate in Cartesian coordinate systems, where large linear displacements and/or continuous rotations of a tool are involved. In tele-operation, pushbutton control can also be used to guide the remote manipulator in emergency cases such as breakage and so on. In this case, the operator can rapidly draw the manipulator from a complicated situation to its home position. This control technique appears to be the simplest and most reliable form of remote control and the most convenient form of trajectory generation in the teach mode (Kulishov, 1988).

In joystick control, the operator uses a hand-controller or a joystick, which has several degrees of freedom and can generate control signals by turning or actuating each of them (see Fig. 3.3). In this case, the operator guides the manipulator arm in desired directions by moving the joystick or applying a force to the joystick in the same direction. The sensors built into the joystick convert the forces into the respective signals, which are routed to a computer generating control signal. Joysticks can work in terms of rate, position and force control.

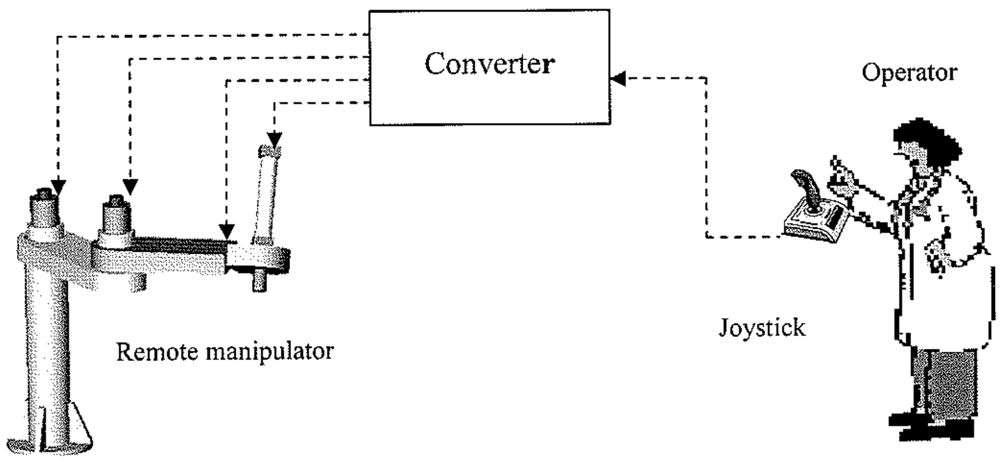

Fig. 3.3: Tele-operation in joystick mode.

Since the joystick and the manipulator are often kinematically dissimilar, this also prevents the operator to completely project him/herself into a remote site. On the other hand, the dissimilarity between the two systems, in some sensitive applications such as tele-medicine, does not create an ergonomic interface, and it might cause the operator to make mistakes.

In a master-slave control scheme, the operator controls the movements of the slave arm by manipulating a controller, which is kinematically similar to the slave arm. Ordinary master-slave manipulators use an antropomorphic configuration of the master or kinematically similar master arm incorporating revolute and prismatic joints (see Fig. 3.4). It means that any kinematic pair in the master should be in a one-to-one correspondence with the relative kinematic pair in the slave. In this configuration, the slave duplicates all of the movements of the operator's hand.

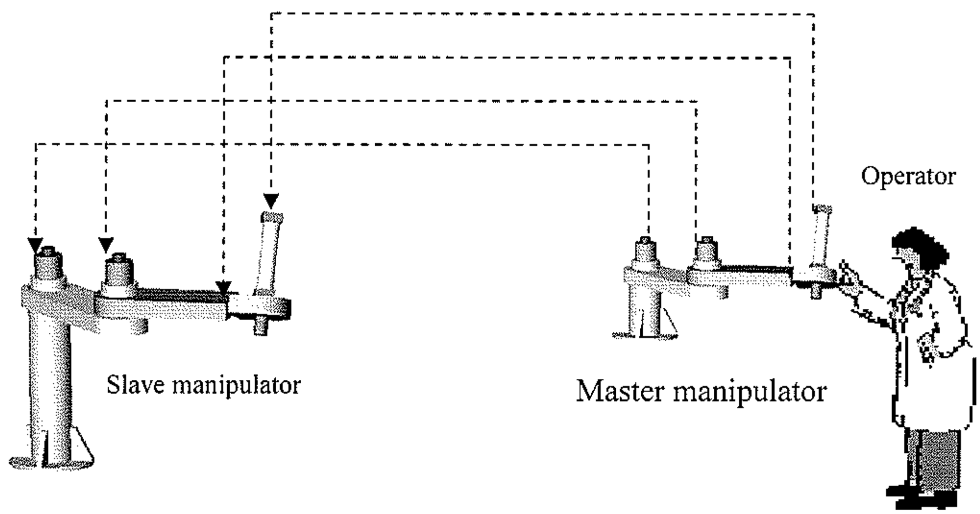

Fig. 3.4: Tele operation in master-slave mode.

Master-slave mechanisms may be different in the linear dimension of their links but they are usually geometrically similar. It is most common to use the master only in terms of the operator's wrist motion mode. In this case, the master duplicates only the motion of the operator's wrist without duplicating those of his forearm and upper arm. The use of the master-slave manipulators controlled solely in terms of the operator's wrist motion gives another unique possibility to reduce the size of the master. Size reduction will lead to mass and inertia reduction, which are very important for the design of masters with force feedback, which need high force transparency.

The principal embodied in tele-operation technique can be best illustrated by considering master-slave manipulators. The geometrically similar master and slave arms substantially simplify the generation of control signals for each degree of freedom. Then, all that is necessary in such a case is the provision of relative position sensors in each axis of the master arm. The point is that the slave itself is a simple mechanical coordinator converter. Any motion in the master arm is taken up and communicated directly to the respective degrees of freedom in the salve. With such manipulators, the operator achieves the sensation of being present inside the work volume. His/her arm can move in a most natural way, and the slave can be moved along the optimal trajectories. Aware at all times of the manner in which the manipulator interacts with the work object, the operator can react with a minimum of delay to any change in the situation within the work volume and avoid any damage to the manipulator and the work object (Kulishov, 1988).

3.3. Bilateral Tele-Operation

Versatility and dexterity of human arm is an extremely valuable property. As his/her muscles exert a force at each of the joints, the operator causes his/her arm to move external objects in a controlled way, that is, he/ she controls both the position and orientation of the arm's member. Owing to symmetric force reflection, there appear to be equal and opposing forces applied not only to the object, but to the arm as well. In the opposite direction, the operator thus senses the reaction of the object being handled (force reflection) via his/ her nervous system and musculature. In the final analysis, the motion of any joint of the arm is controlled by the sum of the reaction of the object acted upon. When the two components strike a balance at all the joints, the arm does not move. Thus the human arm operates as a living bilateral mechanism. A bilateral tele-operation system could generate this effect between an operator and a remote object. The embodiment of bilateral action in master-slave manipulators is essential, because, similar to a human arm, displacements and forces in bilateral master-slave manipulators are reflected from the master to the slave and the other way around. They are called bilateral master-slave manipulators.

If the master has the ability to reflect forces between the manipulator and the work object at the remote site, then the master-slave system has the ability of bilateral transmission of displacement and force. In this system, the operator is well aware of reaction forces between the slave and the object. In these systems, there is not only a one-to-one positional but also force correspondence between the respective degrees-of-freedom in both sides, which would lead to achieving the best of transparency. Figure 3.5 shows the principal of a bilateral master-slave manipulator.

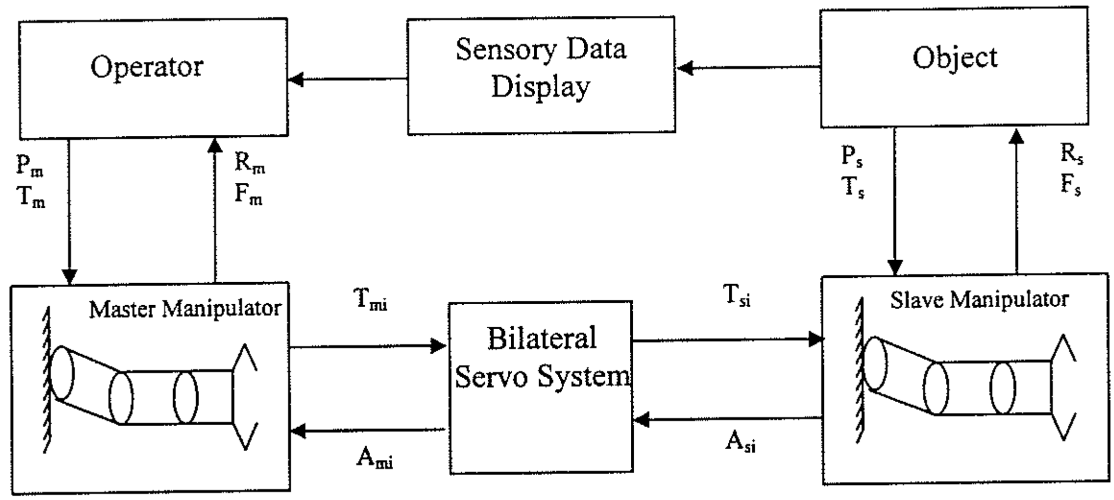

Fig. 3.5: Block digram of a bilateral tele-operation (Kulishov and Lakota,1988).

The human operator moves his/her master arm in space to a desired position and orientation (coordinates R and F), the operator applies the necessary force and torques (P, T), causing the master arm to move in all of its axes and to take up a position whose coordinates are T_{mi} and A_{mi}. The bilateral servo system provides the transfer of these displacements and torques in each axis of the motion from the master arm to the slave arm and back. In response, the slave arm reproduces the coordinates T_{si} and A_{si}, which are the duplications of all motions of the master arm. The reaction of the work object to the slave is reflected by the same servo system back to the master's actuator and then to the control handle and finally is sensed by the human operator. The bilateral servo system consists of a position-servoed subsystem and a torque-servoed subsystem. The former controls the position of the load shaft at the remote site and the latter develops at the operator's shaft a torque corresponding to the load torque. Operating together, these subsystems provide for the transmission of the angular displacements and torques applied to their respective shaft, (Popov, 1987).

Chapter 4

Design of the Hand-Controller

This chapter describes the embodiment design of the four degrees-of-freedom hand-controller in order to assist physicians in controlling a remote robotic wrist performing medical ultrasound examinations and palpation. Section 4.1 reviews the background of the force reflecting hand-controllers. Section 4.2 will study the required specifications for hand-controllers and introduce some design guidelines for achieving the specifications. Section 4.3 develops the embodiment design of the four degrees-of-freedom hand-controller.

4.1. Literature Review

With respect to the design of force reflecting hand-controllers or haptic devices for medical procedure, the haptic devices developed by Rosenberg et al.(US patents No. 5,805,140; 6,271,833, 5,721,566), and by Bevrit et al. (US patent 6,024,576) all have two degrees-of-freedom providing two rotations about a fixed point (also termed center-of-rotation). They all have simple parallel structures[1]. Additional degrees-of-freedom in these devices will unusually enlarge them or will require that the actuators not be grounded[2] (i.e., become non-floating). Similarly, the force feedback mechanisms by Martin et al. (US patent 6,104,382) and Rosenberg (US patent 6,154,198) have only two degrees of freedom providing two rotations about a fixed point and use a parallel structure. The three degree-of-freedom parallel linkage by Adelsein (US patent 5,816,105) provides three translational displacements of the end-point, which are not desirable for our specified tasks. The haptic device by Mor (US patent 6,088,020) has three active and two passive degrees-of-freedom. It does not have a fixed center-of-motion. The adjustable surgical stand by Faraz and Payendeh (US patent 5,824,007) includes two separate pantographs each providing spherical motion about fixed points. It uses a serial linkage mechanism and the actuators are not grounded.

---

[1] A robot is said to be a serial robot if its kinematic structure takes the form of an open loop chain, a parallel structure (manipulator) if it is made up of a closed loop chain [Tsai, 1999].

[2] If the actuator is attached to a fixed base, it is called grounded actuator.

Birglen et al. (2002) reported the development of a three degrees-of-freedom haptic device using a spherical parallel mechanism. The mechanism has an interior fixed center-of- motion, but it does not provide linear motion along the handle of the device, which is necessary for palpation examination. Duriez et al. (2001) describe the development of a parallel robot for simulating the terminal organ that moves on a spherical surface with a variable radius. The mechanism has three degrees of freedom. It was used to simulate abdominal behavior during ultrasound examination. The haptic device developed by Baumann et al. (1997) uses a four degrees-of-freedom parallel manipulator with a remote center-of motion. They used two perpendicular non-identical pantograph-like mechanisms to provide a spherical motion about a remote center-of motion. The actuators of the third and fourth degrees of freedom are floating, which increases the weight and inertia of the haptic, which in turn can destroy force transparency in haptic simulation. The use of non-symmetrical pantographs, however, works against the uniformity requirement, Hayward (1995), which may degrade the performance of the device.

The six degree-of-freedom haptic device developed by Lee (2001) uses parallel structure and non-floating actuators, but to keep the remote center-of-motion at a prescribed location, all degrees of freedom need to be active. It also has a singular configuration inside its workspace, which is not desirable in haptic devices. Yoon et al. (2001) have reported a haptic device with six degrees-of-freedom based on parallel architecture. In order to keep the remote center-of-motion at a prescribed point, all the actuators should move together. These types of manipulators also have kinematically coupled degrees of freedom.

4.2. Design Requirements

4.2.1. Rigidity

Rigidity is the capability of a system to resist the action of external forces with the least deformation. In mechanical engineering rigidity can be defined as the capability of a system to resist the action of the external loads with permitted deformations, which do not destroy the work-capability of a system, Orlov (1979). Rigidity is one of the basic factors in haptic design, which determines and increases force bandwidth of the device.

Improper configuration of the mechanism, non-rigid designed elements such as shafts, linkages and structure and non-rigid revolute and sliding joints can cause malfunctioning of the haptic device. Extra joint slackness spoils the arrangement of the haptic mechanism, increases friction and wear in joints, and decreases accuracy.

One way to increase the rigidity is to use parallel instead of serial manipulator configuration. By employing parallel configuration, one can decrease the weight of the haptic while increasing the haptic force bandwidth. The parallel manipulator could also achieve high positioning accuracy.

Ball bearing types and their arrangements inside the joints must be properly designed to have maximum rigidity and minimum backlash and friction. These three parameters are usually in conflict. Minimizing of backlash and maximizing the stiffness of the ball bearing arrangement require the existence of an axial pre-load in the ball bearing arrangement during assembly. Pre-loading increases ball bearing rigidity and rotational accuracy and eliminates backlash because of more contact points and uniform loading between rolling bodies (Rivin, 1988). The negative effect is high friction inside the ball bearing, which deteriorates haptic performance. It should be noted that ultra-precision deep-groove ball bearings could be produced with a minimum of internal clearance of 0.005 mm. Four-point contact ball bearings have more stiffness and precision due to their four-point contact points between balls and raceways. They also need axial pre-loading during assembly.

With the application of ultra-precision deep-groove ball bearings with a proper arrangement of shaft and housing, one can achieve high stiffness joints and good running smoothness. Cantilever joints have higher joint stiffness than simply supported joints and could be obtained by providing two adjacent ultra-precision deep groove ball bearings on a shaft. By doing so, the joint can also achieve lower endplay.

4.2.2. Singularity-free workspace

In haptic applications, singularities deteriorate haptic performance. Moreover, different from general manipulators, haptic systems cannot avoid singular points, because they are operated by a user's random commands. At singular points, haptic devices cannot reflect forces completely; moreover, actuator saturation, breakdown, and undesirable motions happen.

4.2.3. Compactness

Compactness is a desirable feature. Efficient use of space enables the overall size and weight to be decreased and the strength-to-weight ratio to be increased. Compactness is a key factor in designing haptic devices. This job should be done during embodiment design. Compactness provides more maneuverability for the operator's hand and it could also minimize interference between the operator and the haptic device. On the other hand, compactness would help the haptic device to be desktop.

4.2.4. Cross-coupling

These effects arise due to the complex kinematics and dynamics of serial and parallel manipulators. Kinematic cross-coupling describes the problem of obtaining motion of one degree of freedom of the manipulator without inducing unwanted motion to the power train of the other degrees of freedom. This effect basically comes from static reaction forces and the kinematic arrangement of the manipulator, (Daniel, 1990).

Most of the haptic devices suffer from this effect. Even in some cases, when the operator moves the input device, unintended motions happen in the other degrees of freedoms, which require the operator to lock out the offending joints by grasping the respective elements.

Cross-coupling can also be compensated in the control system, but it makes the controller complicated. This problem could be improved or even eliminated by better kinematical arrangements and mechanical design of input devices.

4.2.5. Backdriveability

The power trains of any force reflecting hand-controller must be backdriveable. This requirement is important when a common position error loop is used for force control, (Daniel, 1990). A mechanism is backdriveable when the operator moves the driven shaft, causing actuator's drive shaft to move. There are two types of backdriveability: acceleration-dependent and velocity-dependent. Minimizing structural and power train inertia and keeping the transmission ratio relatively small can increase acceleration-dependent backdriveability. Therefore, the use of components such as harmonic drives is excluded.

Decreasing a system's friction can increase the velocity-dependent backdriveability. This can be done with the use of non-preloaded high quality anti-friction bearings in joints or by reducing the radial and axial forces on ball bearings. Pre-loaded ball bearings increase internal forces between balls and their raceways, which in turn increase friction forces. By rational designing of mechanical elements and their loading patterns, one can reduce or improve the nature of forces on the joints.

4.2.6. Low inertia

The mass and inertia of the moving elements in a haptic device must be kept as low as possible. Inertia lowers the admittance and backdriveabilty of the haptic devices. A device capable of high endpoint admittance provides the operator with more sensitivity at low force levels, which is especially important when working in low impedance environments, (Daniel, 1990). Having more mass and inertia causes the operator's hand to feel unwanted forces, which in turn influence tele-operation transparency.

Actuators are the main source of mass and inertia in haptics. Parallel manipulators give this ability to put all the haptic's actuators on the ground. By doing so, less torques will be required to move the parts and smaller motors will be needed. Moreover, the distribution of loads in addition to elimination (or at least reduced size) of highly mobile cantilever beams provide parallel manipulators with greater rigidity as well as lighter masses, (Hui, 1995).

Maximum reduction in weight can be achieved by giving haptic elements complete equal strengths. This can be done by a manipulator's force analysis for the working loads. The ideal case is when the longitudinal stresses are distributed equally in every cross-section and at every point in the cross section. This is the condition when equal strength is most fully distributed. Here the material is used to its best possible advantage, and the weight of the part, for the designed stressed level, is the minimum obtainable, (Orlov, 1979; Hayward, 1995).

The use of material with low specific weights is a significant way of lowering the weight of haptic devices. Aluminum alloys are the most widely used light alloys. Aluminum alloys are noted for their low specific weights ($\rho \approx$ 3 kgf/dm^3), satisfactory yield strength [$\sigma_y = (30-180)$ N/mm^2], high machinability, castability, and weldability. It has been used in many haptic devices.

Composite materials have a very low specific weight ($\rho \approx 1.4$ kgf/dm^3) and a satisfactory yield strength [$\sigma_y = (90-365)$ N/mm^2] as well as machinability. Studies by McDougal, (1997) indicate that it is possible to simultaneously raise the lowest natural frequency and decrease the weight of the links of the haptic device. It is also possible to tailor other properties such as structural damping. With conventional materials, these requirements oppose each other.

Plastics also have very low specific weight ($\rho \approx 1.2$ kgf/dm^3), which are even lighter than composite material. It can be successfully used in low weight housings in haptic devices. In many cases, it is advisable to separate parts and make them with different materials and to connect them by press fitting, gluing, welding, and fastening bolts. This is because each part serves different purposes and needs its own best-fitted material to reduce the weight and do its task perfectly. This method is known as composite construction and could be applied in haptic devices.

Counterbalancing is another approach in increasing the admittance of the haptic devices and to reduce forces seen by the operator. A poorly balanced system leads to greater operator fatigue and decreases the transparency of tele-operation. It also reduces peak-torque requirements for joint actuators as well as assuring a more uniform loading of the actuators by means of compensation of gravity-induced forces (Kuleshov and Lakota, 1988). It leads to smaller actuators with smaller inertia. Mass, spring, pneumatic/hydraulic cylinder, cam and electric torque motor counterbalancing have been studied for parallel and serial manipulators, (Rivin, 1988; Gossselin, 2001). Mass counterbalancing seems to increase the overall weight of the haptic, and the pneumatic/hydraulic one is noisy and enhances friction. Motor torque counterbalancing requires a larger size of electric motor, which is associated with larger inertia as well as complicating control software. Spring and cams are promising ways to keep additional weights on the haptic device as low as possible, (Tidwell et al. 1994).

4.2. 7. Workspace

The workspace of a manipulator is the space composed of all points, which can be reached by its arm end. The size and shape of the workspace must be equal to those which are mentioned by ultrasound and palpation tasks (see Chapter 2). An important parameter of the workspace is its degree of redundancy, which means that the operator should reach most of the workspace of the haptic from several directions. This feature is quite important for ultrasound applications, particularly where the physician needs to get visual and force feedback from an internal organ from different directions.

4.2.8. Actuator selection

Actuators are the key elements in haptic devices. Actuators are often electric motors. Several factors must be addressed when selecting a motor for a haptic device. Factors such as, inertia, torque ripple reduction method, required torque, power and size are important for the proper functioning of haptic devices. Torque ripple is the fluctuation about a desired output torque as the motor rotates. Torque ripple can be reduced or even eliminated in brushless DC motors by means of excitation methods and improved motor structure. By doing so, brushless DC motors provide smooth torque at low speeds, which improve haptic transparency. Windings in brushless DC motors are in the stator and magnets are positioned on the shafts. By doing so, rotor inertia is decreased, which helps to respond quickly and provide a good simulation. Therefore, brushless DC motors are often used in many haptic devices.

4.2.9. Human factors

An anthropomorphic design of a hand-controller and a correspondingly remote manipulator increases the operator's comfort and decreases his/her fatigue, which consequently increases the safety of the tele-operation. Hand-controllers or haptic devices must satisfy the requirements of human factor studies. The operator should do his/her job conveniently and without any fatigue, which requires an anthropomorphic design of the hand-controller. The range of motion of each degree of freedom should be adopted regarding the mobility of human body parts such as the wrist, forearm and upper arm during performing specified tasks such as ultrasound and palpation. This feature is quite important in designing master-slave manipulators where the master manipulator's degrees of freedom are in correspondence with human body's joints. Woodson (1987) shows the typical range of motions for wrist, forearm and upper arm separately.

Sanders and McCormic (1987) show the horizontal workspace that can be reached by an average operator. Normal area is the area that can be reached with a sweep of the forearm while the upper arm hangs in a natural position at the side. The Maximum area is the area that could be reached by extending the arm from the shoulder. It is more convenient for an operator to work in an area between the normal and maximum one. This area can be covered by combinatory motion of the forearm and upper arm at the same time. Therefore, kinematic configuration, length of linkages and levers, and angular displacements of degree of freedom should be chosen in a way that the total forearm and upper arm's motion lies between the normal and maximum limits.

This type of motion is needed when the operator uses the hand-controller for positioning of a remote probe. In this type of motion he/she uses the upper and forearm motions. The workspace required by an ultrasound probe (see Chapter 2) can be achieved by wrist movements and small motions of the forearm, which is usually performed in the normal workspace of the forearm. The hand-controller should satisfy the operator's wrist and forearm motions during standard ultrasound procedures. If the hand-controller has a virtual ultrasound probe, the hand grasp's diameter should be between 38.1 and 76.2 (mm), (Woodson, 1987).

4.3. Design of the Hand-Controller

4.3.1. General Description of the Hand-Controller

The hand-controller has four degrees of freedom. It is built upon parallel mechanisms. All actuators are attached to the base (see Fig. 4.a) that is fixed to the ground.

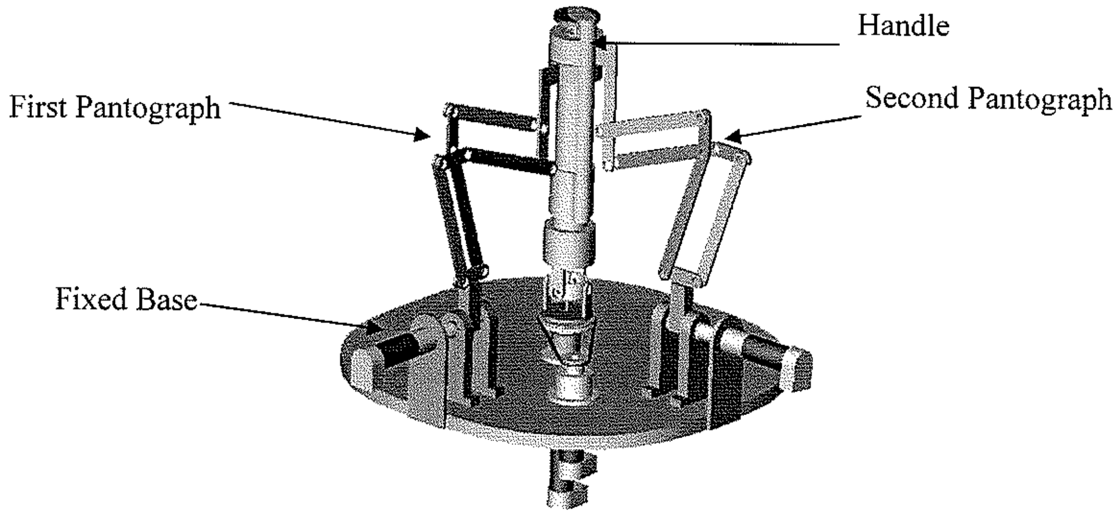

Fig. 4.a: General View of the Hand-Controller

The first two degrees-of-freedom are generated by two identical pantographs pivoted together to provide a hemispherical motion of a handle about a fixed point (see Fig. 4.b). The pantographs are located in two perpendicular planes and are rotated by two grounded direct drive electric actuators.

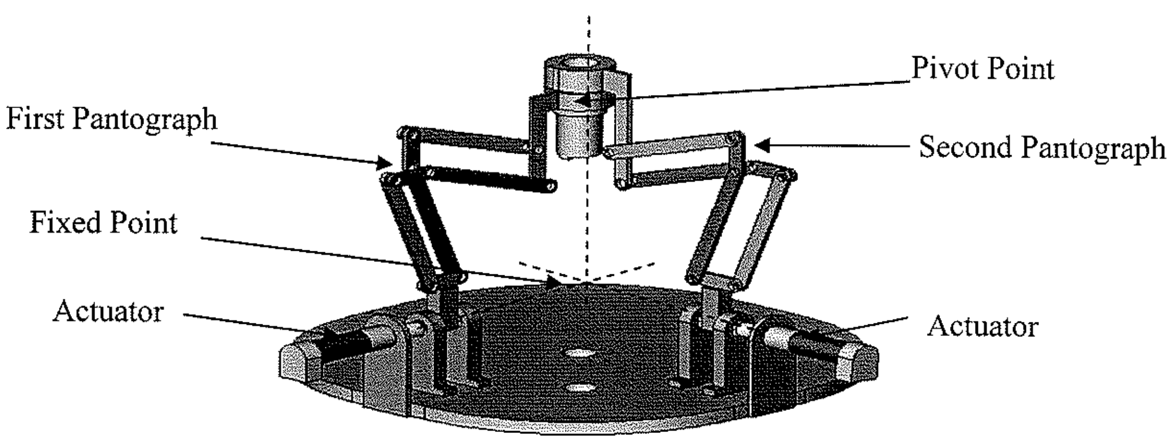

Fig. 4.b: First and Second Degrees-of-Freedom

The third degree-of-freedom represents a sliding motion along the radius of the created hemisphere, which passes through the fixed point. The power train consists of a direct drive electric actuator (see Fig. 4.c), an inner universal joint, a pair of identical decoupling ball bearings (not shown), a closed loop cable drive, a slider and a ball spline shaft. The cable drive consists of six identical pulleys and a closed cable.

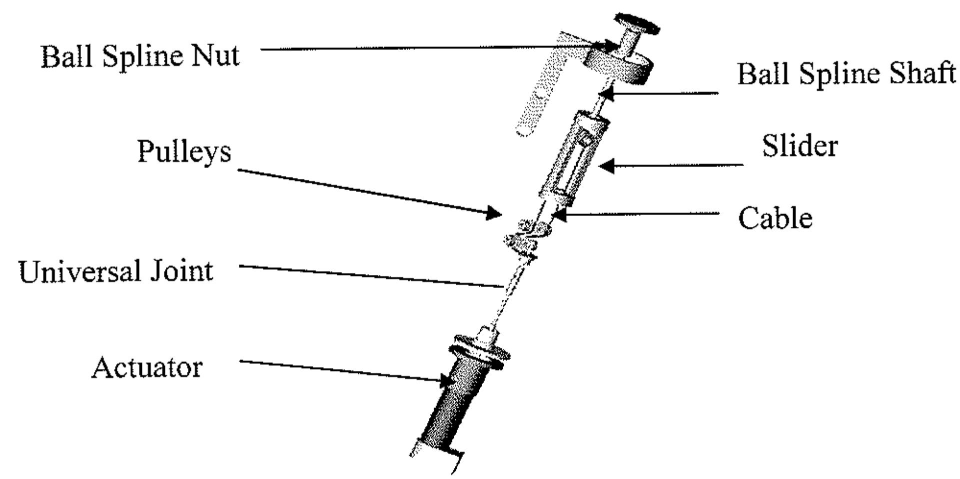

Fig. 4.c: The Third Degree-of-Freedom

The forth degree-of-freedom represents the rotational motion of the handle (see Fig. 4.d). The axis of this degree of freedom is concentric with the pivoted joint. The power train consists of a grounded electric actuator, first cable drive, an outer universal joint, a connecting tube, second cable drive and a ball spline nut.

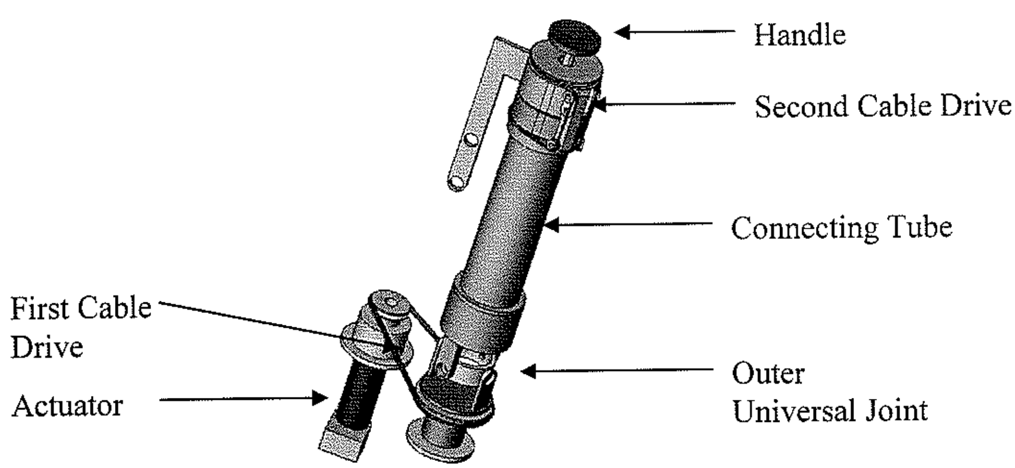

Fig. 4.d: The Forth Degree-of-Freedom

4.3.1. Embodiment design of the hand-controller

This section presents the detailed description of the assemblies and components of the hand-controller. Readers may skip this section if the detailed design is not of interest.

The first embodiment of the present device illustrated in Figs. 4.1 through 4.10. The device has moveable portion MP with a main axis 12 and is provided with an end point P1, which in the illustrated arrangement has a lever 14 rigidly connected thereto for movement relative to a base B (see Fig. 4.1).

The first and second degrees-of-freedom (DoF) are each provided by identical mutually perpendicular six-bar pantograph 16 and 18 respectively which permit the end point P1 to be manipulated in a hemispheric motion about a center point F (see Fig. 4.2), fixed relative to the base B and the location of which will be described below. The links 16L of the pantograph 16 are jointed together by shafts 16S and ball bearings (not illustrated) and the links 18L of the pantograph 18 are jointed together by shafts 18S and ball bearings (not illustrated).

The base link 16LB and 18LB of the pantographs 16 and 18 respectively are integral with their respective arms 20 and 22 which in turn are fixed to shafts 24 and 26 rotatably mounted on the base B on bearing pedestals 28 and 30 respectively.

The center point F is the intersection of the axes 24A and 26A of the shafts 24 and 26 (See Fig. 4.2), which are located in the same plane and as above indicated are mutually perpendicular to each other and the main axis 12. The length of the arms 20 and 22 are identical so that the offsets a_1 and a_2 of the links 16LB and 18LB respectively from their respective shaft axis 24A and 26A are identical.

Each of the shafts 24 and 26 is provided with its respective actuator A_1 and A_2 which may take the form of a grounded electric motor m_1 and m_2 respectively equipped with encoder e_1 and e_2 respectively that determine the position or angular orientation of the shaft 24 or 26 relative to a base position. The actuators A_1 and A_2 are each fixed relative to the base B by mounting arms 32 and 34 respectively.

The sleeves 17 and 19 connect links 16LS and 18LS (links remote form the links 16LB and 18LB) of the pantographs 16 and 18 through suitable bearings as will be described below to the end point P1 so that movement of the pantographs 16 and 18 are transmitted to the end point P1 to move same about the center point F as described above. The links 16LS and 18LS provide essentially the same length offsets a_3 and a_4 respectively from the main axis 12 of the hand-controller.

The offsets a_1, a_2, a_3 and a_4 will normally all be of equal length and the lengths of the links between shafts will be set as in most conventional pantographs i.e. opposed links of equal length.

This assembly consisting of the two pantographs 16 and 18 provides for two degrees of freedom. Actuator A_1 turns and/or measures the turn of the pantograph 16 about the axis 24A (see Fig. 4.2) of the shaft 24 and thus turns (to apply force feed back to the operator when used as a Haptic) and/or measures one of the first two degrees of freedom and causes the links 18L to rotate on their respective shafts 18S. The other of the first two DoF is measured and/or controlled by actuator A_2 that applies the same turning or measuring operations to pantograph 18 as the Actuator A_1 that applies to the pantograph 16 i.e. turns and/or measures the turn of the pantograph 18 about the axis 26A of the shaft 26 that causes links 16L to rotate about the their shafts 16S. It will be apparent that rotation of the pantographs 16 and/or 18 on their respective shafts 24 and 26 pivot the main axis 12 about the center point F (see Fig. 4.2) so that the end point P1 is moveable to define a hemispherical motion about the center point F. It is also apparent that the first and second DoF are decoupled.

The third DoF provides a sliding motion along the main axis 12 which is also the radius of the hemisphere created by the first two degrees of freedom and which has its center at the center point F (see Fig. 4.2).

The operating system for this degree of freedom (see Fig. 4.3) includes an actuator A_3 that normally will include a direct drive electric motor m_3 and encoder e_3. An inner universal joint 40 has one side 40a coupled to shaft 42 (which forms part of the first inner element that includes the system 50 (first portion) and slider 74 (second portion) to be described below) and its other side 40b (second side) coupled directly to the shaft 44 (second inner element) of the actuator A_3 and its pivotal axis 40c aligned with and defining the center point F. The shaft 44 is mounted for rotation relative to the base B by suitable ball bearings or the like schematically represented by the disk 46 in Fig. 4.3.

A cable drive system 50 (first portion) (see Figs. 4.3 and 4.4) drives or is driven by the pulley 52 fixed to shaft 42 and incorporates a plurality of guide pulleys 54 and a turn around pulley 56 that are arranged to insure the closed-loop cable 58 travels in a path having a significant portion of its travel substantially parallel to the axis 12,

A shown in Fig. 4.4, the pulleys 54 are mounted on a first normally lower support 60 on which a second normally an upper support 62 for mounting the pulley 56 is adjustably mounted via a connection schematically represented by the shaft 63 from the lower support 60. The upper support 62 mounts the turn-around pulley 56 to form the cable or belt runs 66 and 68 that are substantially parallel to and are moved by rotation of the pulley 52, 54 and 56 in a direction substantially parallel to the axis 12 as indicted by the arrow 70.

As shown in Fig. 4.5, the tension in the cable 58 is adjusted by turning the shaft 64 which has an offset portion 65 on which the pulley 56 rotates and which provides an offset a_5 so that rotation of shaft 64 changes the position of the periphery of the pulley 56 relative to pulley 42 to thereby adjust the tension in the belt or cable 58. The shaft 64 is locked into adjusted position by any suitable means in the illustrated arrangement Alan screws for example may be provided in the lower portion of the holes 61 (see Fig. 4.4) to engage and lock the shaft 64 on opposite sides of the pulley 56.

The lower support 60 is mounted via a suitable bearing structure 72 on the axial end of shaft 42 remote from the universal joint 40 so that the shaft 42 rotates freely relative to the support 60.

The support platform 60 and the rest of the cable drive system 50 may be prevented from rotation by any suitable means, which is illustrated in Fig. 4.6. In the illustrated arrangement the support 62 is coupled to a lower portion 17a the sleeve 17 by a tongue formed by a cross bar 17b on the sleeve 17 and a mating groove 62a provided on the support 62. Also bolts (not shown) pass through holes (not shown) in the bar forming tongue 17b are threaded into the upper portions of the threaded holes 61 to firmly secure support 62 and sleeve 17 together. The bar 17b provides extend diagonally across the sleeve which is hollow and provides spaces 17c one on each side of the bar 17b (only one shown) that permits the struts 74a and 74b to be received therein so that the top end member 74c is moved up and down within the sleeve 17 as will be described below.

The slider 74 is made of several parts namely a pair of opposed struts 74a and 74b connected at their opposite ends by end members 74c and 74d. When the device is assembled the bar 17b is sliding across the slider 74 between the struts 74a and 74b on the side of the top end member 74c remote from the shaft 76 and then connected to the sleeve 17 as shown.

A slider 74 (second portion) is fixed to one side of the cable route 58 at point indicated as point Y (Fig. 4.3) and is connected to a ball spline and shaft 76 system through a ball bearing 78 (Fig. 4.3). The ball bearing 78 decouples the rotational motion of the ball spline shaft 76 from the slider 74. The ball spline shaft 76 as is well known is a linear motion system, in that balls accommodated in the spline nut transmit torque while permitting linear or axial movement on precision raceways on a spline shaft.

The other side of the cable 58 passes through slider 74 without any contact with the slider 74. The cable drive system 50 particularly the cable 58 converts the rotational motion of the actuator A_{ε} and the inner universal joint 40 into the sliding one of the slider 74. The axis of the sliding motion of the slider 74 is concentric with the main axis 12 of the device (Figs. 4.1, 4.2 and 4.3). The universal joint 40 allows the third degree-of-freedom to idly follow the first two DoF provided by the pantographs 16 and 18 while transmitting rotational motion of its own degree of freedom.

The end point P1 is in the illustrated arrangement is at the end of shaft 76 remote from the base B and may be connected directly to other elements such as handle 14 to achieve the desired purpose. The fourth subassembly illustrated in Figs. 4.1, 4.7 and 4.8 is optional and is only provided if the system is to have 4 DoF i.e. if rotational motion of the end point P1 is to be provided. The axis of rotation is concentric with the main axis 12, which is concentric with the shaft 76 and 42 and with the sleeves 17 and 19.

Referring to Fig. 4.7 this 4^{th} DoF is provided by an outside universal joint 90 concentric with the inner universal joint 40 (see Fig. 4.8) so its pivot point is also aligned with the center point F. One or a first side 90a of the outer universal joint 90 is connected to a first outside element 94 that as will be described below is connected to the shaft 76 to apply rotational forces thereto and thereby to the end point P1. A second side 90S of the outside universal joint 90 is mounted on the base B via a suitable rotatable pedestal 98 that is rotable on the base B via bearing schematically indicated by the disk 46. A pulley 100 of the belt or cable drive system 102 is fixed to rotate with the pedestal 98 to dire or be driven by the universal 90 as will be described below. The outer universal 90 has a hollow ring 90c to which the sides 90 and 90S are pivotably connected in the conventional manner to provide that hollow interior in which the inner universal 40 is received.

The belt or cable drive system 102 further includes a belt or cable 104 that drivingly connects the pulley 100 to the pulley 106 of the Actuator A_4. The actuator A_4 will normally include a grounded electric motor m_4 and encoder e_4, to drive and/or monitor the movement of the element 94.A preferred form of drive for fourth degree-of-freedom is illustrated in Figs. 4.8 and 4.9 and represents rotation on an axis of rotation concentric with the main axis 12.

The power train for this subassembly consists of belt or cable drive system 102 described above and the second cable drive 400. The second cable drive 400 consists of an lower pulley 420 embedded in the upper part of connecting tube 94, two guiding pulleys 421, two tension adjuster mechanisms 422, closed loop cable 423 and an upper pulley 424 which is connected to and drives the spline nut 75 about the axis 12. The upper pulley is mounted on the sleeve 17 via ball bearings (not shown) that permit the pulley 424 is mounted on the sleeve 17 via ball bearings (not shown) that permit the pulley 424 to rotate on the axis 12 relative to the sleeve 17. The guiding and tension adjuster pulleys 422 and 424 are mounted on sleeve 17 of link 16LS block.

The tension adjuster mechanism consists of pulleys 422a, links 422b and tightening nuts 422c. By turning and tightening the link 422b and the nut 422c respectively, the user is able to adjust the cable tension. Cable 423 transmits motion from lower pulley 420 to upper one 424. The ball spline nut 75 permits relative axially movement between the pulley 424 and the shaft 76 while transmitting rotational movement.

The connecting tube or housing 94 is jointed to sleeve 19 of link 18LS of the second pantograph 18 through a ball bearing (not shown) that decouples the rotational motion of connecting tube 94 from link 18LS.

In some cases it may be desirable to have a sleeve P2 or the like that encircles the controller 10 and is connected to the handle 14 to provide an auxiliary end point P2 which may be grasped by the user by either one of or both hands to facilitate manipulation of the hand-controller 10. This construction allows the user to hold the handle in two places i.e. one hand on top at P1 and another encircling the housing 94 at P2 so that these movements may provide a one-to-one mapping for the user's wrist and elbow movements respectively. Such an arrangement is shown in Fig. 4.9.

In the illustrated version the handle 14 has been shown located in the 90° segment between the pantographs 16 and 18 for convenience so it is visible, it will normally be on the opposite side i.e. in the 270° segment between the pantographs 16 and 18 to provide 270° of free movement. It will be apparent that if 360° movement is desired the handle 14 may be eliminated.

Turning to Fig. 4.10 wherein the operation of the device is illustrated schematically the centerline CL indicates the datum centerline of the device and assuming the device is oriented vertically this line CL will extend vertically from the center point F.

The axis 12 is manipulated so that the plane PL containing the point P1 extends at any suitable selected an angle β_1 measured from the CL on "X" axis (assuming CL is the Z axis) and the point P1 is at second angle β_2 measured from the "Z" axis of CL on plane PL the "Y" axis direction. These angles β_1 and β_2 are determined by the pantographs that have been pivoted from their respective datum positions which for the purpose of this description is the location when the centerlines CL and 12 coincide. In effect rotation of the pantographs 16 and 17 on their respective axes 24A and 26A result in mutually perpendicular displacements of the centerline 12 relative to centerline CL as indicated by the arrows 450 and 452. Thus, movement of the pantographs 16 and 18 about their respective axes 24A and 26A results in adjusting the size of angle β_1 and β_2 and thereby the positioning of point P1 relative to the centerline or axis CL.

The third degree-of-freedom moves the endpoint P1 axially along the axis 12 as indicated by the arrow 456 in Fig. 4.10 and the fourth degree-of-freedom rotates the endpoint P1 around the axis 12 as indicated by the arrow 458.

The above-described combination will be used as a hand-controller with force reflecting capability. It may be used to control the motion of, and reflect the forces from a remote wrist performing selected operations such as palpation or ultrasonic diagnosis.

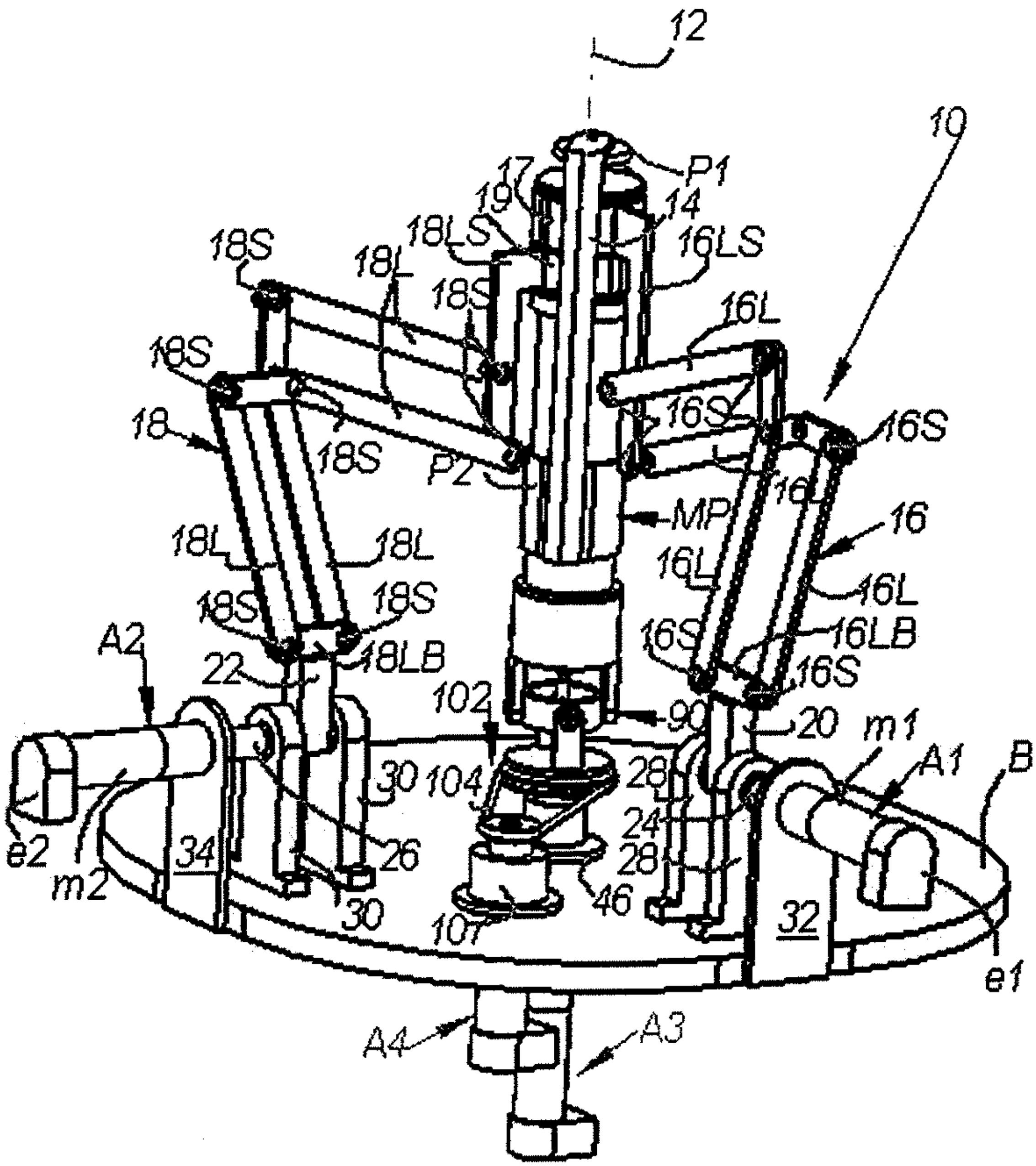

Fig. 4.1: General view of the hand controller.

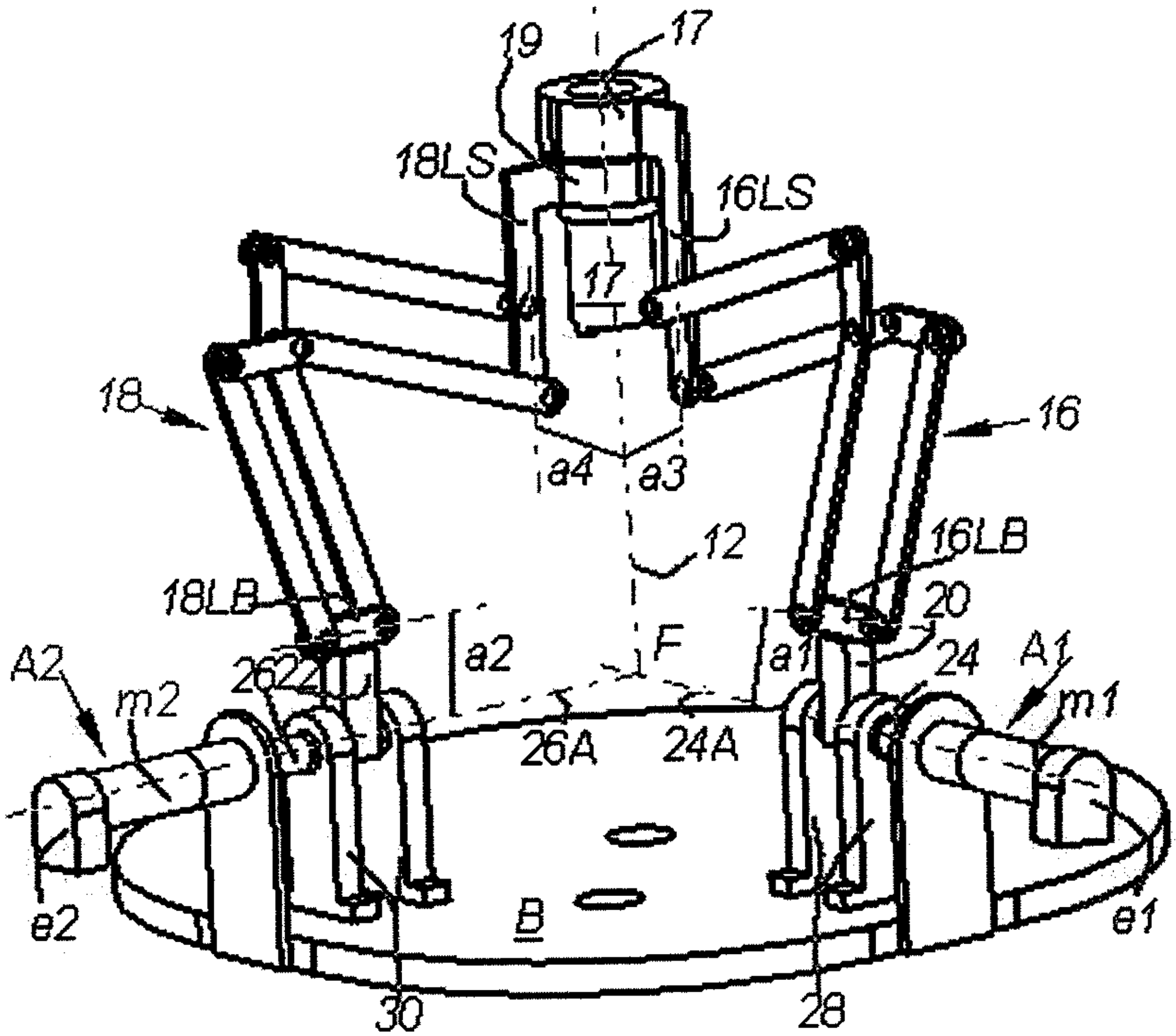

Fig. 4.2: The pantographs for applying the first and second degrees of freedom.

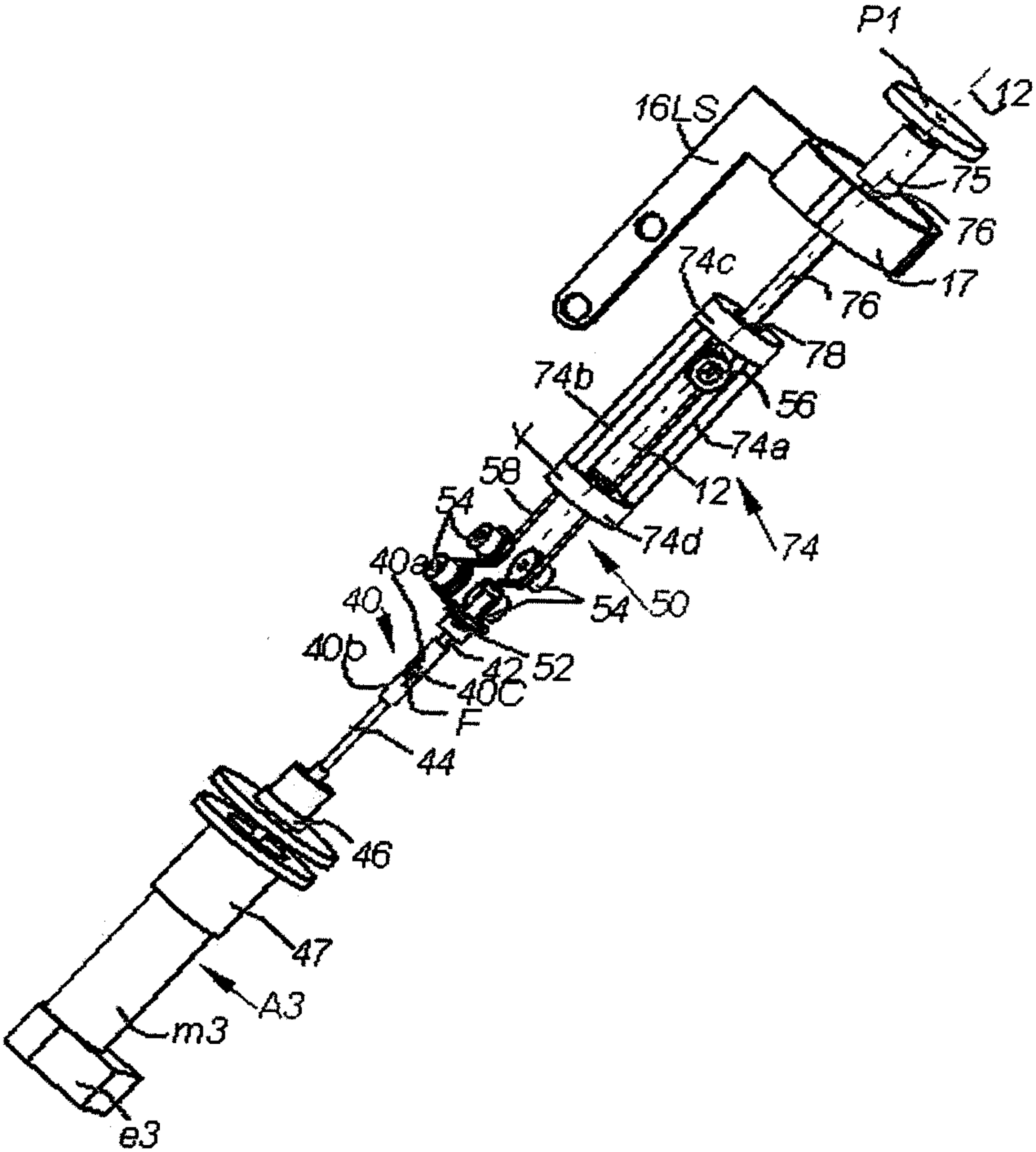

Fig. 4.3: The power train for the third degree of freedom.

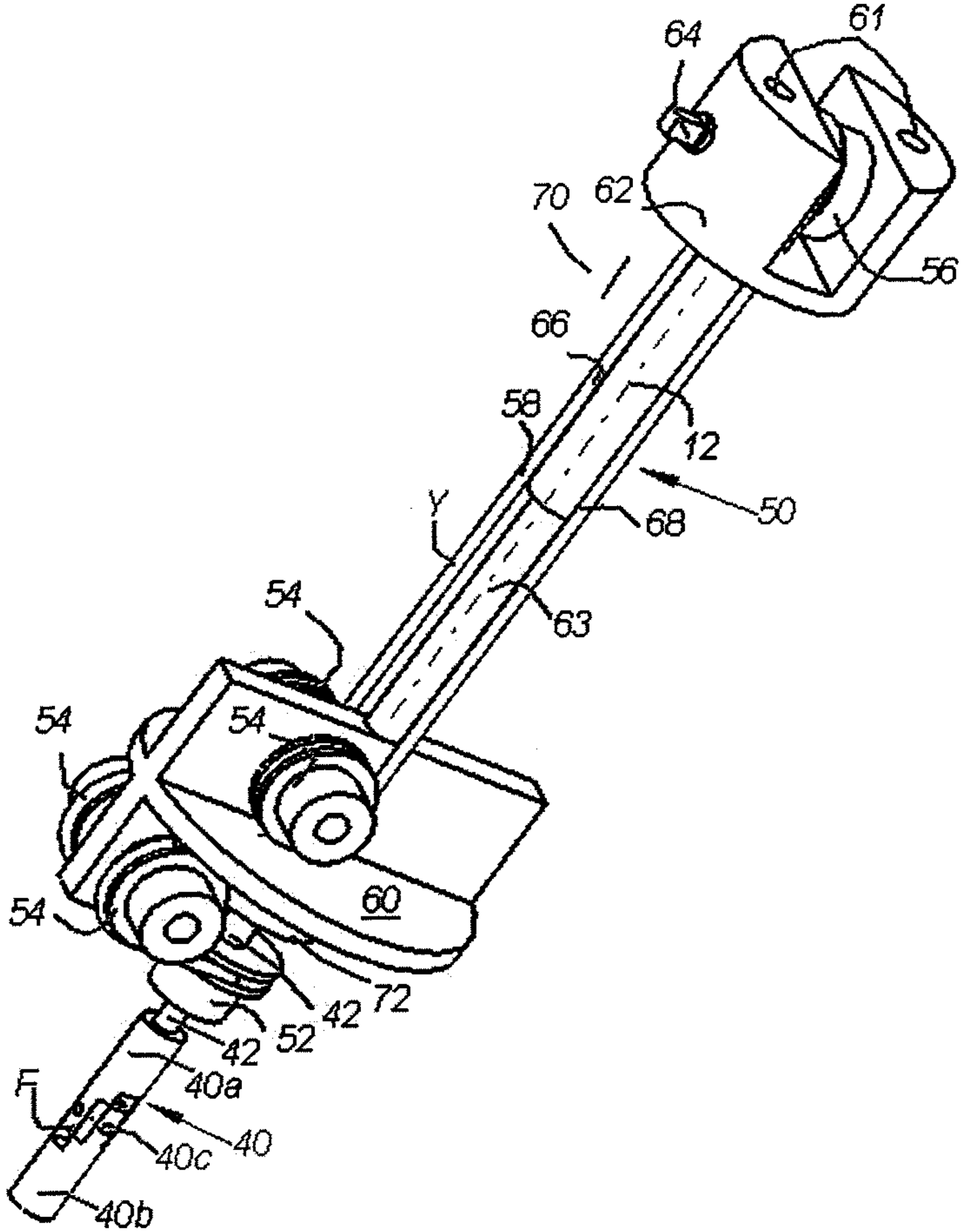

Fig. 4.4: Detail of the cable drive.

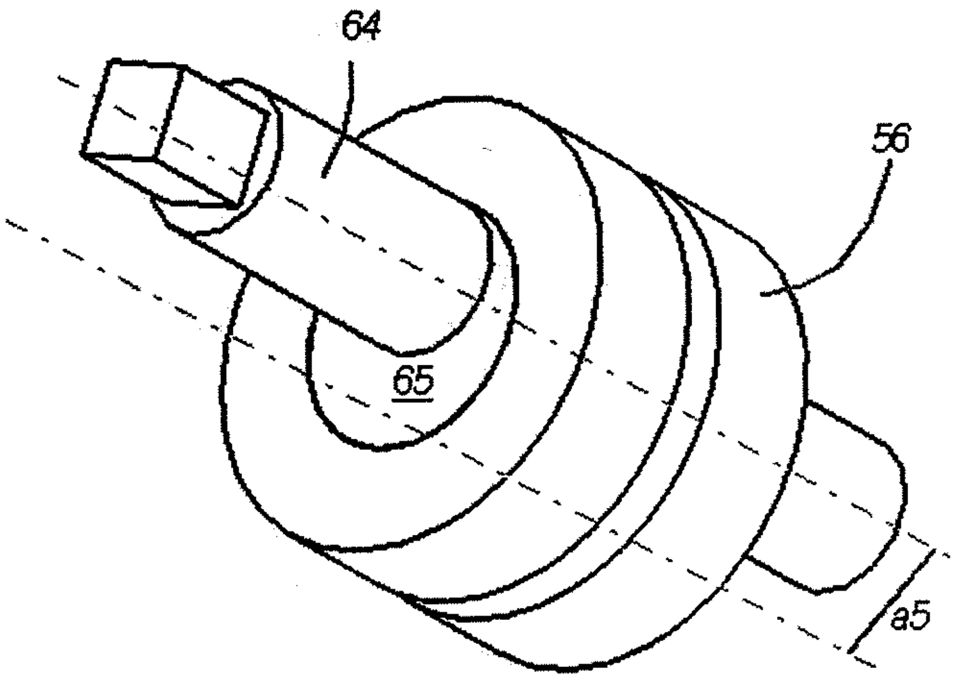

Fig. 4.5: Cable tensioning mechanism.

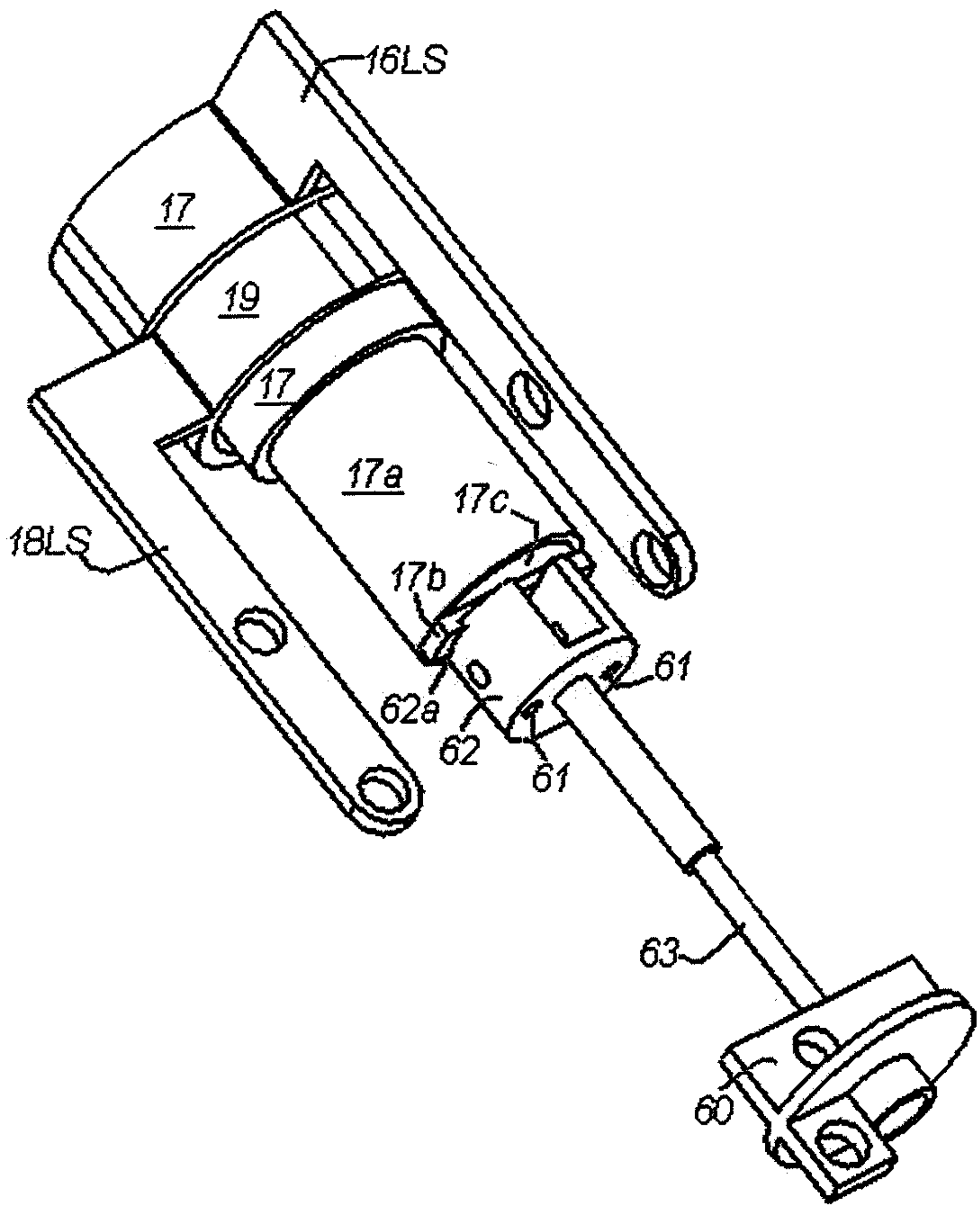

Fig. 4.6: The interconnection between the pulley mounting and one of the pantographs.

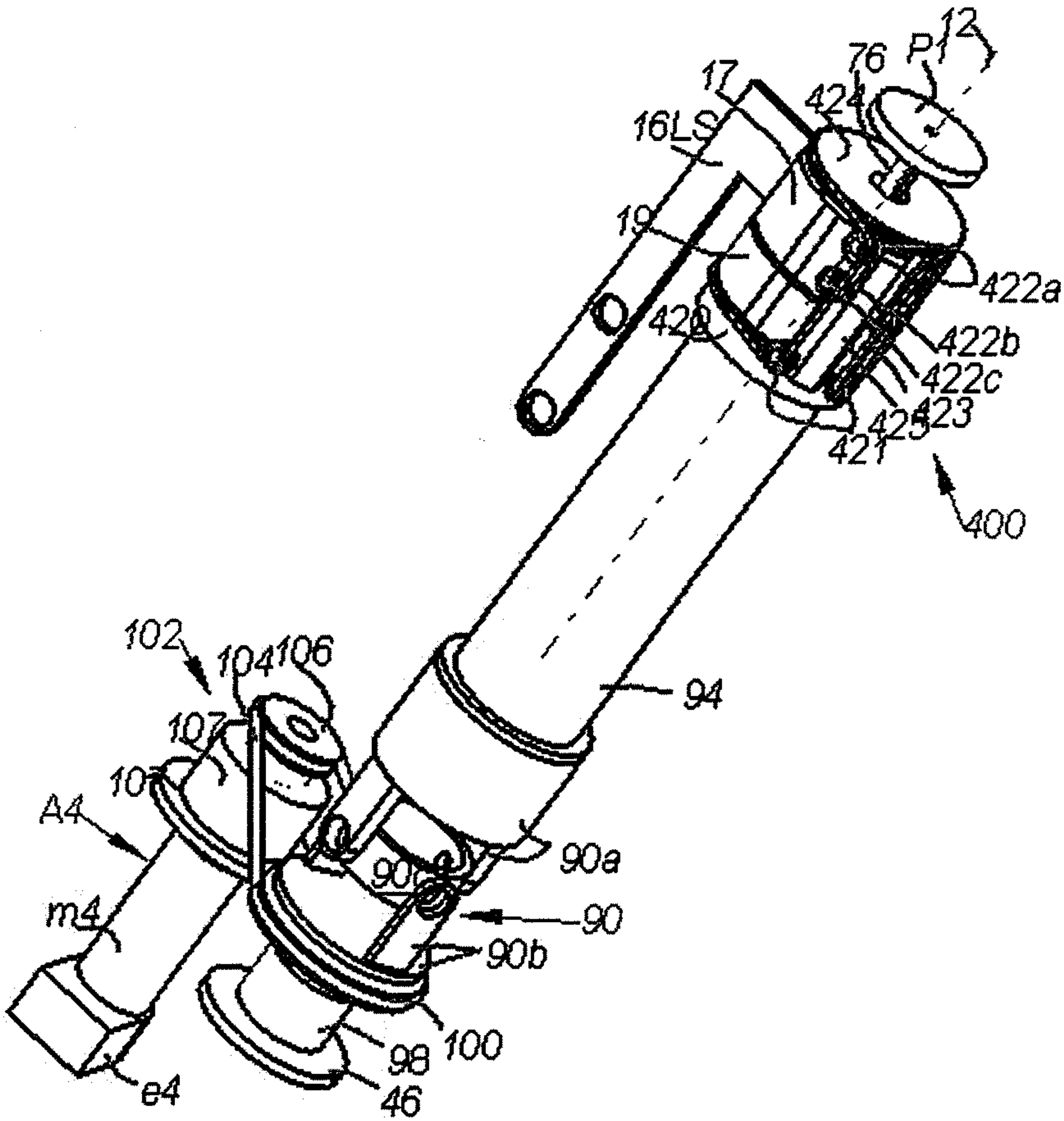

Fig. 4.7: The power train for the fourth degree of freedom.

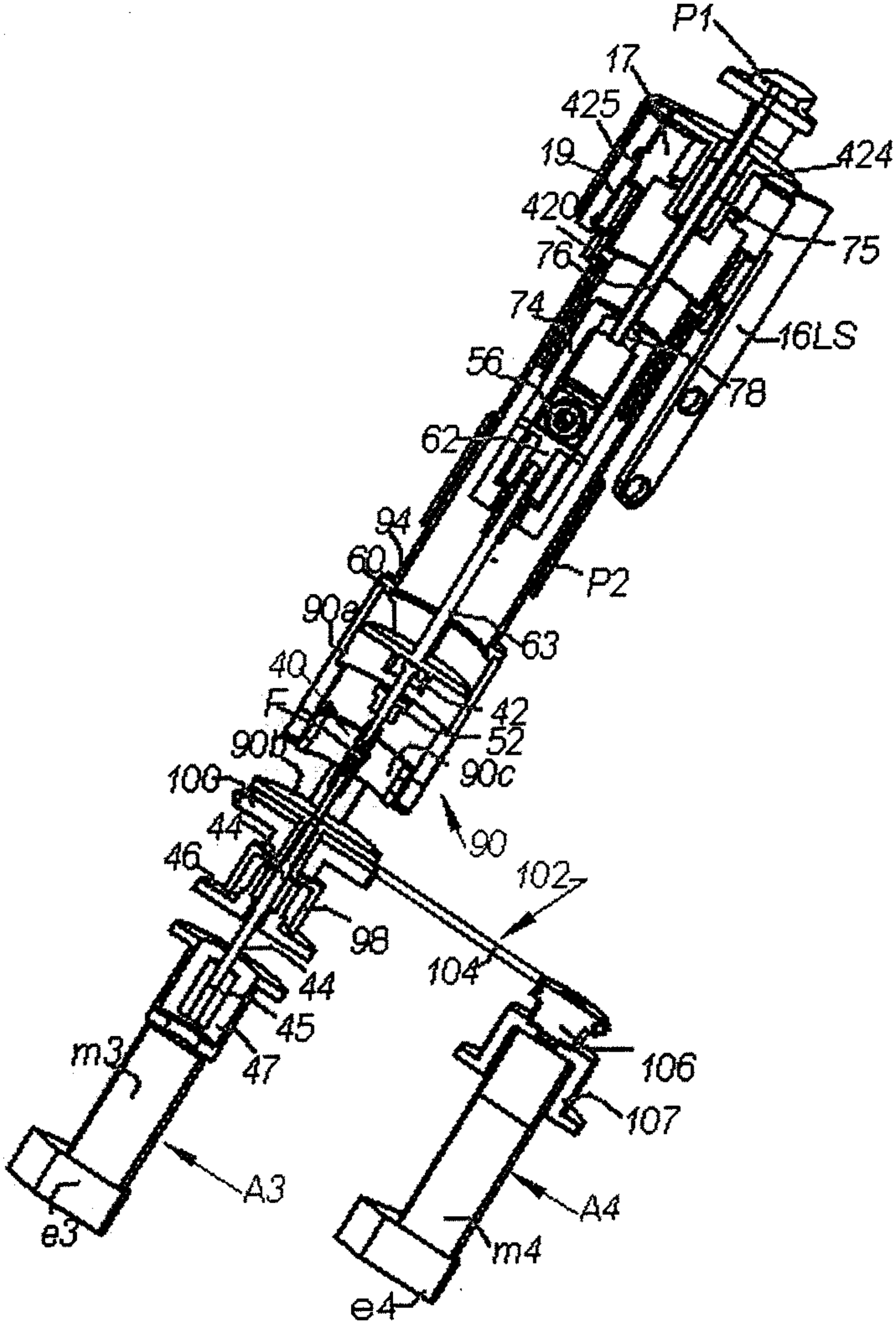

Fig. 4.8: The relationship between the third and fourth DOF in cross section.

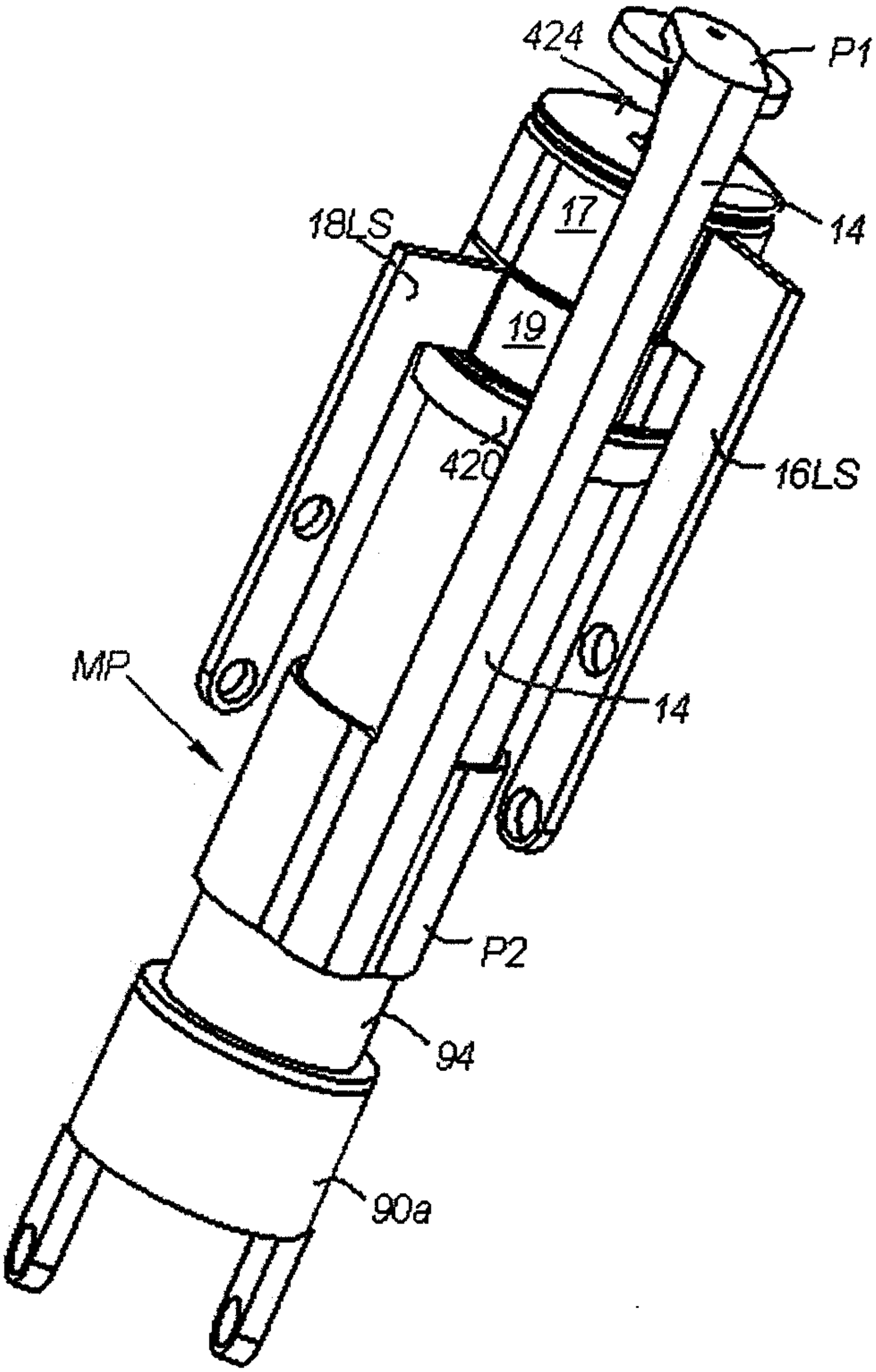

Fig. 4.9: The connection between pantographs and manipulated end point.

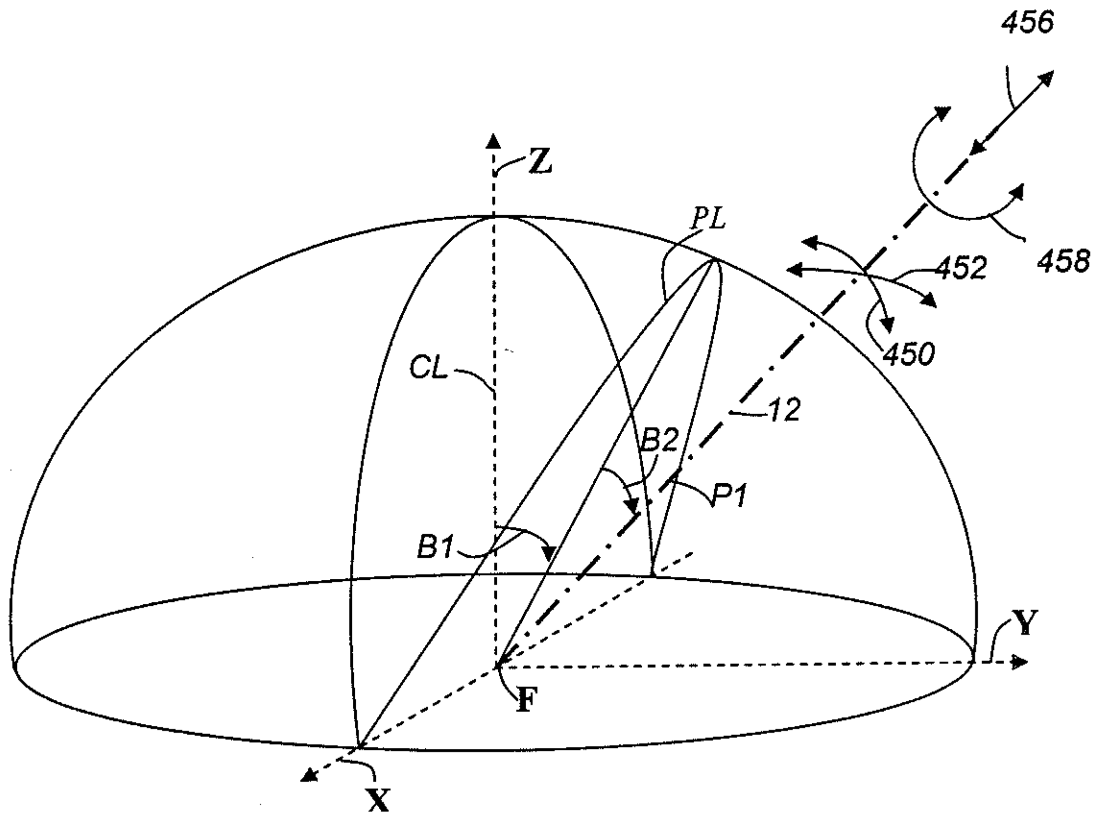

Fig. 4.10: The movements of the endpoint.

Chapter 5

Design of the Robotic Wrist

This chapter describes the embodiment design of the four degrees-of-freedom robotic wrist to enable physicians to perform ultrasound examination and palpation on a remote patient. Section 5.1 reviews the background of robotic wrists and manipulators. Section 5.2 introduces the required specifications for robotic wrists. Section 5.3 studies safety aspects that should be followed during the design of medical manipulators. Section 5.3 develops the embodiment design of a four degrees-of-freedom robotic wrist.

5.1. Literature Review

As far as various relevant designs of the wrist are concerned, the dexterous split equator joint by Stanisic et al. (US patent 6,026,703) and Wiitala (2000), desribes a device with all points of the links moving on spheres. Thus, there is no remote center-of –motion outside the mechanism. The compact wrist actuators by Rosheim (US patents, 4,686,866, 4,723,460, 6,418,811) have three degrees of freedom with linear actuators. These devices provide spherical motion of an end-point, which is inside the mechanism. The spherical robotic wrist by Dien et al. (US patent 4,628,765) consists of two perpendicular semi-circular yokes providing a spherical motion, with no remote center-of motion. The yokes can be heavy, need precision machining and usually exhibit backlash. The stereotactic apparatus for locating or removing lesions developed by Shelden et al. (US patent 4,638,798) provides the required motions for ultrasound and palpation. However, the actuators in this device are floating, making it bulky and heavy. Grounded actuation is a basic parameter of designing any wrist. The wrist for detecting very small breast anomalies by Souluer (US patents 6,192,143, 6,351,549 and 6,400,837) consists of a positioning device, fully adjustable bed and detection head, which should work together to position/orient the probe over the breast for palpation. The device is not only big, but also cannot provide the required motions for ultrasound diagnosis. Funda et al. (US patent 6,201,984) developed a remote center-of motion device for endoscopic surgery. The device provides a spherical motion about a fixed point with two circular guides. Available circular guides are bulky, heavy and difficult to be machined precisely. The actuators are also floating, which would not fulfill the requirements of the wrist design. The remote center-of-motion robot for surgery by Taylor et al. (US patent 5,397,323) has four degrees of freedom and uses a serial linkage mechanism. All the actuators are mounted on the proximal part of the device (not on the ground) and located on the same plane as the work point. Thus, it is not easy to install this device on the implement of a manipulator. The tele-operated surgical instrument developed by Madhani et al. (1998) and laparoscopic positioning stand by Faraz and Payandeh (1998) have similar structures as the one belonging to Taylor et al. (US patent 5,397, 323). The two degrees-of-freedom spherical parallel manipulator by Hong (US patent 6,355,048) can have both interior and exterior remote center-of-motions, but the work done by Ouerfelli and Kumar (1994) shows that these type of manipulators have singular points in their workspace. The laparoscopic workstation by Cavusoglu et al. (1999) uses three linear actuators with grounded motors (but appear to be coupled) for the first three degrees of freedom and one floating actuator for the fourth degree of freedom. The parallel wrist by Vischer and Clavel (2000) provides a three degrees-of-freedom rotational motion about a fixed working point. However, the remote center-of motion is enclosed within the mechanism at some configurations. The roll motion is also limited to 120 degrees. Salcudean et al.(patent) and Zhu et al. (2000) developed an ultrasound robot in order to reduce the joint's fatigue of the ultrasound technicians. They used a pantograph to generate a conical motion around a fixed point on the patient with using a serial configuration and floating actuators. They balanced the whole manipulator by adding counterbalance weights to the system to be pushed back by the patient upon feeling any discomfort during examination. Adding counterbalance weights increases the overall weight of the system, which in turn increases the impact forces between the patient and the robot in unwanted situations. For providing palpation motion for abdominal ultrasound, the whole manipulator should be moved up and down, which is not desirable from the safety aspects. They implemented different control algorithms such as force control and visual servoing. Mitsubishi et al. (2001) developed a remote ultrasound diagnostic system consisting of circular guides connected in a serial configuration and embedded with gears of high ratio. The system seems to be heavy and bulky. They also developed a six degrees-of-freedom force reflecting hand-controller with a different kinematical configuration than its ultrasound robot, which requires a large amount of coordinate mapping between the hand-controller and the manipulator. They implemented impedance control on their system. The ultrasound wrist developed by Gourdon et al. (1999) uses a differential mechanism with bevel gears, which has kinematically coupled degrees-of-freedom. Hamlin and Sanderson (1994) used a six-bar pantograph in different configurations to make modular parallel manipulators with novel spherical joints.

5.2. Design Requirements

In addition to the factors discussed for designing haptic devices (see chapter 4) such as structural rigidity, a large and singularity-free workspace, compactness, kinemtically decoupled degrees-of-freedom, backdriveability, low mass and inertia, remote actuation or grounded actuators, low cost, simple fabrication process and having a kinematically similar configuration with its hand-controller (Chapter 4), there is another important factor, which must be taken into consideration during the design of medical robots. The next section addresses safety aspects, which must be considered during the mechanical design of medical robots.

5.3. Safety Aspects

The health and safety requirements for industrial robots suggest that they should not operate in contact with people but they should be isolated in a cell with safety interlocks. The only exception is that, the robot may be programmed by a skilled operator in the cell. During programming, the robot can move only under reduced speed conditions while the operator keeps out of the reach of the moving arm. If the medical robots were to operate under the same requirements as industrial robots, they clearly would be very limited in their capabilities and applications (Davis, 2003).

A further consideration is that manufacturers of industrial robots seldom make available to the suppliers of medical robotic systems all the specific details of software and hardware of their industrial robots. Only if such full details are supplied, can the medical group assure themselves that the necessary safety features are in place so that they can take responsibility for the system they propose to use (Davis, 2003).

The modification of industrial robots to make them fit for medical applications seems to be very difficult since implementing required safety aspects of medical robots to them ends up in a huge number of modifications, which make this job somehow impossible. However, it might be acceptable to use a standard robot for feasibility study purposes to try out concepts and ideas prior to the implementation of special purpose medical robots. Therefore, one solution can be designing special purpose medical robots to perform specific jobs.

Extensive work is underway by the Japanese to develop and quantify safety aspects of medical robots. Yamada et al. (1997) and Ikta and Nokata (1999) studied how to reduce the probability of an accident and how to minimize the injuries after an accident.

Ikta and Nokata (1999), have developed a safety measure (danger index) to quantify the safety level of manipulators. The danger index is defined based on impact force between the patient and the manipulator. Different researchers have suggested the following safety regulations and their effects on minimizing the impact force and increasing safety. These factors should be considered during the design of medical manipulators:

1- Ikta and Nokata (1999) showed that replacing the robot's structure material from steel to aluminum brings the danger indexfrom 100% to 34% and replacing aluminum with plastic brings the danger index to 18%. However, weight can also be minimized by adopting appropriate robot structures and their material and also mathematical optimization techniques.

2- Covering the robot manipulator with shock absorbing material such as rubber could reduce the impact force. Covering the manipulator's structure with rubber could reduce the danger index to 50%, (Ikta and Nokata, 1999).

3- Having compliance in the manipulator's joints can decrease the danger index. However, existing techniques for providing compliance to the joints would make the whole system quite bulky (Morita and Sugano 1995; and Okada et al. 2001).

4- Increasing the impact area between the patient and the manipulator could decrease impact stress, which is basically achieved by making the robot's links curvy. Sharp edges can generate larger impact stresses on the patient (Ikta and Nokata, 1999).

5- Covering the robot's linkages with slippery material such as Teflon could release impact force by slipping on the less frictional surfaces. When using Teflon instead of steel, the danger index reduces from 100% to 80% (Ikta and Nokata, 1999).

6- The primary axes of the manipulator should be gravitationally balanced to prevent from falling due to complete power loss. This feature could help patients to easily push away the manipulator in emergency cases (Zhu, et al. 2000).

7- The Manipulator's joints must be backdriveable, which enables the patient and medical staff to remove the manipulator in emergency cases.

8- Manipulators should be moved with the lowest velocity to have a minimum of kinetic energy during motion.

9- Having the minimum number of joints with low mass and inertia.

10- All the actuated joints should be equipped with torque overload clutches. These clutches are usually mounted between the actuator and the driven members of the manipulator.

11- Position sensors such as potentiometers and encoders should be duplicated to monitor output motion as well as the motor shaft. There might be breakage and/or slippage in the power train from the input actuator to the output members. And the operator must be informed about the proper action of all sensors.

12- System must fail only in a safe, predictable manner. This can be achieved by design approaches such as using power-off brakes, or using pneumatic actuators with their valves to maintain air pressure during the absence of power.

13- Use mechanical constraints and electrical switches to limit the manipulator's motion to a safe volume or trajectory (Khodabandehloo et al., 2003).

14- Manipulator structure must enable reasonable access to the patient in emergency cases (Khodabandehloo et al., 2003).

15- The electrical actuator should be as far away as possible from the patient and they must be isolated from the manipulator to prevent electrical shocks.

5.4. Design of the Robotic Wrist

5.4.1. General description of the robotic wrist

The wrist has four degrees of freedom. It is built upon parallel mechanisms. The base will be attached to the implement of a manipulator with prismatic joint (see Fig. 5.a). The first two degrees-of-freedom are generated by two identical pantographs pivoted together to define a hemispherical motion of a probe about an exterior fixed point.

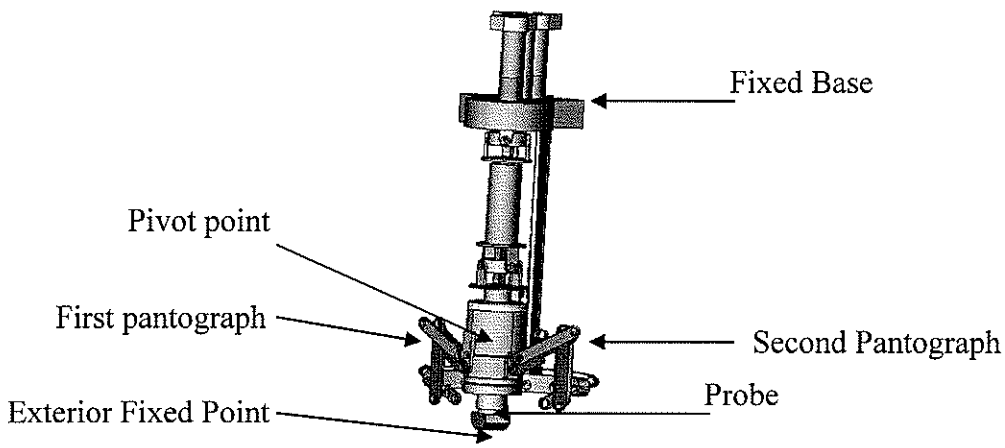

Fig. 5.a: General View of the Robotic Wrist.

Fig. 5.b shows the power train of each pantograph. It consists of an electric actuator, cable drive, a pantograph, a moveable section and finally the probe.

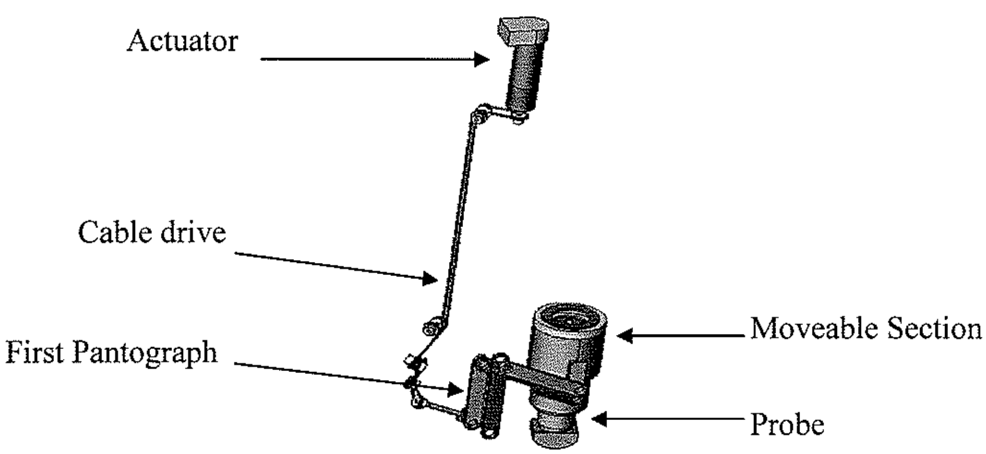

Fig. 5.b: First and Second Degrees-of-Freedom's Power Train.

The third degree-of-freedom is a linear motion of the probe along the radius of created hemisphere (see Fig. 5.c). It consists of an electric actuator, a universal telescoping joint, a moveable section and a linear drive inside the moveable section (not shown). Telescoping joint transmits torque while there is linear motion along its axis.

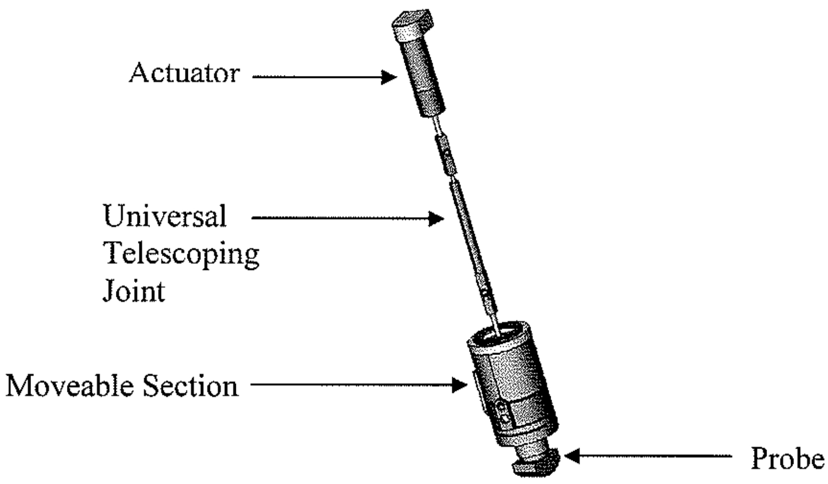

Fig. 5.c: Third Degree-of-Freedom's Power Train.

The forth degree-of-freedom is a rotational motion of the probe about the radius of created hemisphere (see Fig. 5.d). It consists of an electric actuator, a first cable drive, a universal telescoping joint, second cable drive, a moveable section and finally the probe.

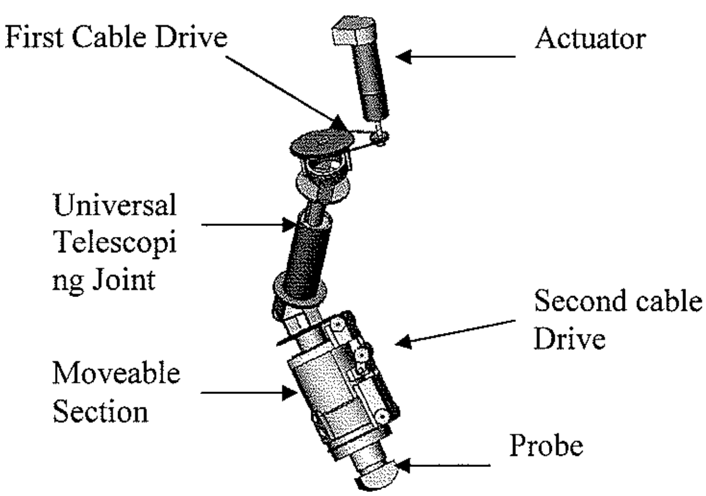

Fig. 5.d: Forth Degree-of-Freedom's Power Train.

5.4.2. Embodiment design of the robotic wrist

This section presents the detailed description of assemblies and components of the robotic wrist. Readers may skip this section if the detailed design is not of their interest. Similar parts of the hand-controller described in Chapter 4 to those equivalent parts of the wrist 10A are called by similar names in the following description of the wrist 10A.

Referring to Figures (5.1) and (5.2), the device is provided with moveable portion or section MPA having a main centerline 212 and end point or probe PA that is being manipulated. This probe PA is primarily manipulated about a center point or a center of motion point FCM (see Fig. 5.3). The probe PA may also be manipulated as will be described below for axial and or rotational motion relative to the main centerline 212 of the main or moveable section MPA in which the operating modules (described below) are to be amounted. This moveable section MPA is oriented as will be described below by a pair of pantographs 216 and 218 which operate or are operated to orient the section MPA particularly the probe PA in a manner similar to the operation of the pantographs 16 and 18 in the positioning of the end point P1.

A pair of six-bar pantographs 216 and 218 similar to the pantographs 16 and 18 of the above-described controller are mounted on a frame 220 suspended from the base BA defines the first two DoF of the probe PA (which is the wrists equivalent to the end point P1 and is manipulated in a manner similar or equivalent to the movements of the end point P1 of the hand-controller 10 described in Chapter 4). The frame in the illustrated arrangement (see Figs. 5.2 and 5.6) is formed by a pair of pillars 222 and 224 to which is attached a substantially semi circular bar 226 on which the turning axels 228 and 230 (see Fig. 5.3) of the pantographs 216 and 218 are mounted.

The axes 232 and 234 of the axels 228 and 230 are positioned in axial plains perpendicular to the main axis 212 and are space 90 degrees apart. These axes 232 and 234 are set at the same selected angel α relative to the main axis 212 so that they are in effect in the same cone relative to the datum centerline CL_1 of the moveable section MPA which is equivalent to the centerline CL of the device 10 described above and is thus coaxial with the axis 212 when the axis 212 is in neutral position - in the illustrated arrangement when the axis 12 is substantially vertical.

The point of intersection of projections of axes 228 and 230 with each other and with main axis 212 (and with the centerline CL_l) defines the location of the center of motion FCM.

The pantographs 216 and 218 operate in the same manner as the pantographs 16 and 18 described above in that as they are rotated with their respective shafts 228 and 230 (the plain of each pantograph is located in the plain of their respective shafts 228 and 230) to define a hemispherical motion of the point PA (which may for example indicate the surface of an ultrasound or palpation probe) about a remote center of motion (FCM) (see Figs. 5.3, 5.4 and 5.5).

In the Fig. 5.3, position of the center of motion FCM, which is fixed relative to the base BA is shown aligned with the extreme free end PAF of the probe PA. It will be apparent that the axial extension of the probe relative to the moveable section MPA as will be described below and as schematically indicted in Fig. 5.3 by the arrow 235 will change the operation or movement of the probe PA for a given change in movement of the pantographs 216 and 218. It is preferred to position the center of motion FCM so that axial movement of the probe PA may position the free end PAF on opposite sides of the center of motion FCM.

As indicated above, the rotatable shafts 228 and 230 are each is fixed to and positioned in fixed relation to the base BA via the frame 220. Mounted on the base BA are a pair of actuators A_5 and A_6 each of which may include its motor m_5 or m_6 and suitable encoders e_5 and e_6 that drives (or is driven by) and measures the rotation of its respective pantograph 216 and 218 respectively via their respective shafts 228 and 230.

The motors m_5 and m_6 have gearboxes for torque increase or speed reduction if desires and may also be directly coupled to shaft 228 and 230 respectively in applications whereby motor closeness to the FCM is not of concern, however it is preferred to couple each of the motors m_5 or m_6 to its respective shaft 228 and 230 via the belt or cable drives 236 or 238 respectively.

The cable drive 236 and 238 are essentially the same except one 236 connects actuator A_5 with shaft 228 and the other 238 connects the actuator A_6 to the shaft 230. Thus only the drive 238 will be described with reference to Figs. 5.2, 5.3, 5.5 and 5.6 it being understood that the drive 236 is essentially the same.

As shown the shaft 240 (see Fig. 5.5) of the motor m_6 has a pulley 242 mounted thereon and drives a cable 244 that passes over and is guided by suitable guide pulleys 246 some of which may also function as tensioners to tension the cable 244 and drives pulley 248. The pulley 248 has a companion pulley 250 fixed for rotation therewith and this pulley 250 drives a second cable 252 that drives the shaft 230 via pulley 254. A suitable tensioning pulley 256 may be provided, if desired.

As indicated the first degree of freedom is generated by motor m_5 and the cable drive that turns the pantograph 216 about the axis 232 of the shaft 228. The drive m_6 for second degree of freedom may but need not be idle when the first is operated but when activated rotates the second pantograph 218 with its shaft 230 i.e. about its axis 234.

The detail of the pantographs is shown is Fig. (4.2). The lengths of the links in each pantograph 216 and 218 comply with the conventional length conditions used in most pantographs.

The first and second pantographs 216 and 218 as above indicated are located in two perpendicular planes. The pantographs 216 and 218 each connect to the device via their respective sleeves 260 and 262 i.e. the pantograph 218 has its link 264 remote from the shaft 230 connected to the sleeve 260 (see Figs. 5.3, 5.4 and 5.5) and similarly the pantograph 216 has its link 266 remote from its shaft 228 fixed to the sleeve 262. The sleeves 260 and 262 are concentric with and may rotate relative to each other about the axis 212. These two degrees defined by the pantographs 216 and 218 are decoupled.

The third DoF of the end point PA is provided by a shaft system 270 (see Fig. 5.7) formed by three shafts interconnect by a pair of inner universal joints namely a first inner universal 278 inter connecting shafts 276 and 284 and a second inner universal joint 280 interconnecting the shafts 274 and 282 (which is part of shaft 284). The shaft 272 is driven buy actuator A_7 that normally will include a motor m_7 and an encoder e_7. The shaft 272 is in effect the motor shaft of the motor m_7 and the shaft 284 is made of an inner shaft 282 and outer shaft 283 coupled together to permit relative axial movement while prohibiting relative rotational movement. Outer shaft 283 is connected to one side of the first inner universal joint 278.

The shaft 276 coupled to the other side of the first inside universal joint is an output shaft that couples to the various modules (described below) that may interchangeably be received in the sleeves 260 and 262 of the mobile section MPA to drive same if required.

The fourth DoF is provided by the mechanism shown in Figs. 5.8, to 5.11. This fourth DoF is a rotation about the radius of the hemisphere created by the first two degrees of freedom and which is coaxial with the main axis 212 i.e. the rotational axis of the sleeves 260 and 262 is main axis 212.

The roll or rotation motion is provided by the actuator A_8 that normally includes a grounded electric motor m_8 and an encoder e_8. The rotational motion from the electric motor m_8 is transmitted through a first cable or belt drive 290 composed of pulley 292, cable or belt 294 and pulley 296 that is attached to one side 298 of a second outside universal joint 300 that is concentric with the second inside universal joint 280.

The other side 301 of universal joint 300 is coupled to an inner shaft 302 that telescopes within the concentric outer shaft 304 and these two shafts 302 and 304 are splined together by spline 306 and mating element 305 secured to shaft 304 (see Figs. 5.9) and (5.11)) so that the shafts 302 and 304 rotate together but permit relative axial movement there between in the same manner as the shafts 282 and 284.

The outside shaft 304 at its end remote from the universal joint 300 is fixed to one side 308 of a first outside universal joint 310 which is concentric with the first inside universal joint 278. The other side 312 of the is connected to a pulley 314 which forms the driving pulley for a second cable or belt drive system 316 wherein a belt or cable 318 passes over a plurality of properly positioned idle or guiding rollers 320 and a driven pulley 322 mounted on the sleeve 260 of the moveable section MPA for rotation about the axis 212 and fixed to a rotably driven module element to drive the module as will be described below.

A suitable cable or belt tensioning system 324 is provide for the belt or cable 318 and is formed by a pulley 326 mounted on an arm 328 whose position is adjustable to change the position of pulley 326.

The guide rollers 320 and the tensioning systems 324 of the drive system 316 are mounted on the sleeve 260 of the pantograph through a series of modular blocks 340, 342 and 344 (see Figs. 5.8 and 5.9).

The first cable drive 290, drives the second outside universal joint 300 which in turn drives the first outside universal 310 via the telescoping shafts 302 and 304 interconnected by the spline 306 and the universal 310 the drives the cable system 320 thereby transmitting torque from a fixed rotation source A_8 to a moving joint in space in any orientation (see Figs. 5.8 and 5.9). This allows a module (described below) mounted in the sleeves 260 and 262 of the moveable portion or section MPA to be rotatably driven and to idly follow the movement of the moveable portion MPA by the first two DoF for the moveable section MPA so that torques is transmitted to drive the fourth DoF of the wrist 10A.

Figure 5.10 shows the relationship of the actuators A_7 and A_8 and their respective driving relationships with the second inside universal 280 and second outside universal 300 respectively and the concentric relationship of the two second universals 280 and 300. As indicated above, the two first universals namely first inside universal 278 and first outside universal 310 have a similar concentric relationship to that shown in Fig. 5.10 for the second inside 280 and second outside 300 universals and above described for the inside and outside universals 40 and 90 of the device 10 described above.

The wrist 10A may include more than one module designed so that the modules can be easily substituted for one another i.e. quickly attached and/or detached in the sleeves 260 and/or 262 of the moveable section MPA.

The wrist 10A in the illustrated embodiments is provided with two interchangeable modules 500 and 600 each of which may be quickly attached and detached (see Figs. 5.12 to 5.15).

The first module 500 has two degrees of freedom (see Figs. 5.12 and 5.13).This module 500 transmits the rotation of pulley 314 to the working probe 532 forming the end point PA. It also converts motion of the fourth degree of freedom, i.e., the rotation of shaft 276 into the sliding motion of the working probe 532. The module 500 has an outside housing 526 that is received in and detachably mounted in the moveable section MPA in any suitable manner. In the arrangement illustrated in Fig. 5.13 a retractable coupling pin pins the module in position and functions to prevent rotation of a slider 528 as will be described below.

The shaft 276 is coupled to a ball screw drive shaft 525 of the module 500 via a self-aligning coupling 502 and drives a ball screw's nut 527 fixed to a slider 528 (see Fig. 5.13). Linear guides 529 are fixed to a slider 528, and end support 533, respectively and prevent rotation of the nut 527 with the shaft 525 while permitting relative axial sliding movement between the guides 529 and the end support 533. The end support 533 is fixed to sleeve 260 of the pantograph 218 by a coupling pin schematically indicated at 506 to prevent rotation of the end support 533 and thereby through guides 529 prevent rotation of the slider 528. The ball screw drive shaft 525 is mounted on end support 533 by a ball bearings (not shown). The linear guides 529 are connected to slider 528 by two linear ball bushing (not illustrated). Slider 528 is mounted on connector 530 via a decoupling ball bearing (not shown). Thereby to decouple the rotating motion of connector 530 imparted by the drive 316 from sliding motion of the slider 528 so that the module can achieve three modes of motion (rotational, sliding and spiral as needed).

The connector 530 also connects the working probe 532 with a ball spline nut 531 that prevents relative rotational movement of the probe PA and the housing 526 while permitting relative axial movement parallel to axis 212 there between. The housing 526 is connected to pulley 322 by coupling pin schematically indicated at 508 and receives it rotary motion from pulley 322 driven via drive 316 as above described. Obviously the rotary motion imparted to the housing 526 is transferred to the probe PA by the spline nut 531. Probe 532 is preferably attached to the connector 530 through an off-the-shelf six axes force/torque sensor (not shown).

When the module 500 is in operative position (see Fig. (5.13)), ball screw's shaft 525 is connected to the shaft 276 by -the- shelf self aligning coupling 502 and the housing 526 of the module 500 (or 600) is mounted within the outer housing formed by sleeve 260 on suitable bearings (not shown) and pinned in place by pin 506 (and 508) as described above. This module in combination with the four degrees of freedom allows the wrist to orient and palpate.

The second module 600 (see Figs. 5.14 and 5.15) converts the rotary motion of the shaft 276 into a sliding motion of the probe 638 (probe PA) along the radius of the hemisphere created by the action of the pantographs 216 and 218 to provide a wrist with three degrees of freedom. This module 600 has housing 640 in which the inner elements of the module 600 are contained.

A drive shaft or ball-screw 634 of this module 600 is coupled to the shaft 276 via a self aligning coupling 602 (see Fig. 5.15) similar to the coupling 502 described above) and rotation of the ball-screw shaft 634, tends to rotate nut 637, which is connected rigidly to slider 642 and which in turn is connected via extension 644 to the probing device 638 forming the end point PA. Slider 642 is restrained from rotation by the linear guides 636 (two shown) connected to the slider 642 by sets of linear ball bushings (not shown) that permit relative axial movement between the guides 636 and the slider 642. Therefore, rotation of the ball-screw shaft 634 causes the nut 637 and slider 642 moves along the ball-screw 634.

The linear guides 536 are rigidly connected to plates 635 and 639, which are in turn fixed to the housing 640. The housing 640 is connected to sleeve 260 by coupling pin 604. This module does not receive any motion from pulley 322.In combination with the first three degrees of freedom, this module is able to perform the palpation action and reports on all arising forces from palpation.

Fig. 5.16 schematically indicates the action of the wrist 10A. As illustrated the angle θ_1 and θ_2 (which are essentially equivalent to the angles β_1 and β_2 of the embodiment of Figs. 4.1 to 4.10) between the datum centerline CL_1 for the moveable section MPA and the actual central or main axis 212 at the center of movement FCM measured in the planes relative to the x and y axes respectively in the same manner as angles β_1 and β_2.

These angles θ_1 and θ_2 are determined by the action of the two pantographs 216 and 218 in the same manner as the pantographs 16 and 18 determined the angles β_1 and β_2 as described in chapter 4 for the hand-controller. The end point PA may be moved by the pantographs 216 and 218 in two mutually perpendicular directions as indicated by the arrows 700 and 702 and depending on the module used i.e. module 500 or 600 may be moved both axially as indicated by the arrow 704 and rotated around the axis 212 as indicated by the arrow 706 when the module 500 is used or when the module 600 is used there is no movement as schematically indicated by the arrow 706.

The device 10A may be set so that axial travel of the probe PA along the axis 212 between the points A and B as indicated by the dimension D may set so that one extremity of travel point A is on one side of the center FCM and the opposite extremity point B is on the opposite side of center FCM along the axis 212. It will be apparent that movement of the end point PA moves on a hemisphere based on the position of the end point PA relative to the point FCM and will have having a radius measure along axis 212 from point PA to the point FCM. When the point PA is to the left of the point FCM in Fig 5.16 the point PA moves in a convex pattern, but when PA is on the opposite side of the point FCM it moves in a concave pattern when the pantographs 216 and 218 are manipulated.

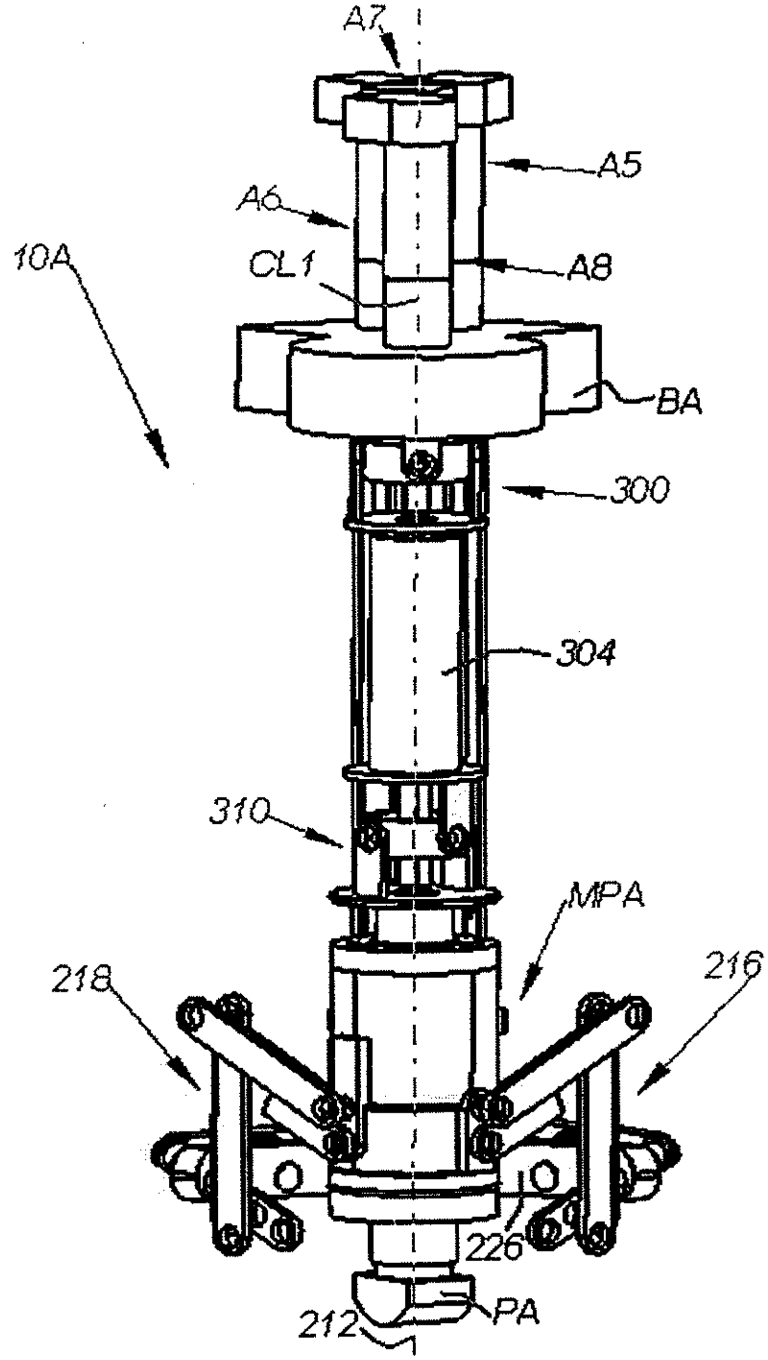

Fig. 5.1: General view of the wrist.

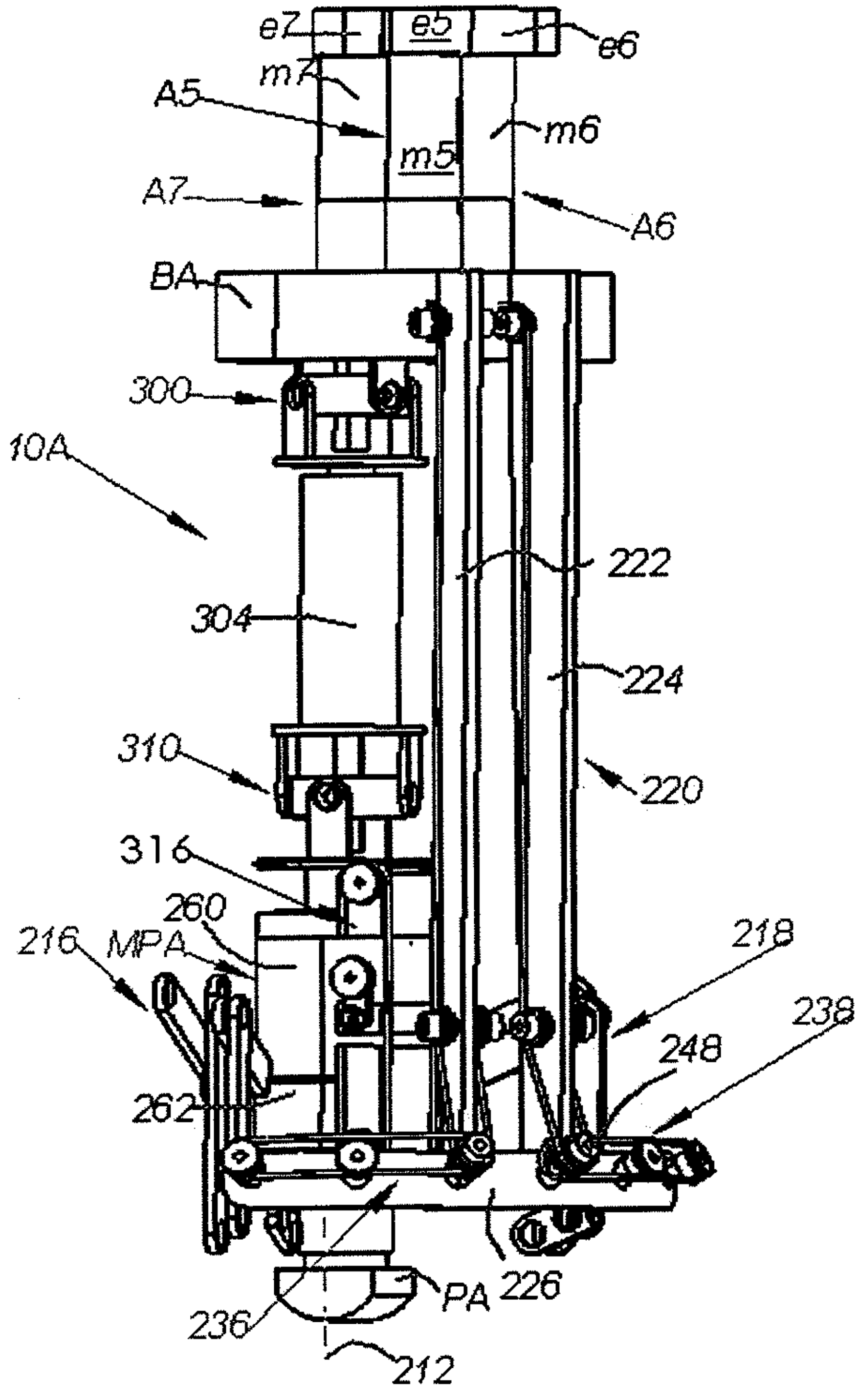

Fig. 5.2: General side elevation view of wrist.

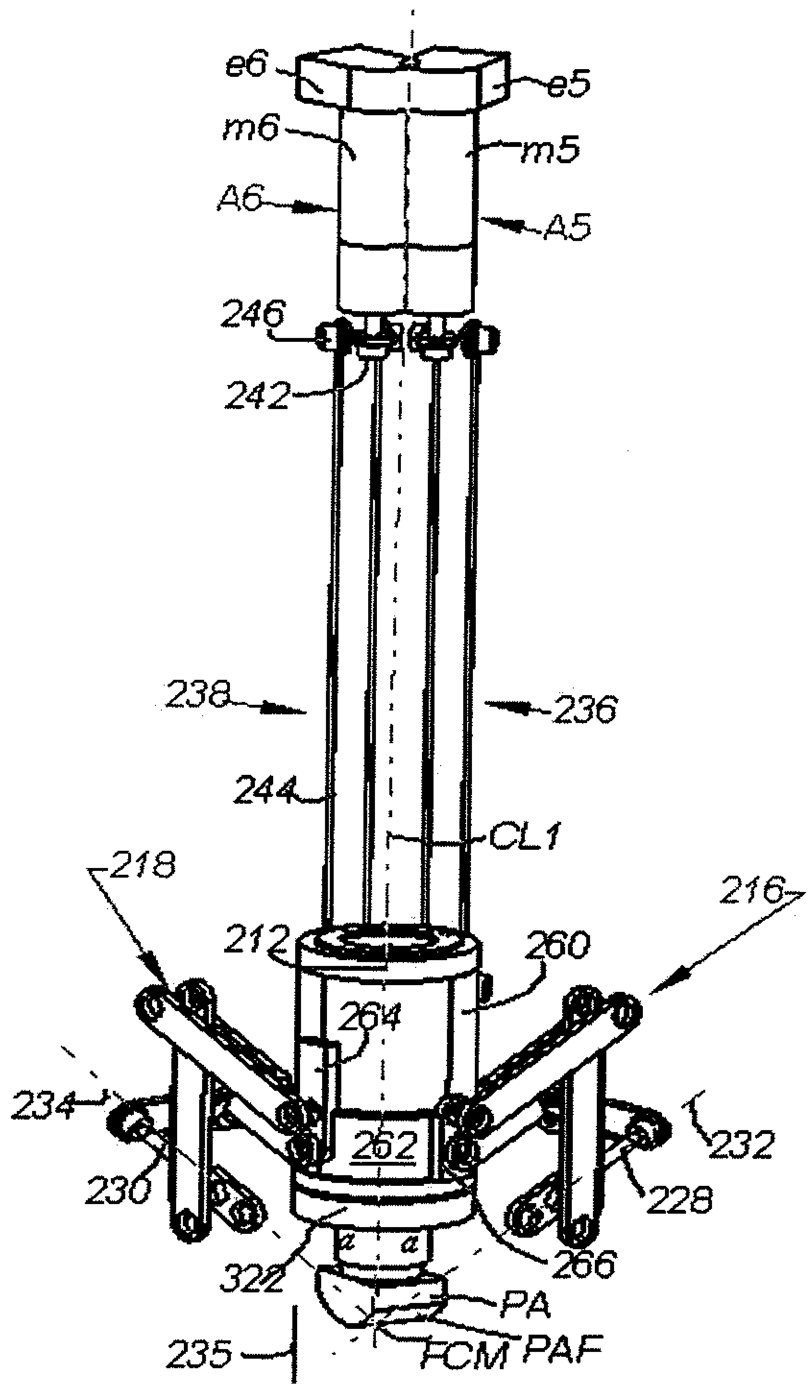

Fig. 5.3: The location of the center point of the device.

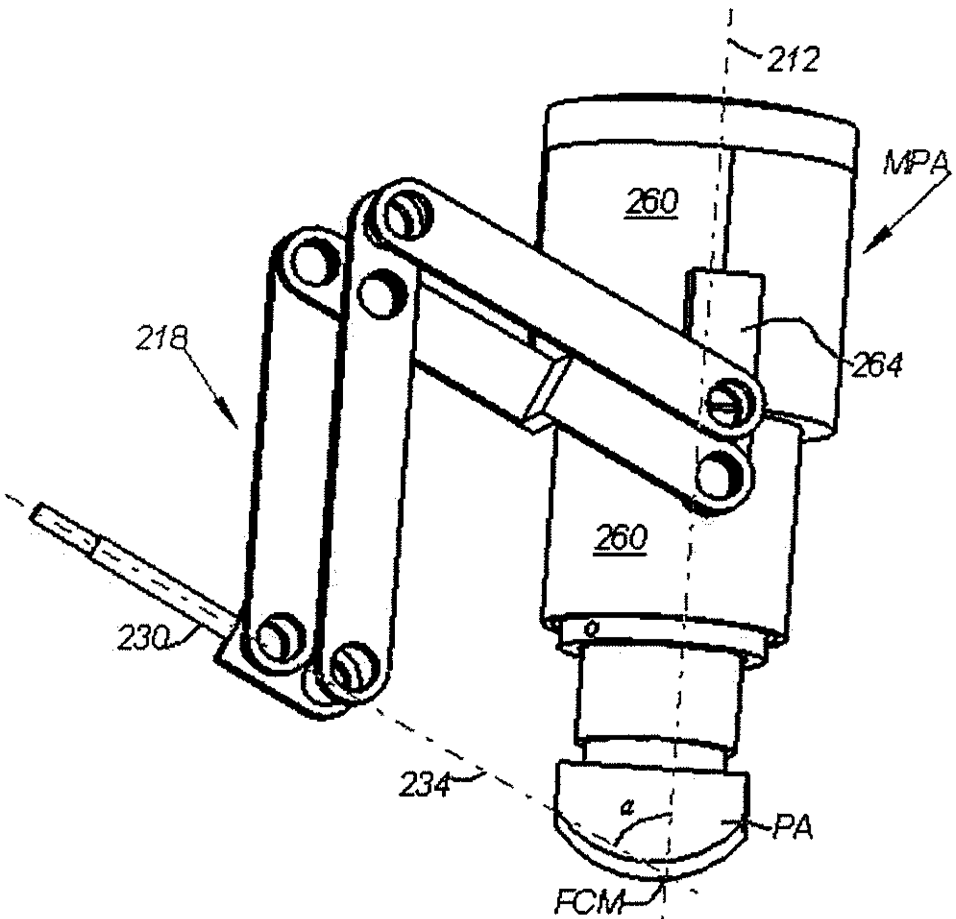

Fig. 5.4: Detail of one pantograph for the first or second degree of freedom.

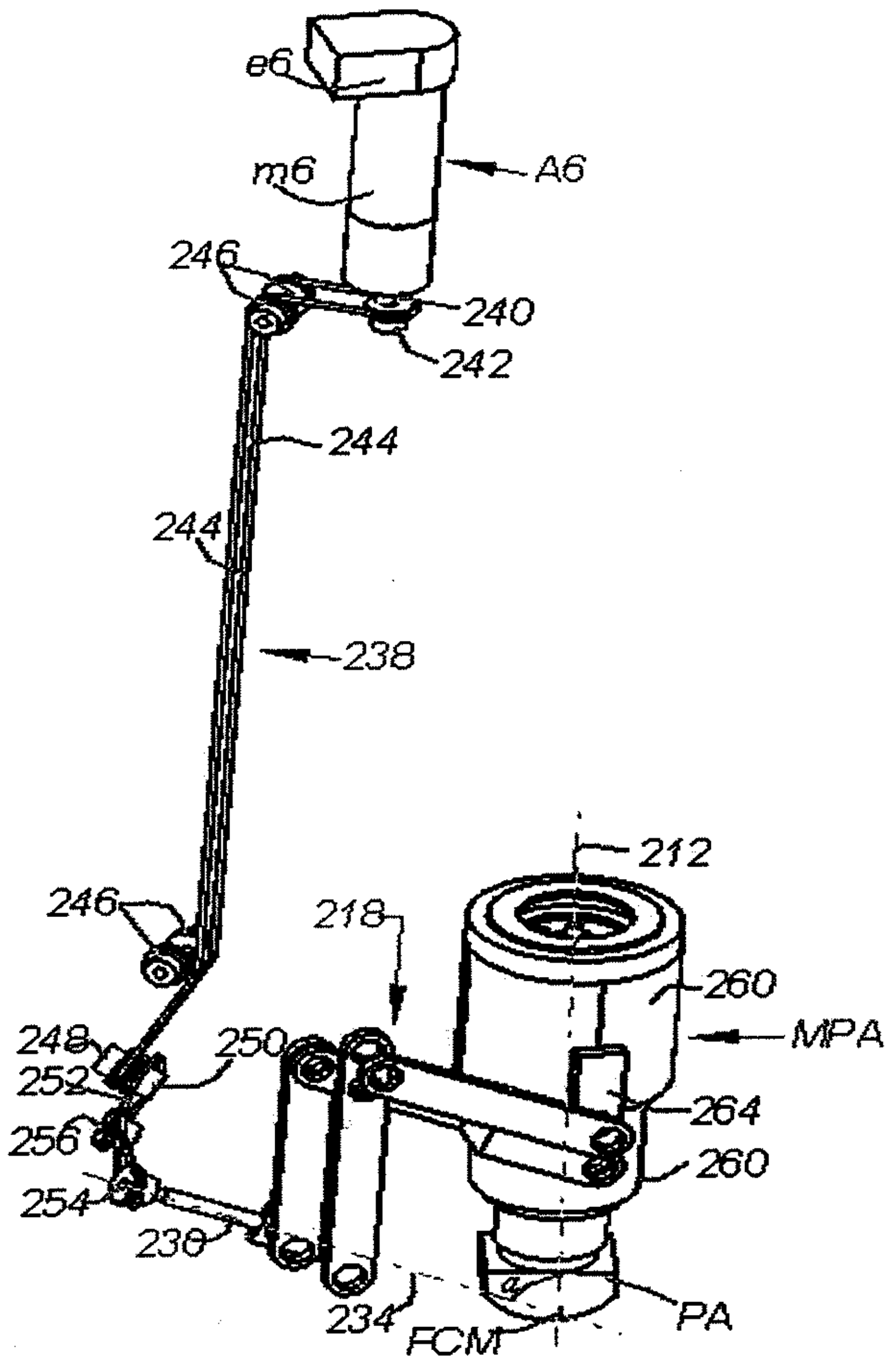

Fig. 5.5: Cable drive arrangement for the pantographs.

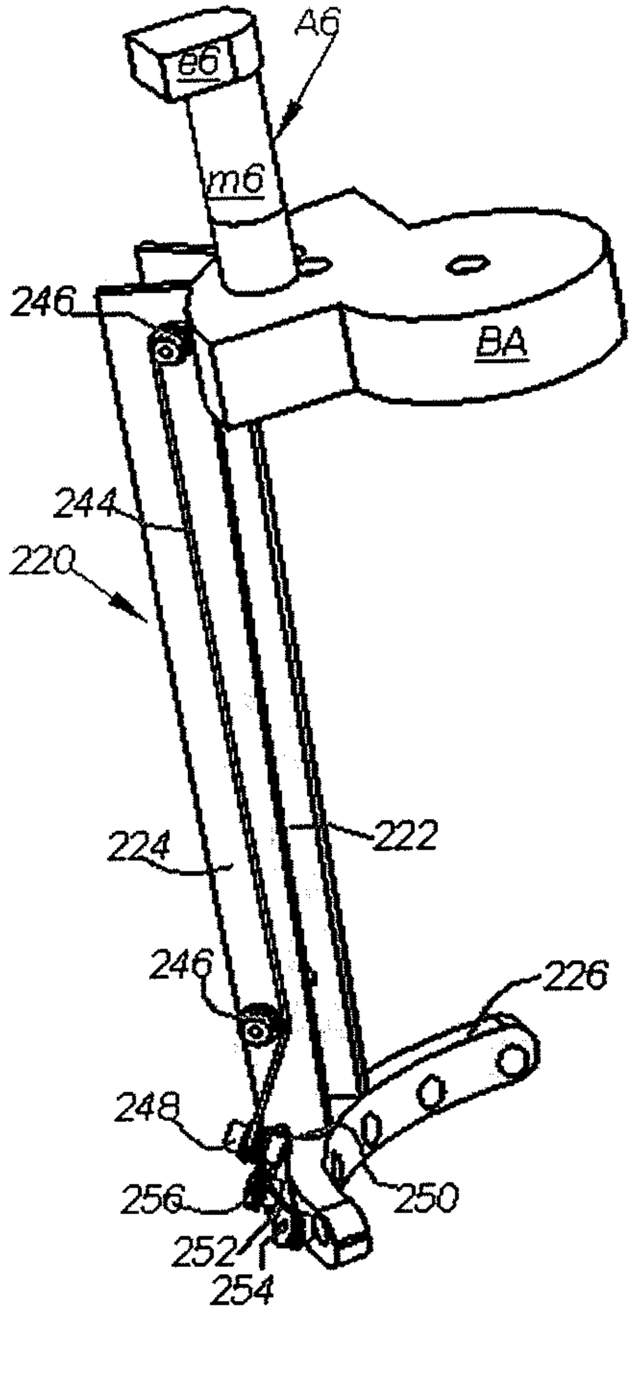

Fig. 5.6: Support arrangement for the actuators, cable drives and pantographs.

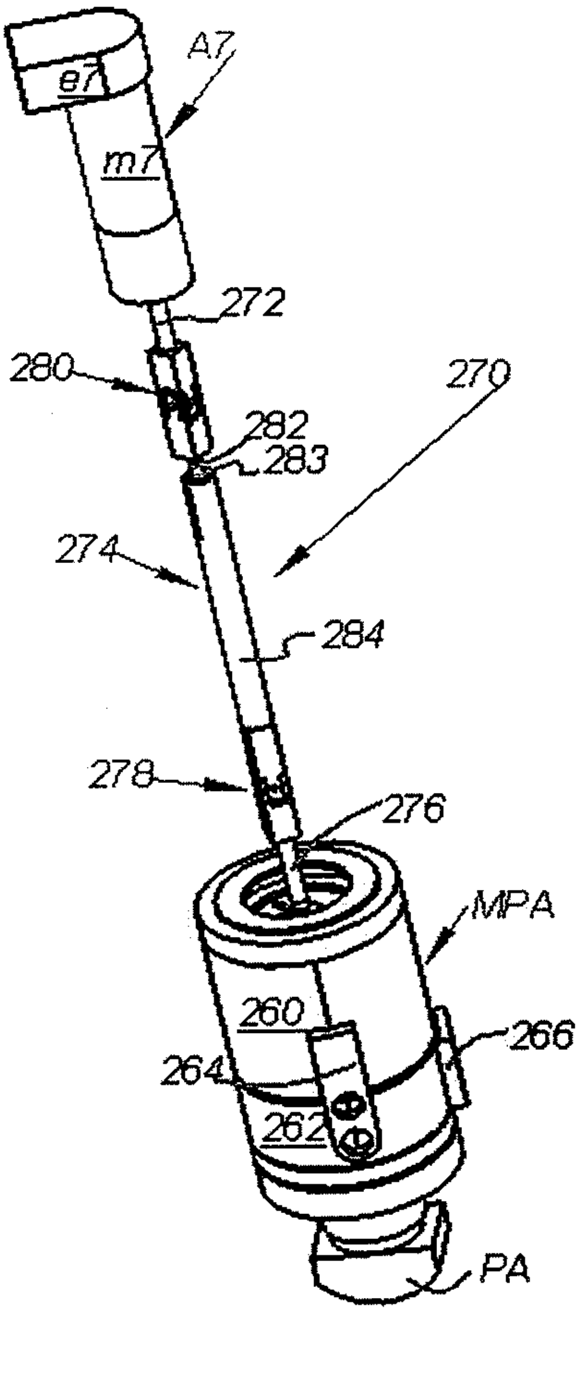

Fig. 5.7: The power train for the third degree of freedom.

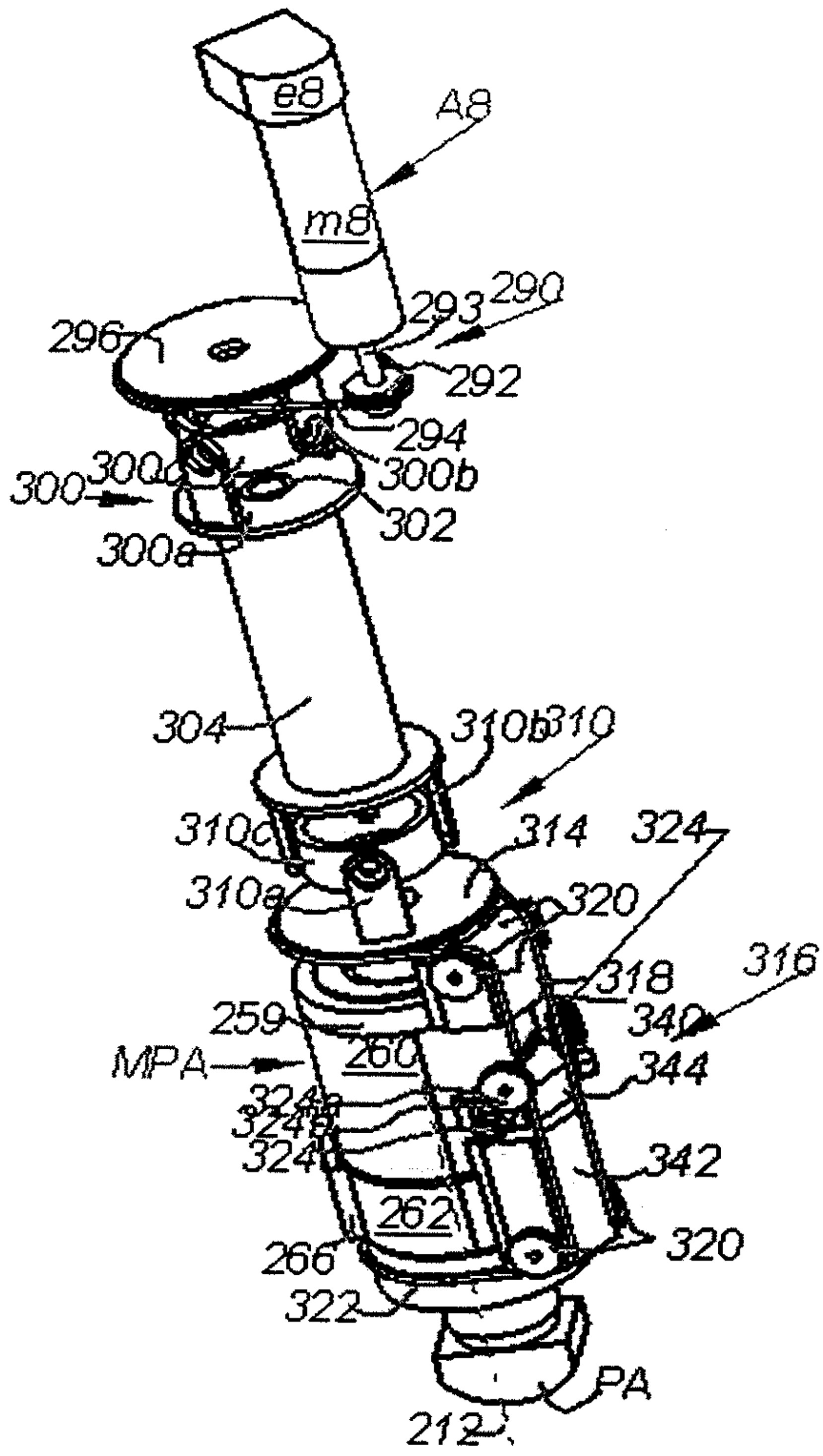

Fig. 5.8: The power train for the fourth degree of freedom.

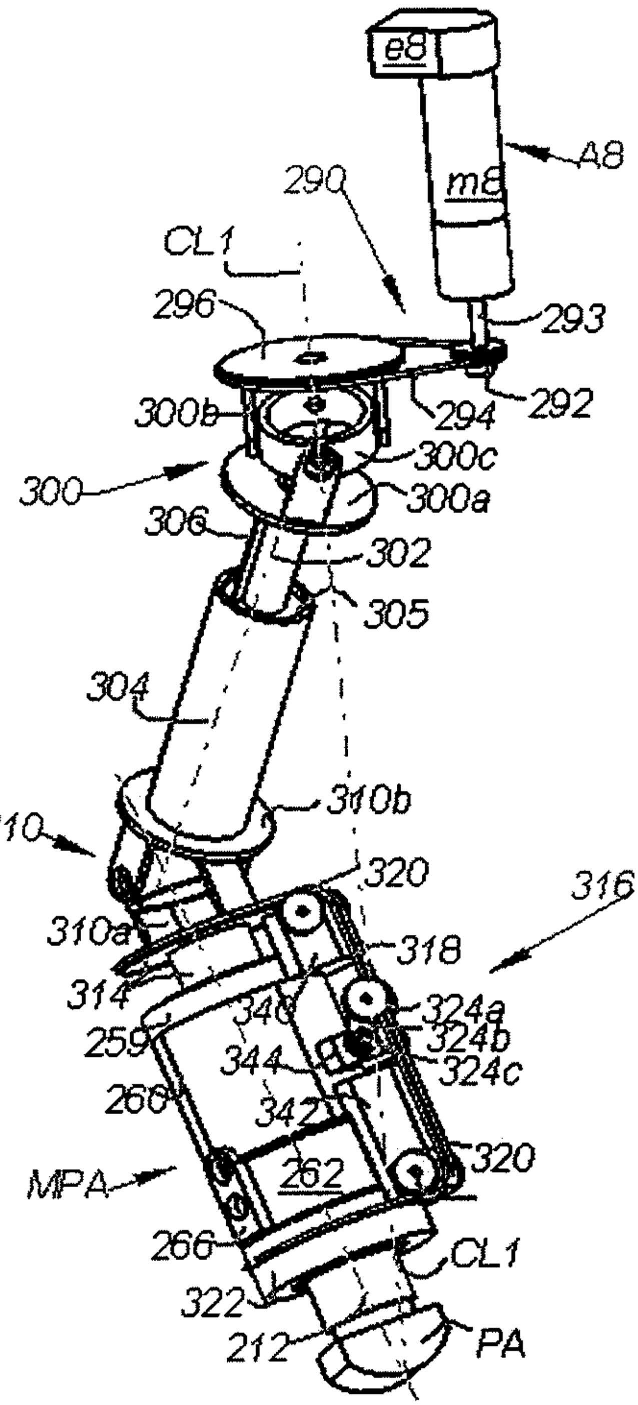

Fig. 5.9: The fourth degree of freedom in a different position.

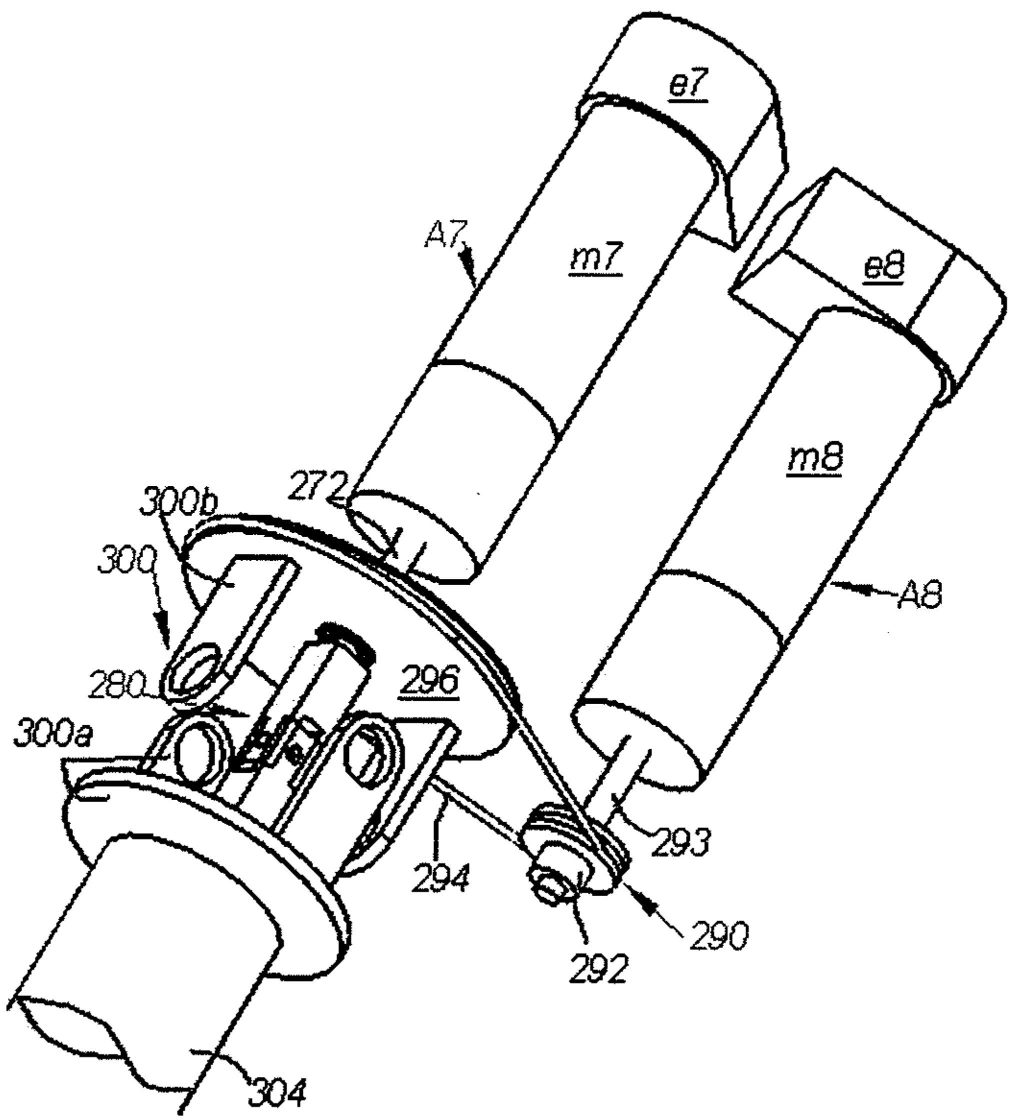

Fig. 5.10: The connection between the third and the fourth degrees of freedom.

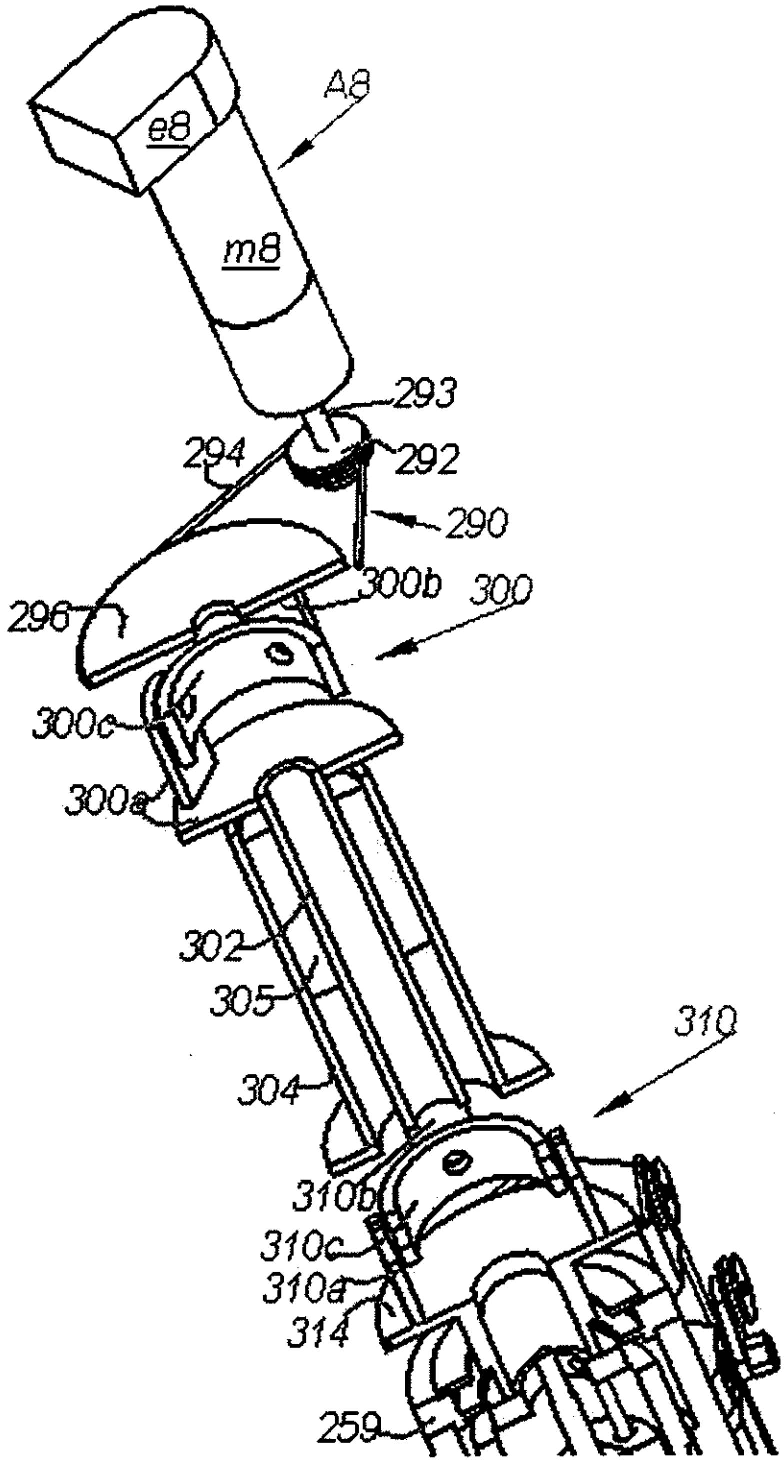

Fig. 5.11: Cross sectional view of the power train of the fourth degree of freedom.

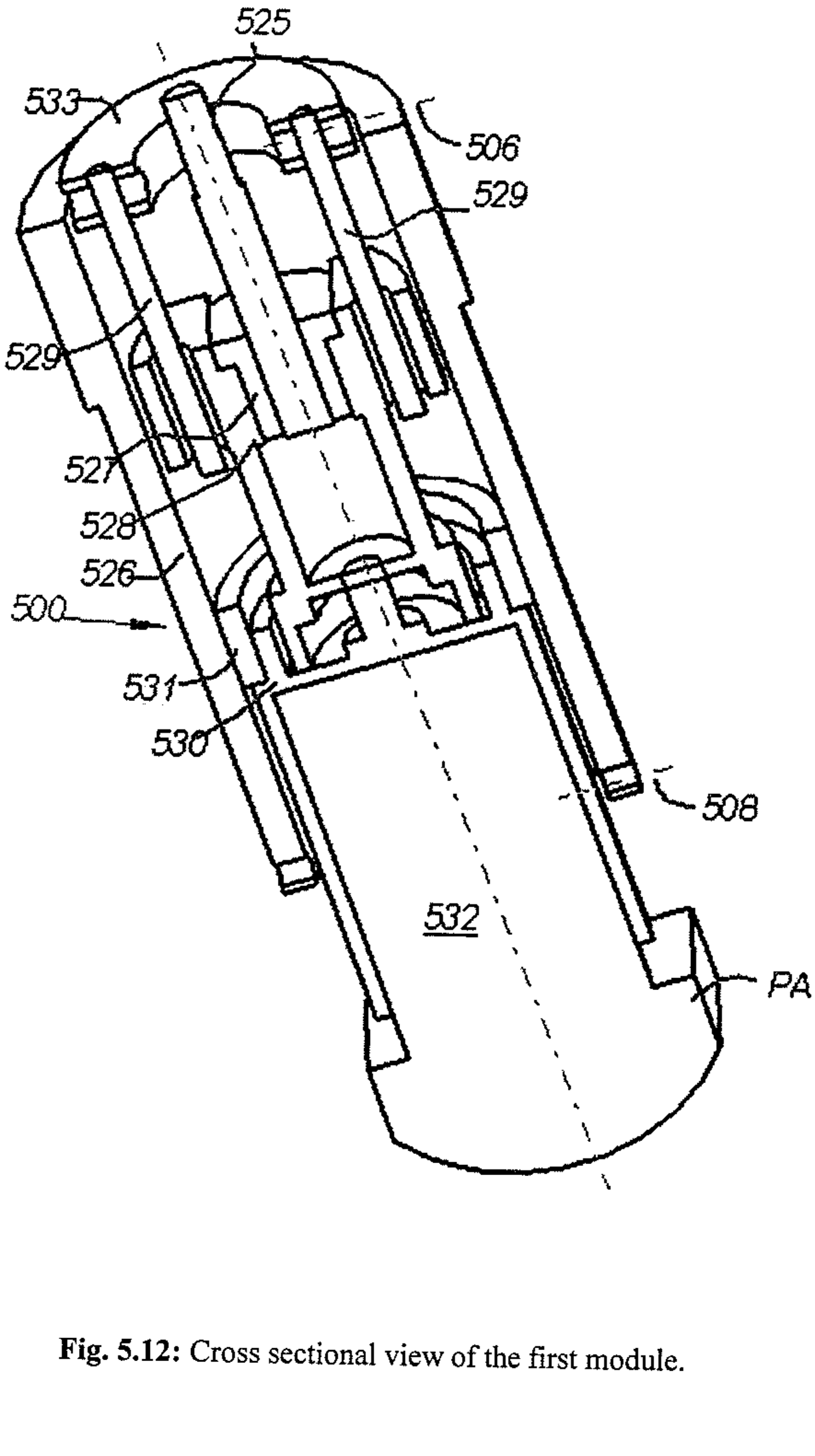

Fig. 5.12: Cross sectional view of the first module.

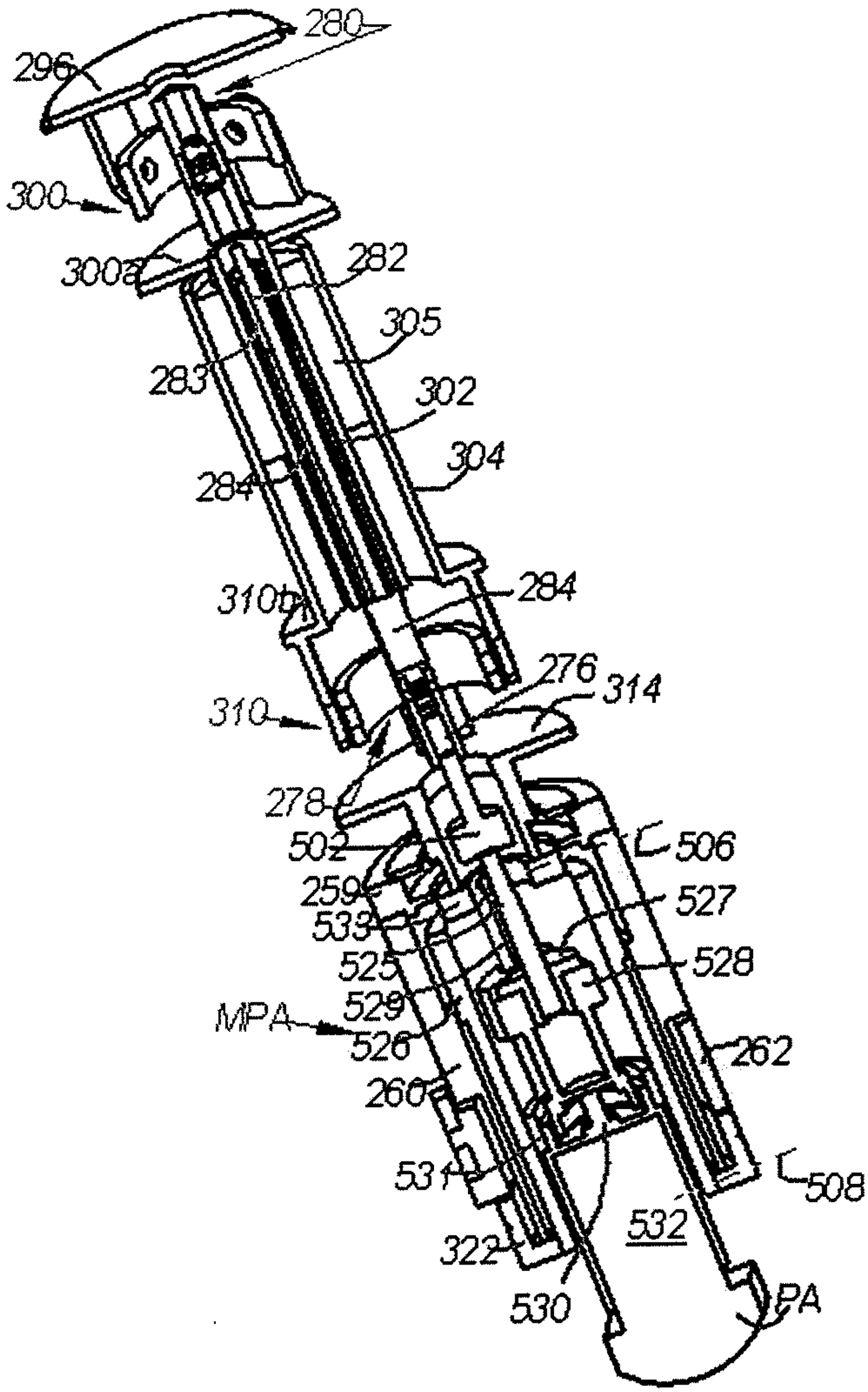

Fig. 13: Cross sectional view of the first module inside the wrist.

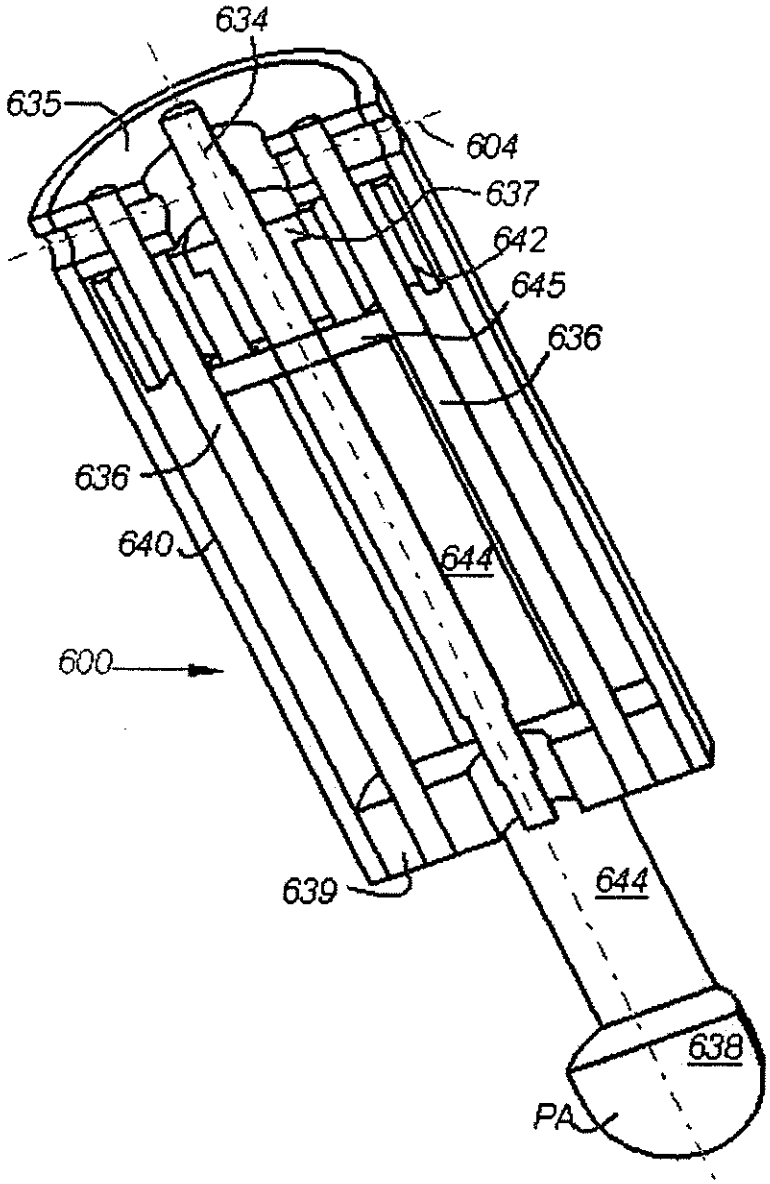

Fig. 5.14: Cross sectional view of the second module.

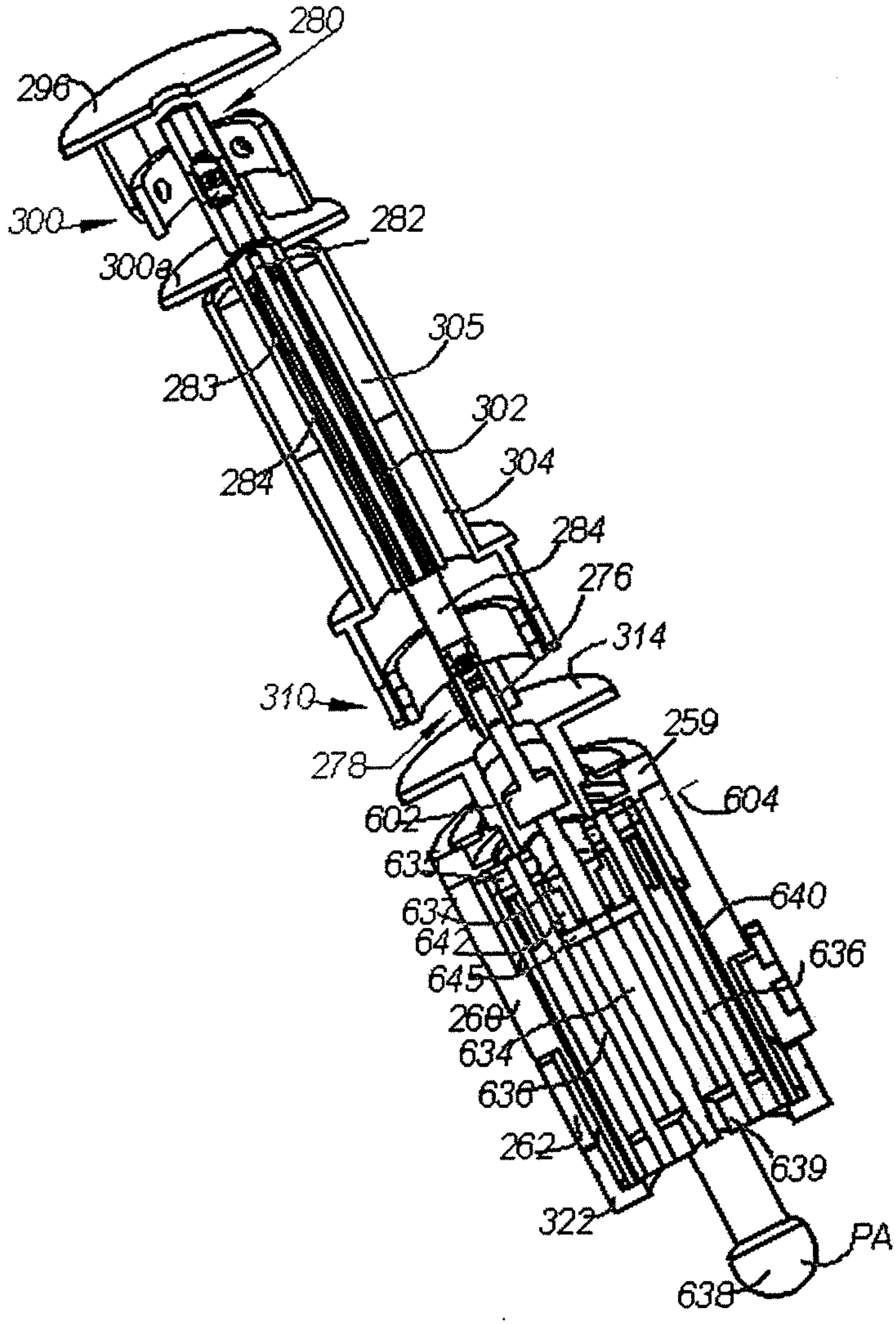

Fig. 5.15: Cross sectional view of the second module inside the wrist.

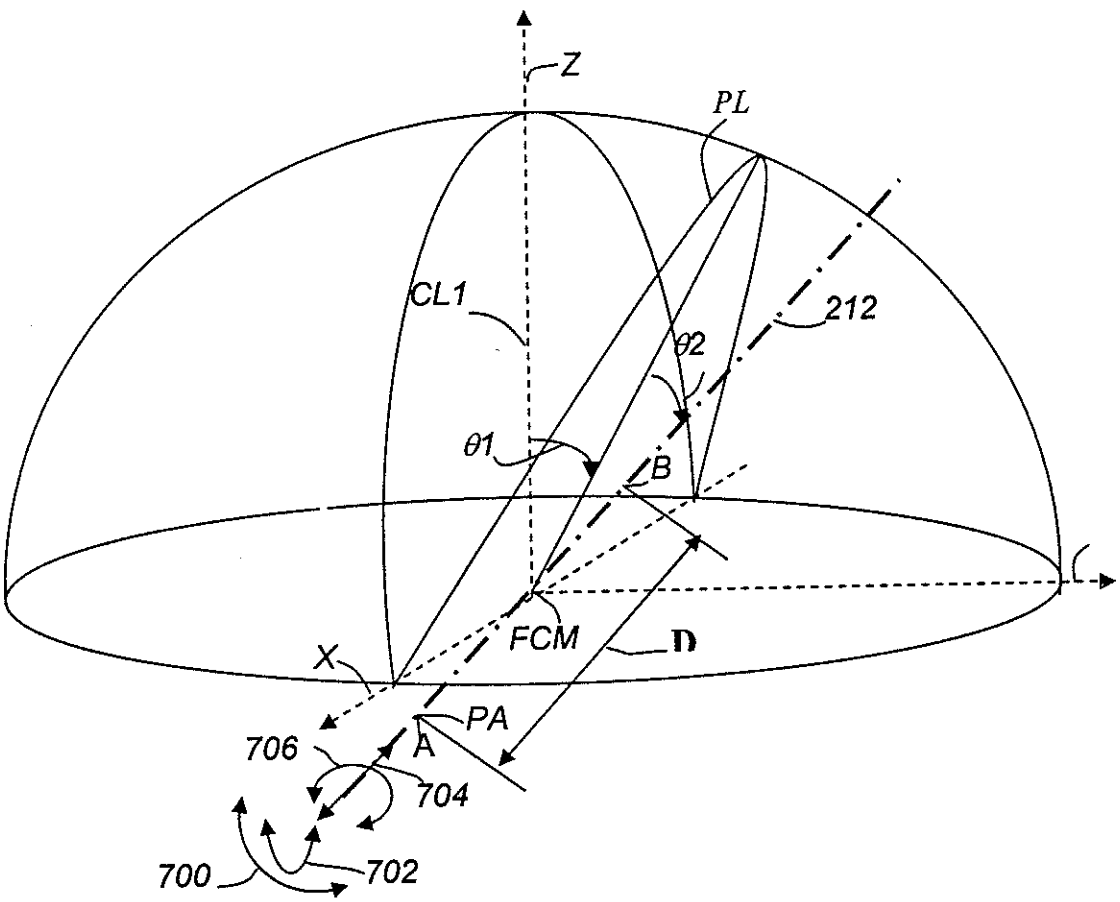

Fig. 5.16: The movements of the wrist's endpoint.

Chapter 6

Kinematic Analysis of the Proposed Design

This chapter develops the kinematic analysis of the hand-controller and wrist. Kinematic deals with the aspects of motion without regarding the forces and torques that cause it. As the hand-controller and wrist have the same kinematic configurations, we only develop one set of kinematic equations. Section 6.1 will develop the forward kinematic analysis based on the Danavit-Hartenberg method. Section 6.2 investigates the inverse kinematic solutions for all four degrees of freedom of the devices. Section 6.3 derives the Jacobian matrix. Section 6.4 uses inverse Jacobian analysis to investigate the existence of singular points for both the hand-controller and the wrist. Section 6.5 graphically shows different shape of workspaces for the hand-controller and the wrist.

6.1. Forward Kinematics

Since both hand-controller and wrist mechanism have similar kinematics configurations, therefore the kinematics equations for them are identical. Different methods such as homogenous transformations, geometric approach and Danavit-Hartenberg (D-H) methods have been proposed to solve the forward kinematic problem of parallel manipulators. Choosing a specific method depends mainly on the complexity of the kinematics configuration and number of degrees of freedom. D-H method is used here. The motions of the moving platform (end-effector) can be achieved by a four degree-of-freedom serial link manipulator, which has a similar kinematic chain as its original parallel one. Figure 6.1 shows structure of the equivalent manipulator with its assigned D-H coordinate systems. The first two degree-of-freedom are revolute joints, the third one is prismatic and the fourth one is revolute joint. In this configuration, all actuators are directly connected to their respective joints. The first two degrees of freedom comprise a universal joint with a fixed center point F, which is the intersection of the first two actuator's centerlines. Due to the kinematic symmetry between the pantographs in our manipulator, we derive the following equations based on the assumption that joint 1 is fixed to the ground and simulates the first pantograph's motion. In this case, joint 2 simulates the second pantograph's motion and idly follows joint 1. Similarly, we can derive the equations based on fixing joint 2 to the ground as pantograph 2. In this case, joint 1 simulates the first pantograph's motion and idly follows joint 2.

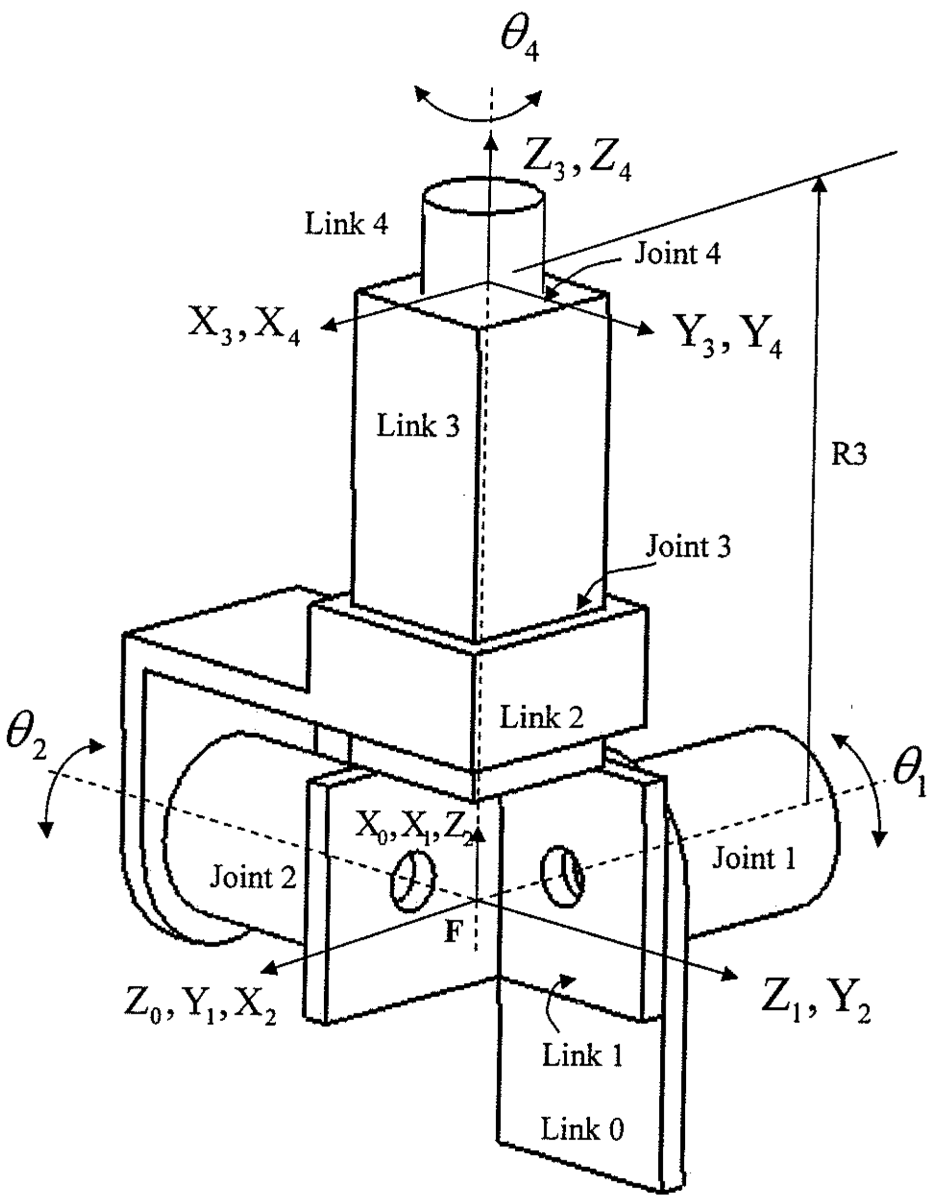

Fig. 6.1: Schematic diagram of serial manipulator in spherical coordinate system.

The procedure that is used for establishing Danavit-Hartenberg coordinate systems is summarized as follows. The links and joints are numbered sequentially. For the intersecting joints, it is recommended to assign the coordinate systems on the intersection point F (Tsai, 1999). Z_0 axis of the fixed coordinate system is aligned with the joint axis 1 and X_0 is perpendicular to Z_0 axis. Z_1 is aligned to the joint axis 2 and X_1 is in the direction of vector cross product of Z_0 and Z_1. Z_2 axis is aligned with the prismatic joint axis 3. Z_4 axis is aligned with Z_3. All Y axes are determined according to the right hand rule.

With reference to Fig. 6.1, the joint variables are θ_1, θ_2, R_3 and θ_4. θ_1 is the angle required to rotate the X_{i-1} axis into alignment with the X_i axis about the positive Z_{i-1} axis according to the right hand rule. Unlike revolute joints, the location of the prismatic joint coordinate system has no effect on relative displacement. Therefore R_3 or in general d_i is the only translational distance between the second and third coordinate systems.

The offset distance between two adjacent joint axes, Z_{i-1} and Z_i , is a_i. α_i is the twist angle between two adjacent joint axes. For the coordinate systems assigned in the Fig. 6.1, the D-H parameters are listed in Table 6.1.

Table 6.1: D-H parameters of the manipulator.

Joint	α_i (deg)	a_i	d_i	θ_i (deg)
1	90	0	0	θ_1
2	90	0	0	$90+\theta_2$
3	0	0	R_3	0
4	0	0	0	θ_4

The general D-H transformation matrix is.

$$ {}^{i-1}A_i = \begin{pmatrix} C\theta_i & -C\alpha_i S\theta_i & S\alpha_i S\theta_i & a_i C\theta_i \\ S\theta_i & C\alpha_i C\theta_i & -S\alpha_i C\theta_i & a_i S\theta_i \\ 0 & S\alpha_i & C\alpha_i & d_i \\ 0 & 0 & 0 & 1 \end{pmatrix} \quad (6.1) $$

The trailing subscript *i* and the leading superscript *i-1*denote that transformation takes place from the $(i\text{-}1)^{th}$ coordinate system to the i^{th} coordinate system. According to D-H parameters (see Table 6.1), the D-H transformation for the manipulator is as follows:

$$ {}^{0}A_1 = \begin{pmatrix} C\theta_1 & 0 & S\theta_1 & 0 \\ S\theta_1 & 0 & -C\theta_1 & 0 \\ 0 & 1 & 0 & 0 \\ 0 & 0 & 0 & 1 \end{pmatrix} \quad (6.2) \qquad {}^{1}A_2 = \begin{pmatrix} -S\theta_2 & 0 & C\theta_2 & 0 \\ C\theta_2 & 0 & S\theta_2 & 0 \\ 0 & 1 & 0 & 0 \\ 0 & 0 & 0 & 1 \end{pmatrix} \quad (6.3) $$

$$ {}^{2}A_3 = \begin{pmatrix} 1 & 0 & 0 & 0 \\ 0 & 1 & 0 & 0 \\ 0 & 0 & 1 & R_3 \\ 0 & 0 & 0 & 0 \end{pmatrix} \quad (6.4) \qquad {}^{3}A_4 = \begin{pmatrix} C\theta_4 & -S\theta_4 & 0 & 0 \\ S\theta_4 & C\theta_4 & 0 & 0 \\ 0 & 0 & 1 & 0 \\ 0 & 0 & 0 & 1 \end{pmatrix} \quad (6.5) $$

In forward kinematics, the joint variables are given and the problem is to find where the end-effector or moving platform is with respect to the base coordinate system. By substituting (6.2), (6.3), (6.4) and (6.5) into (6.8), the D-H matrix for our manipulator is as follow:

$$ {}^{0}A_1\,{}^{1}A_2\,{}^{2}A_3\,{}^{3}A_4 = {}^{0}A_4 = \begin{pmatrix} -C\theta_1 S\theta_2 C\theta_4 + S\theta_1 S\theta_4 & C\theta_1 S\theta_2 S\theta_4 + S\theta_1 C\theta_4 & C\theta_1 C\theta_2 & R_3 C\theta_1 C\theta_2 \\ -S\theta_1 S\theta_2 C\theta_4 - C\theta_1 S\theta_4 & S\theta_1 S\theta_2 S\theta_4 - C\theta_1 C\theta_4 & S\theta_1 C\theta_2 & R_3 S\theta_1 C\theta_2 \\ C\theta_2 C\theta_4 & -C\theta_2 S\theta_4 & S\theta_2 & R_3 S\theta_2 \\ 0 & 0 & 0 & 1 \end{pmatrix} $$

(6.6)

Any point such as ${}^{4}P = \begin{bmatrix} p_x & p_y & p_z & 1 \end{bmatrix}^T$ in the end-effector coordinate (X_4, Y_4, Z_4) can be found in the base coordinate (X_0, Y_0, Z_0) according to ${}^{0}P_4 = {}^{0}A_4 . {}^{4}P$.

6.2. Inverse kinematics

In the study of the inverse kinematics, the end-effector or moving platform (i.e., ${}^{0}A_{n}$)is known and the problem is to find the joint variables needed to bring the end-effector to the desired position and orientation. Loop-closure Equation (6.6) can be applied to solve the inverse kinematic problem. By pre-or post multiplying the loop closure equation by the inverse matrix ${}^{i-1}A_{i}$ one can obtain alternative loop-closure Equations.

The inverse matrixes are as follows:

$$({}^{0}A_{1})^{-1} = \begin{pmatrix} C\theta_1 & S\theta_1 & 0 & 0 \\ 0 & 0 & 1 & 0 \\ S\theta_1 & -C\theta_1 & 0 & 0 \\ 0 & 0 & 0 & 1 \end{pmatrix} \quad (6.7) \qquad ({}^{1}A_{2})^{-1} = \begin{pmatrix} -S\theta_2 & C\theta_2 & 0 & 0 \\ 0 & 0 & 1 & 0 \\ C\theta_2 & S\theta_2 & 0 & 0 \\ 0 & 0 & 0 & 1 \end{pmatrix} \quad (6.8)$$

$$({}^{2}A_{3})^{-1} = \begin{pmatrix} 1 & 0 & 0 & 0 \\ 0 & 1 & 0 & 0 \\ 0 & 0 & 1 & -R_3 \\ 0 & 0 & 0 & 1 \end{pmatrix} \quad (6.9) \qquad ({}^{3}A_{4})^{-1} = \begin{pmatrix} C\theta_4 & S\theta_4 & 0 & 0 \\ -S\theta_4 & C\theta_4 & 0 & 0 \\ 0 & 0 & 1 & 0 \\ 0 & 0 & 0 & 1 \end{pmatrix} \quad (6.10)$$

By equating the general form of the D-H matrix (${}^{0}A_{4}$) to a given D-H martix, we have:

$${}^{0}A_{4} = \begin{pmatrix} n_x & o_x & a_x & p_x \\ n_y & o_y & a_y & p_y \\ n_z & o_z & a_z & p_z \\ 0 & 0 & 0 & 1 \end{pmatrix} \quad (6.11)$$

By pre-multiplying Equation (6.6) at $({}^{0}A_{1})^{-1}$, one can obtain:

$$\begin{pmatrix} n_xC\theta_1 + n_yS\theta_1 & o_xC\theta_1 + o_yS\theta_1 & a_xC\theta_1 + a_yS\theta_1 & p_xC\theta_1 + p_yS\theta_1 \\ n_z & o_z & a_z & p_z \\ n_xS\theta_1 - n_yC\theta_1 & o_xS\theta_1 - o_yC\theta_1 & a_xS\theta_1 - a_yC\theta_1 & p_xS\theta_1 - p_yC\theta_1 \\ 0 & 0 & 0 & 1 \end{pmatrix}$$
$$= \begin{pmatrix} -S\theta_2C\theta_4 & S\theta_2S\theta_4 & C\theta_2 & R_3C\theta_2 \\ C\theta_2C\theta_4 & -C\theta_2S\theta_4 & S\theta_2 & R_3S\theta_2 \\ S\theta_4 & C\theta_4 & 0 & 0 \\ 0 & 0 & 0 & 1 \end{pmatrix} \quad (6.12)$$

By equating matrix elements (3,4) on both side of Equation (6.12), we have,

$$p_x S\theta_1 - p_y C\theta_1 = 0 \tag{6.13}$$

A solution for θ_1 is found immediately by solving Equation (6.13),

$$\theta_1 = \tan^{-1}(\frac{p_y}{p_x}) \quad (-\pi/2 \le \theta_1 \le \pi/2) \tag{6.14}$$

By equating matrix elements (1,4) and (2,4) on both side of Equation (6.12), we have,

$$p_x C\theta_1 + p_y S\theta_1 = R_3 C\theta_2 \tag{6.15}$$

$$p_z = R_3 S\theta_2 \tag{6.16}$$

A solution for θ_2 is found by solving Equations (6.15) and (6.16) at the same time.

$$\theta_2 = \frac{p_z}{p_x C\theta_1 + p_y S\theta_1} \quad (-\pi/2 \le \theta_1 \le \pi/2) \tag{6.17}$$

$$R_3 = \frac{p_z}{S\theta_2}. \tag{6.18}$$

By equating matrix elements (3,1) and (3,2) on both sides of Equation of (6.21), we have:

$$C\theta_2 C\theta_4 = n_z \tag{6.19}$$

$$-C\theta_2 S\theta_4 = o_x \tag{6.20}$$

A solution for θ_4 can be found by solving Equations (6.19) and (6.20) at the same time,

$$\theta_4 = \tan^{-1}(-\frac{o_x}{n_z}) \quad (-\pi/2 \le \theta_4 \le \pi/2) \tag{6.21}$$

6.3. Jacobian

In many applications, it is necessary to move the end-effector of a manipulator along some desired paths with a prescribed speed. In the direct velocity problem, the input joint rate s are given and the objective is to find the velocity state of the end-effector or moving platform. For the inverse velocity problem, the velocity state of the moving platform is given and the input joint rates are to be found.

6.3.1. Direct velocity

The Jacobian matrix, (J), is a linear transformation matrix that maps an n-dimensional velocity vector $\dot{q}$ into a m-dimensional velocity vector $\dot{X}$, according to $\dot{X} = J\dot{q}$. For manipulators, the Jacobian matrix or simply Jacobian, is defined as the matrix that transforms the joint rates in the actuator space to the velocity state in the end-effector space.

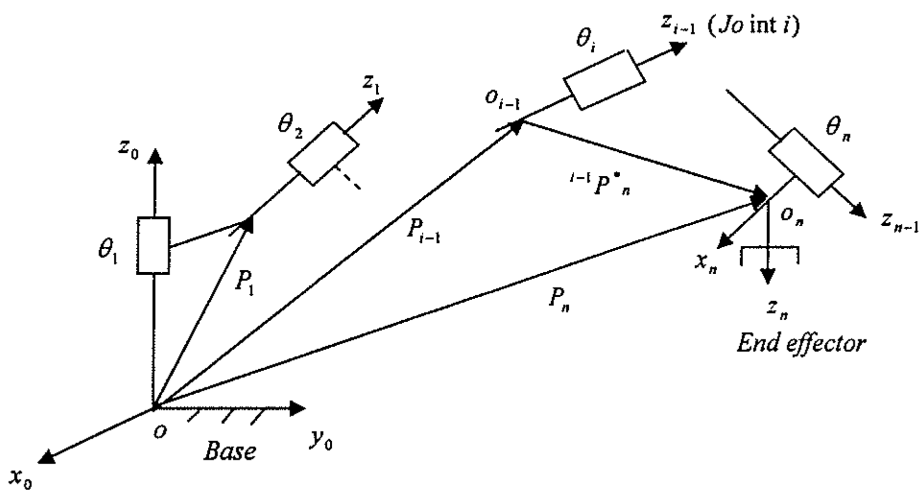

Fig. 6.2: Link parameter of a serial manipulator (Tsai, 1999).

Figure 6.2 shows a schematic of a typical serial manipulator. The velocity of the end-effector can be expressed in terms of the joint rates as follows:

$$V_n = \sum_{i=1}^{n} \left[\dot{\theta}_n (z_{i-1} \times {}^{i-1}P_n^{*}) + z_{i-1}\dot{d}_i\right] \qquad (6.22)$$

$$\omega_n = \sum \dot{\theta}_i z_{i-1} \qquad (6.23)$$

where $\dot{\theta}_i$ and $\dot{d}_i$ are the rate of rotation about and translation along the i^{th} joint axis, z_{i-1} is unit vector along the i^{th} joint axis. P_n denotes the position vector of the origin of the end-effector frame, and P_{i-1} denotes the position vector of the origin of the $(i-1)^{th}$ frame relative to the fixed frame. Further, ${}^{i-1}P_n^*$ denotes the vector pointing from o_{i-1} to o_n and is expressed in the fixed frame. According to Jacobian definition, we have

$$\dot{X} = \begin{pmatrix} v_n \\ \omega_n \end{pmatrix} = J\dot{q} \qquad (6.24)$$

where

$$J = (J_1, \quad J_2, \quad \ldots, \quad J_n) \qquad (6.25)$$

$$J_i = \begin{pmatrix} Z_{i-1} \times {}^{i-1}P_n^* \\ Z_{i-1} \end{pmatrix} \quad \text{(revolute joint)} \qquad (6.26)$$

$$J_i = \begin{pmatrix} Z_{i-1} \\ 0 \end{pmatrix} \quad \text{(prismatic joint)} \qquad (6.27)$$

$$Z_{i-1} = {}^0R_{i-1} \begin{pmatrix} 0 \\ 0 \\ 1 \end{pmatrix} \qquad (6.28)$$

$${}^{i-1}P^*{}_n = {}^0R_{i-1}\,{}^{i-1}r_i + {}^iP_n^* \qquad (6.29)$$

$${}^{i-1}r_i = \begin{pmatrix} a_i C\theta_i \\ a_i S\theta_i \\ d_i \end{pmatrix} \qquad (6.30)$$

${}^{i-1}r_i$ denotes the vector $o_{i-1}o_i$ expressed in the $(i-1)^{th}$ link frame. The left hand side of Equation (6.31) is a (6×1) vector composed of the elements of v_n and ω_n, while the right- hand side is a product of the Jacobian matrix and the vector of the joint rates. The vector of the joint rates consists of all the actuated joint rates, $\dot{q}_i$ where $i = 1,2,\ldots,n$. The i^{th} column of the Jacobian matrix, J_i, represents the effect of the i^{th} joint rate on the velocity state of the end-effector. We study the Jacobian of the four degrees of freedom manipulator by calculation of vectors z_{i-1} and ${}^{i-1}P_n^*$ based on Equations (6.28) and (6.29), for $i = 1,2,3,4$.

$$Z_{i-1} = {}^0R_{i-1}\begin{pmatrix}0\\0\\1\end{pmatrix} \tag{6.31}$$

$$Z_0 = {}^0R_0\begin{pmatrix}0\\0\\1\end{pmatrix} = \begin{pmatrix}1 & 1 & 1\\1 & 1 & 1\\1 & 1 & 1\end{pmatrix}\begin{pmatrix}0\\0\\1\end{pmatrix} = \begin{pmatrix}0\\0\\1\end{pmatrix} \tag{6.32}$$

$$Z_1 = {}^0R_1\begin{pmatrix}0\\0\\1\end{pmatrix} = \begin{pmatrix}C\theta_1 & 0 & S\theta_1\\S\theta_1 & 0 & -C\theta_1\\0 & 1 & 0\end{pmatrix}\begin{pmatrix}0\\0\\1\end{pmatrix} = \begin{pmatrix}S\theta_1\\-C\theta_1\\0\end{pmatrix} \tag{6.33}$$

$$Z_2 = {}^0R_2\begin{pmatrix}0\\0\\1\end{pmatrix} = {}^0R_1{}^1R_2\begin{pmatrix}0\\0\\1\end{pmatrix} = \begin{pmatrix}C\theta_1 & 0 & S\theta_1\\S\theta_1 & 0 & -C\theta_1\\0 & 1 & 0\end{pmatrix}\begin{pmatrix}-S\theta_2 & 0 & C\theta_2\\C\theta_2 & 0 & S\theta_2\\0 & 1 & 0\end{pmatrix}\begin{pmatrix}0\\0\\1\end{pmatrix} = \begin{pmatrix}C\theta_1C\theta_2\\S\theta_1C\theta_2\\S\theta_2\end{pmatrix} \tag{6.34}$$

$$Z_3 = {}^0R_3\begin{pmatrix}0\\0\\1\end{pmatrix} = {}^0R_1{}^1R_2{}^2R_3\begin{pmatrix}0\\0\\1\end{pmatrix} = \begin{pmatrix}C\theta_1 & 0 & S\theta_1\\S\theta_1 & 0 & -C\theta_1\\0 & 1 & 0\end{pmatrix}\begin{pmatrix}-S\theta_2 & 0 & C\theta_2\\C\theta_2 & 0 & S\theta_2\\0 & 1 & 0\end{pmatrix}\begin{pmatrix}1 & 0 & 0\\0 & 1 & 0\\0 & 0 & 1\end{pmatrix}\begin{pmatrix}0\\0\\1\end{pmatrix} = \begin{pmatrix}C\theta_1C\theta_2\\S\theta_1C\theta_2\\S\theta_2\end{pmatrix} \tag{6.35}$$

$${}^3P_4^* = {}^0R_3{}^3r_4 + {}^4P_4^* = \begin{pmatrix}-C\theta_1S\theta_2 & S\theta_1 & C\theta_1C\theta_2\\-S\theta_1S\theta_2 & -C\theta_1 & S\theta_1C\theta_2\\C\theta_2 & 0 & S\theta_2\end{pmatrix}\begin{pmatrix}0\\0\\0\end{pmatrix} + \begin{pmatrix}0\\0\\0\end{pmatrix} = \begin{pmatrix}0\\0\\0\end{pmatrix} \tag{6.36}$$

$${}^2P_4^* = {}^0R_2{}^2r_3 + {}^3P_4^* = \begin{pmatrix}-C\theta_1S\theta_2 & S\theta_1 & C\theta_1C\theta_2\\-S\theta_1S\theta_2 & -C\theta_1 & S\theta_1C\theta_2\\C\theta_2 & 0 & S\theta_2\end{pmatrix}\begin{pmatrix}0\\0\\R_3\end{pmatrix} + \begin{pmatrix}0\\0\\0\end{pmatrix} = \begin{pmatrix}R_3C\theta_1C\theta_2\\R_3S\theta_1C\theta_2\\R_3S\theta_2\end{pmatrix} \tag{6.37}$$

$$ {}^{1}P_4^* = {}^{0}R_1 {}^{1}r_2 + {}^{2}P_4^* = \begin{pmatrix} C\theta_1 & 0 & s\theta_1 \\ S\theta_1 & 0 & -C\theta_1 \\ 0 & 1 & 0 \end{pmatrix} \begin{pmatrix} 0 \\ 0 \\ 0 \end{pmatrix} + \begin{pmatrix} R_3 C\theta_1 C\theta_2 \\ R_3 S\theta_1 C\theta_2 \\ R_3 S\theta_2 \end{pmatrix} = \begin{pmatrix} R_3 C\theta_1 C\theta_2 \\ R_3 S\theta_1 C\theta_2 \\ R_3 S\theta_2 \end{pmatrix} \tag{6.38} $$

$$ {}^{0}P_4^* = {}^{0}R_0 {}^{0}r_1 + {}^{1}P_4^* = \begin{pmatrix} 1 & 0 & 0 \\ 0 & 1 & 0 \\ 0 & 0 & 1 \end{pmatrix} \begin{pmatrix} 0 \\ 0 \\ 0 \end{pmatrix} + \begin{pmatrix} R_3 C\theta_1 C\theta_2 \\ R_3 S\theta_1 C\theta_2 \\ R_3 S\theta_2 \end{pmatrix} = \begin{pmatrix} R_3 C\theta_1 C\theta_2 \\ R_3 S\theta_1 C\theta_2 \\ R_3 S\theta_2 \end{pmatrix} \tag{6.39} $$

Substituting the expressions above into Equations (6.26) and (6.27), we obtain

$$ J_1 = \begin{pmatrix} -R_3 S\theta_1 C\theta_2 & R_3 C\theta_1 C\theta_2 & 0 & 0 & 0 & 1 \end{pmatrix}^T \tag{6.40} $$

$$ J_2 = \begin{pmatrix} -R_3 C\theta_1 S\theta_2 & -R_3 S\theta_1 S\theta_2 & R_3 C\theta_2 & S\theta_1 & -C\theta_1 & 0 \end{pmatrix} \tag{6.41} $$

$$ J_3 = \begin{pmatrix} C\theta_1 C\theta_2 & S\theta_1 C\theta_2 & S\theta_2 & 0 & 0 & 0 \end{pmatrix}^T \tag{6.42} $$

$$ J_4 = \begin{pmatrix} 0 & 0 & 0 & C\theta_1 S\theta_2 & S\theta_1 S\theta_2 & -C\theta_2 \end{pmatrix} \tag{6.43} $$

or

$$ \begin{pmatrix} \dot{x} \\ \dot{y} \\ \dot{z} \\ \omega_x \\ \omega_y \\ \omega_z \end{pmatrix} = \begin{pmatrix} -R_3 S\theta_1 C\theta_2 & -R_3 C\theta_1 S\theta_2 & C\theta_1 C\theta_2 & 0 \\ R_3 C\theta_1 C\theta_2 & -R_3 S\theta_1 S\theta_2 & S\theta_1 C\theta_2 & 0 \\ 0 & R_3 C\theta_2 & S\theta_2 & 0 \\ 0 & S\theta_1 & 0 & C\theta_1 C\theta_2 \\ 0 & -C\theta_1 & 0 & S\theta_1 C\theta_2 \\ 1 & 0 & 0 & S\theta_2 \end{pmatrix} \begin{pmatrix} \dot{\theta}_1 \\ \dot{\theta}_2 \\ \dot{R}_3 \\ \dot{\theta}_4 \end{pmatrix} \tag{6.44} $$

Thus,

$$ \dot{x} = -R_3 S\theta_1 C\theta_2 \dot{\theta}_1 - R_3 C\theta_1 S\theta_2 \dot{\theta}_2 + C\theta_1 C\theta_2 \dot{R}_3 \tag{6.45} $$

$$ \dot{y} = R_3 C\theta_1 C\theta_2 \dot{\theta}_1 - R_3 S\theta_1 S\theta_2 \dot{\theta}_2 + S\theta_1 C\theta_2 \dot{R}_3 \tag{6.46} $$

$$ \dot{z} = R_3 C\theta_2 \dot{\theta}_2 + S\theta_2 \dot{R}_3 \tag{6.47} $$

$$ \omega_x = S\theta_1 \dot{\theta}_2 + C\theta_1 C\theta_2 \dot{\theta}_4 \tag{6.48} $$

$$ \omega_y = -C\theta_1 \dot{\theta}_2 + S\theta_1 S\theta_2 \dot{\theta}_4 \tag{6.49} $$

$$ \omega_z = \dot{\theta}_1 - S\theta_2 \dot{\theta}_4 \tag{6.50} $$

The Equation (6.44) is simulated with constant average velocities (see Chapter 2) over the theoretical workspace of each degree of freedom within 60 Seconds. The range of motions and their velocities are as follows:

$-90^{\circ} < \theta_1 < +90^{\circ}$, $\dot{\theta}_1 = 3(\deg/s)$

$-90^{\circ} < \theta_2 < +90^{\circ}$, $\dot{\theta}_2 = 3(\deg/s)$

$+60 < R_3 < +140$ (mm), $\dot{R}_3 = 5(\text{mm/s})$

$-90^{\circ} < \theta_4 < +90^{\circ}$, $\dot{\theta}_4 = 3(\deg/s)$

The velocity state of the moving platform $(\dot{x}, \dot{y}, \dot{z})$ and $(\omega_x, \omega_y, \omega_z)$ are shown in Figs. 6.3 and 6.4 respectively.

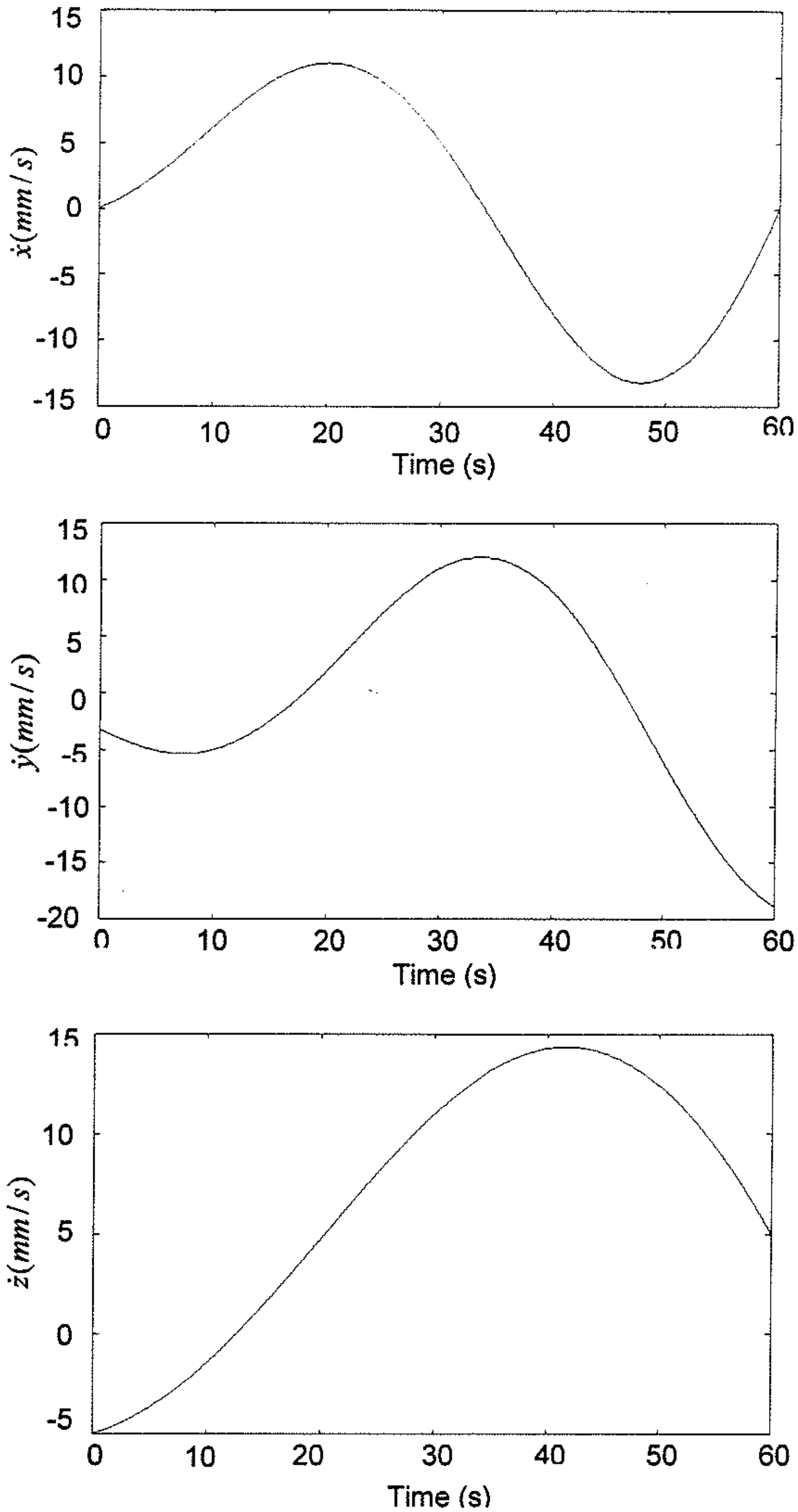

Fig. 6.3: Simulation results for direct velocity problem $(\dot{x}, \dot{y}, \dot{z})$.

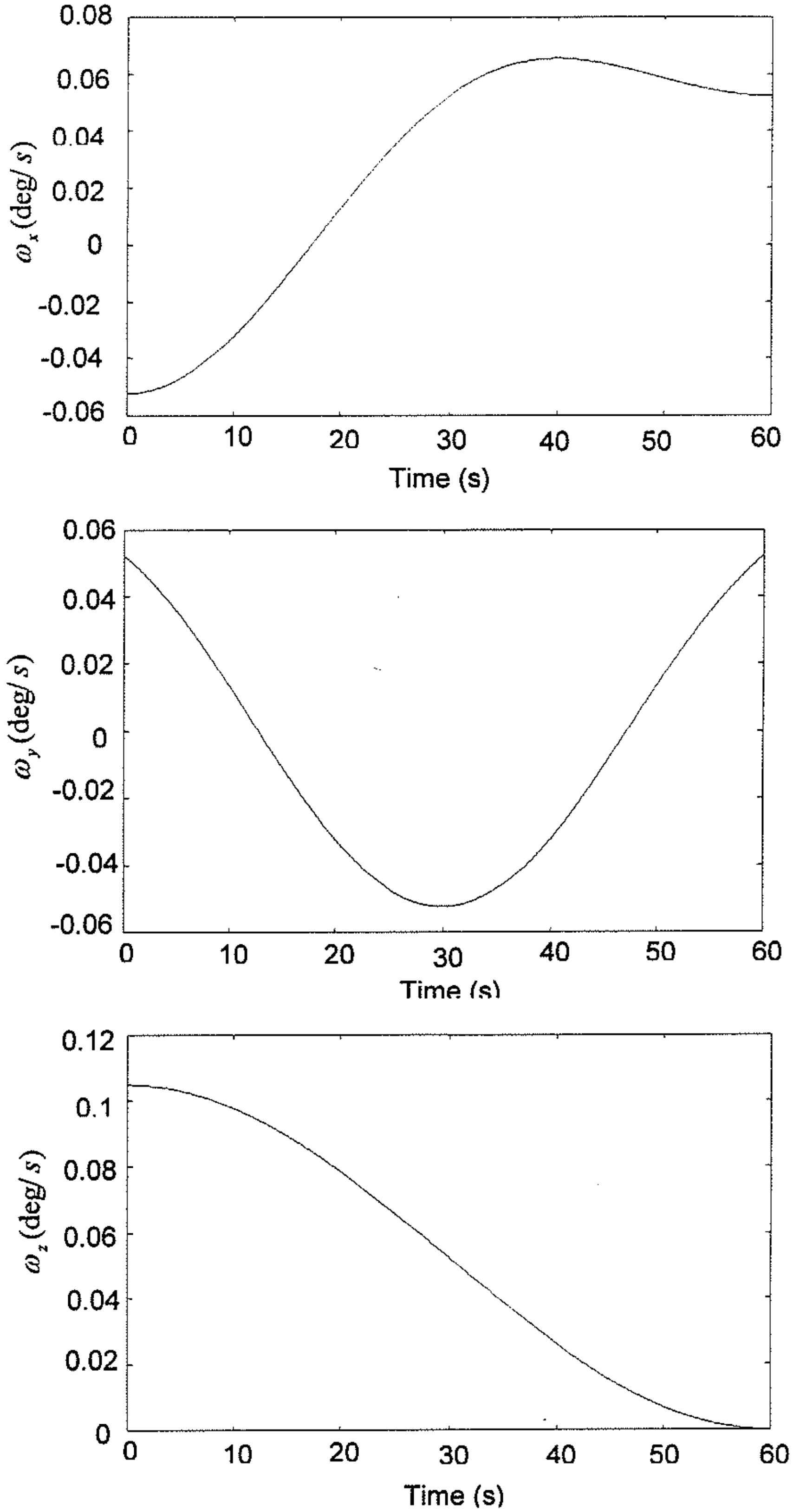

Fig. 6.4: Simulation results for direct velocity problem $(\omega_x, \omega_y, \omega_z)$.

6.3.2. Inverse velocity

In the inverse velocity (known also as inverse Jacobian) problem, we have,

$$\dot{q} = J^{-1}\dot{X}. \tag{6.51}$$

It is obvious that the required joint rates depend on the condition of the Jacobian matrix. In some manipulator configurations the Jacobian is not invertible. In such a case there are infinite joint rates for the Equation (6.51) and the manipulator loses one or more degrees of freedom and it will not be able to move in some directions in the moving platform space.

An important limitation of parallel manipulators is that singular configurations may exist within their workspace where the manipulator gains one or more degrees of freedom and therefore loses its stiffness completely. To identify the singular configurations, we equate the determinant of the Jacobian of the first three degree-of-freedom to zero.

$$|J| = \begin{vmatrix} -R_3S\theta_1C\theta_2 & -R_3C\theta_1S\theta_2 & C\theta_1C\theta_2 \\ R_3C\theta_1C\theta_2 & -R_3S\theta_1S\theta_2 & S\theta_1C\theta_2 \\ 0 & R_3C\theta_2 & S\theta_2 \end{vmatrix} = R_3{}^2C^2\theta_2 = 0 \tag{6.52}$$

Then singularity occurs when: $R_3 = 0, or \theta_2 = \pm 90^\circ$ or similarly when $\theta_1 = \pm 90^\circ$. The manipulator cannot physically reach to the point since $R_3 = 0$ is outside the real workspace. The angles θ_1 and θ_2 can reach to either + or - 90°, but they cannot physically reach to the opposite side of their workspace due to interferences among shafts and other parts of the manipulator. When $\theta_1 = 90^\circ$ and $-90^\circ < \theta_2 < 90^\circ$, the manipulator loses three degrees of freedom and the only remaining degree-of-freedom is a rotation about the axis 26A (see Fig. 6.5). In this configuration, rotational motion of the input link, which is in the stretched out position, results in no output motion of the moving platform and the third and fourth degree-of-freedom become completely locked due to the nature of the inner and outer universal joints at 90°. The same kind of singularity happens when $\theta_2 =$ +90 and $-90^\circ < \theta_1 < 90^\circ$, which is shown in Fig. 6.5.

When $\theta_1 = \pm 90^\circ$ and $\theta_2 = \pm 90^\circ$, it generates four possible areas (S_1, S_2, S_3 and S_4) (see Figs. 6.6 and 6.7), where the axis 12 is co-planer with the axes 24A and 26A. In these configurations the hand-controller can possibly gain one extra degree-of-freedom (in the direction of circular arrow) while all the actuators are locked. These kinds of singularities happen where the redundancies of the pantographs and the inner and outer universal joints exist at the same position. At the same time umder these conditions, the moving platform also loses its third and fourth degree-of-freedom due to the nature of the universal joints at 90°. Due to the orientation of the intermediate part of the outer universal joint in area S_1 (see Fig. 6.8), the hand-controller does not gain any extra degree-of-freedom.

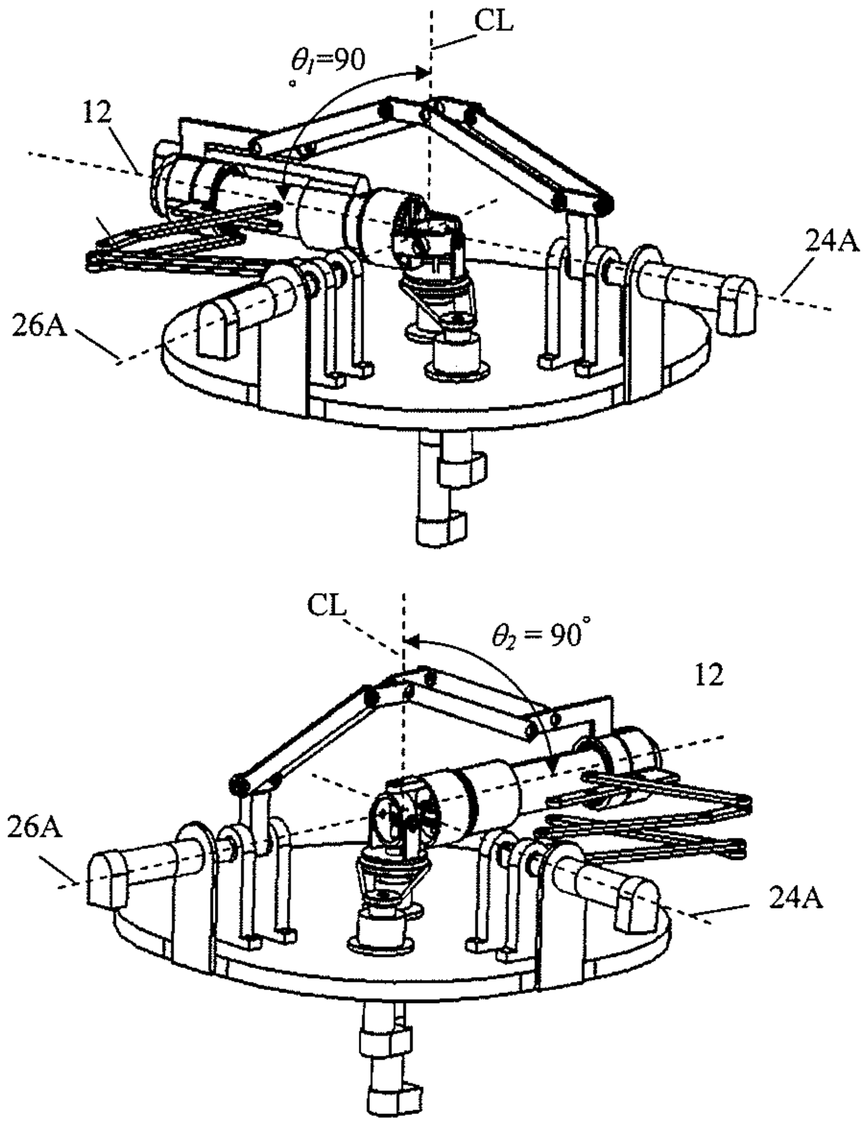

Fig. 6.5: Singular configurations where the manipulator loses three degrees of freedom.

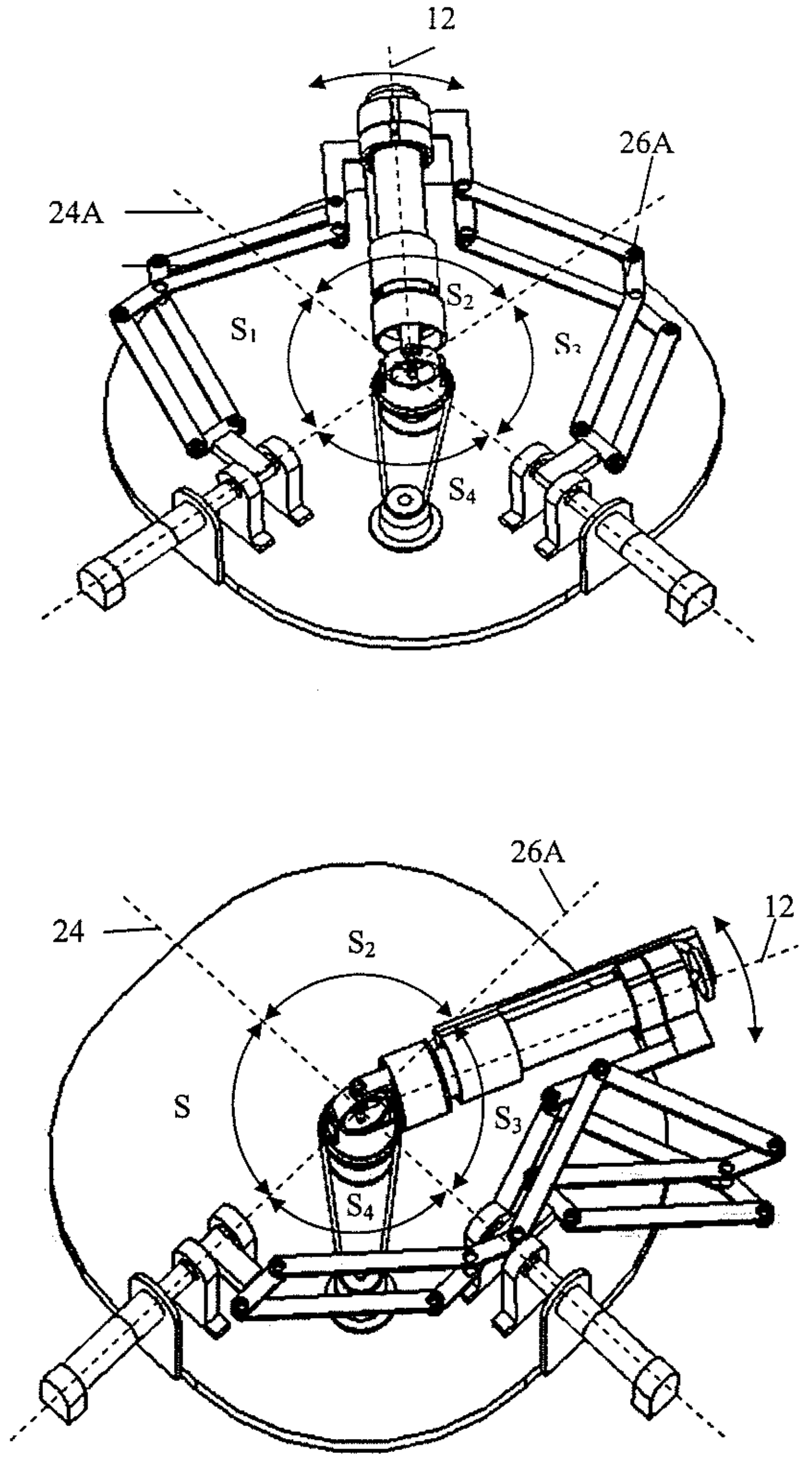

Fig. 6.6: Singular configurations where the manipulator loses two degrees of freedom and gains one extra degree-of-freedom.

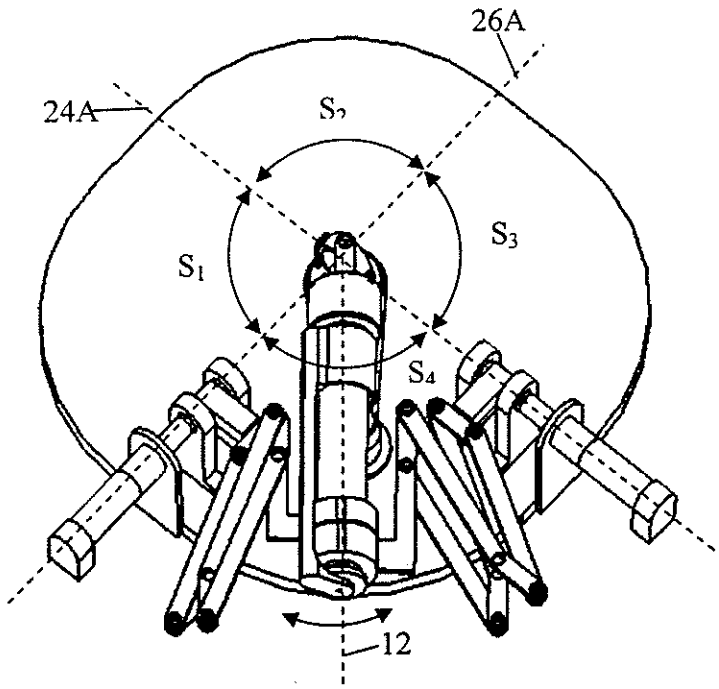

Fig. 6.7: Singular configuration where the manipulator loses two degrees of freedom and gains one extra degree-of-freedom.

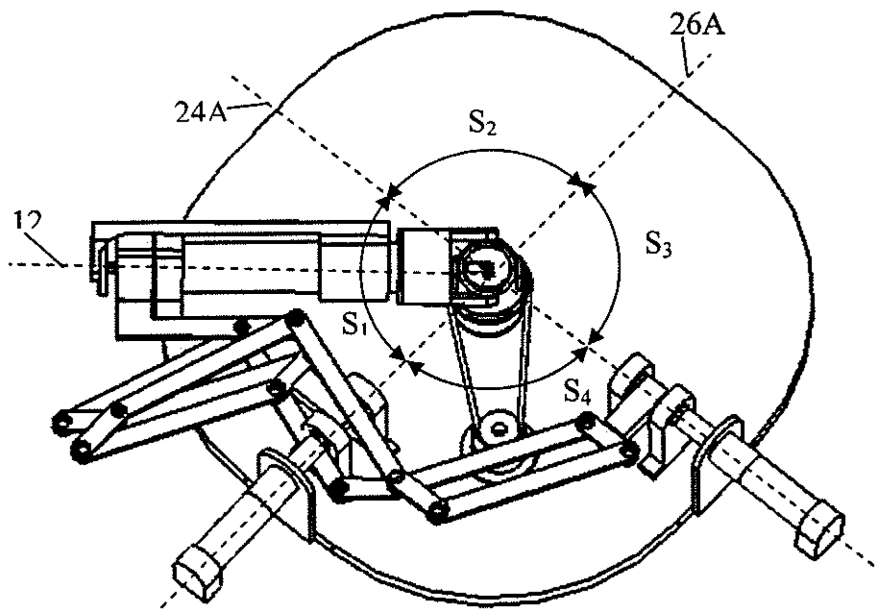

Fig. 6.8: Singular configuration where the manipulator loses two degrees of freedom.

The manipulator theoretically shows a hemispherical workspace in which all the singular points are located on the great circle of the hemisphere. The useful workspace can be selected far from the singular points, which will be discussed in the next section. Similar observations can be made for the wrist's structure. However, the wrist cannot reach to those singular points due to mechanical constraint inside its structure.

6.4. Workspace

6.4.1. Hand-controller

The hand-controller provides two points for the operator to hold (see Fig. 4.1). If the operator holds the hand-controller at point P1, he/she needs to move his/her forearm or upperarm or both of them together to move the manipulator. By doing so, the workspace created is S_1 (see Fig. 6.9), which has a conical contour and is limited between two cap spheres with radius R_4 and R_3 about a common fixed center F. This is the workspace of the axis 12 at point P1, which is outside the parallel manipulator. In the hand-controller, $R_4 = 355$ (mm), $R_3 = 275$ (mm) and vertex angle θ is up to120° but for ultrasound and palpation tasks the angle is limited to 90°. The difference between R_4 and R_3 is 80mm, which provides enough radial movement during ultrasound and palpation examinations. This workspace is more useful during positioning the end-effector of a remote manipulator working in a spherical coordinate system in master slave mode. It should be noted that the hand-controller has a full rotation of (0-360°) around the axis 12 in this workspace.

By adding handle 14 (see Fig. 4.1), the operator can manipulate the hand-controller at point P2, which needs the operator's wrist and slight forearm movements. In such a case, the axis 12 and its point P2 has another workspace S_2, which is inside the parallel manipulator (see Fig. 6.9). This workspace has been designed not to have any interference with the other parts of the parallel manipulator. The operator can move his/her wrist freely in this area. The shape of S_2 is similar to S_1 but in a smaller scale in that $R_1 = 60$ (mm), $R_2 = 140$ (mm) and the vertex angle θ is 90°. This workspace is useful for orienting a remote wrist holding an ultrasound probe.

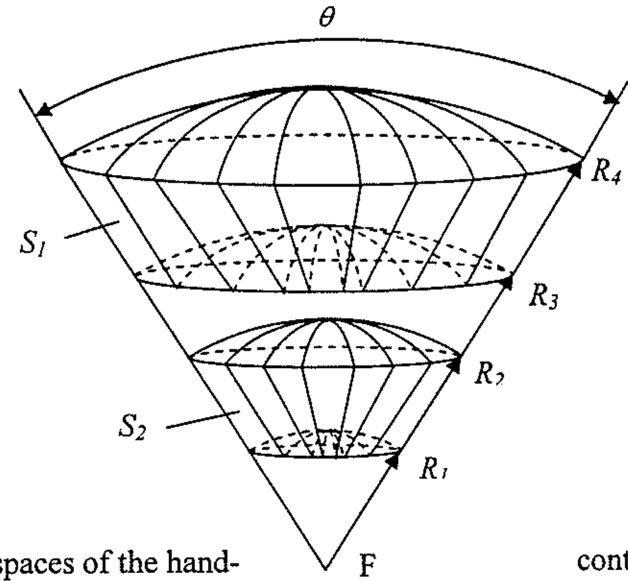

Fig. 6.9: Workspaces of the hand-controller.

6.4.2. Wrist

The wrist has two modules; the first and second one generate motions necessary for performing ultrasound and deep palpation respectively. A typical workspace of the wrist is shown in Fig. 6.10. This is the workspace generated by axis 212 (see Fig. 5.1), at its end point PA. The first workspace is S_1, which has a conical contour and is limited by a cap sphere at its upper end. R_1 varies between 0 and 30 (mm), and maximum vertex angle is 90°. This workspace is useful for ultrasound examinations. The second workspace is S_2, which has a conical contour and is limited by a cap sphere at its lower end. R_2 varies between 0 and 70 (mm), and maximum vertex angle is 90°.

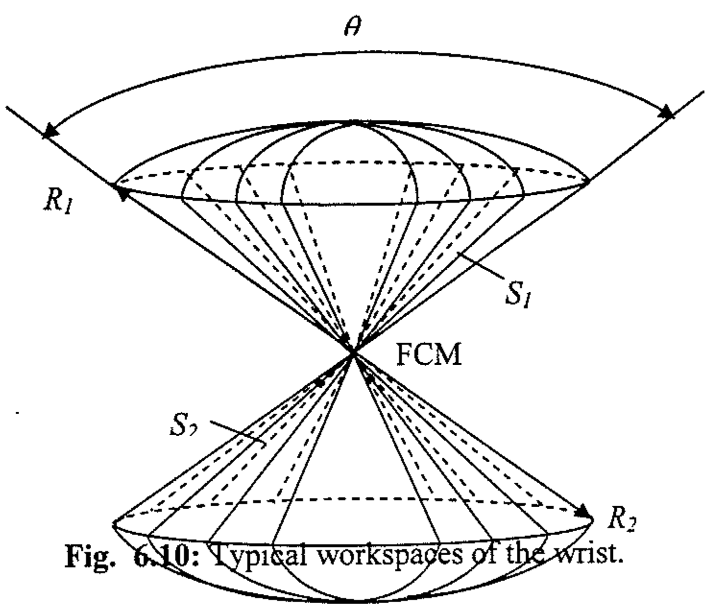

Fig. 6.10: Typical workspaces of the wrist.

Chapter 7

Prototype of the Hand-Controller and the Wrist

7.1. Hand-Controller's Mechanical Specifications

Figure 7.1 shows the four degrees-of-freedom hand-controller, which has been prototyped to verify the concepts developed during the embodiment design described in Chapter 4. The fabricated model has up to three active degrees of freedom and the fourth degree of freedom is passive. It consists of two perpendicular pantographs 1 and 2 to provide a spherical motion around an interior center point F. These two pantographs together provide the first two degrees of freedom. A third unit 3 creates a linear motion along the radius of the created hemisphere, which provides the third degree of freedom. The fourth degree of freedom 4 has been made passive (for simplicity of proof of concept), which means that it does not have any power train and its decoupling system with the third degree of freedom has also been eliminated.

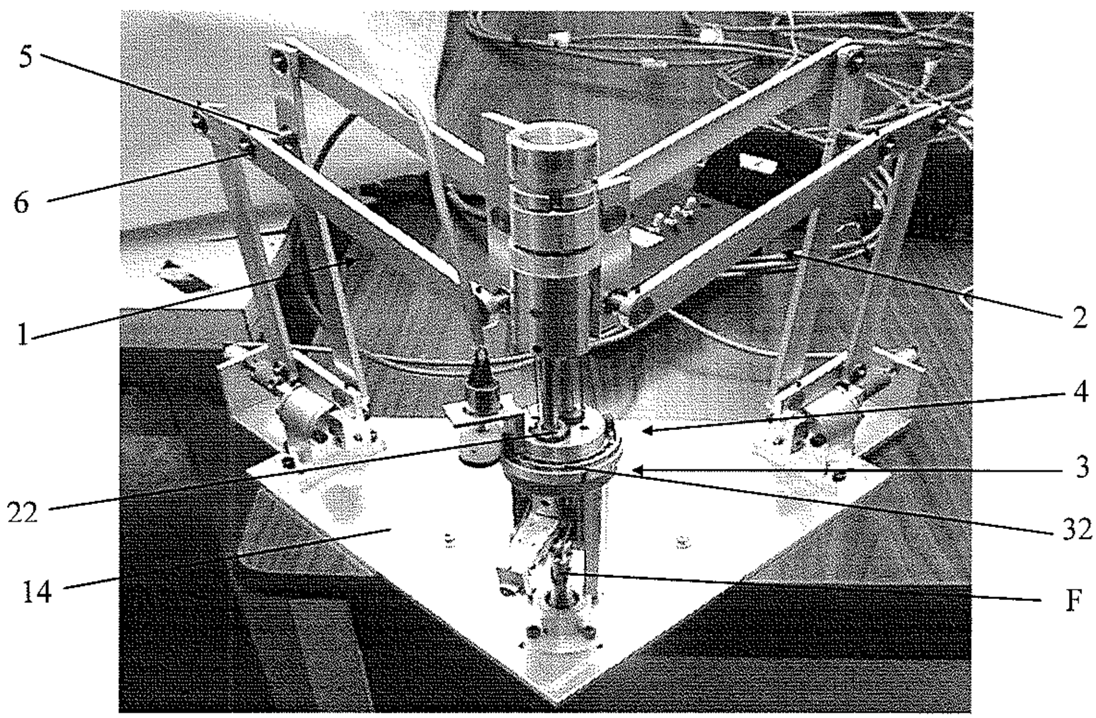

Fig. 7.1: General view of the hand controller.

The structure of the pantograph's linkages has been made of aluminum. The linkages are connected together by shafts and deep-groove ball bearings. One end of each shaft 5 is sited in the hole of the linkages and is secured by very small setscrews, and the other end of the shafts is jointed to its counterpart hole by an ordinary no-shielded deep-groove ball bearing 6 (SDP/SI) (see Fig. 7.1). Shielded ball bearings impose large amount of friction in any revolute joint, which is not desirable in haptic applications. The selected ball bearings show 0.0002-0.0005 (in) radial play (SDP/SI). A slight joint compliance has been observed because of using only one ball bearing in each revolute joint. This effect can be eliminated by using two tandem deep-groove ball bearings in each joint of the pantographs for future developments. The pantographs are connected to the base plate 14 by means of housings 7, which include two single-row deep-groove ball bearings (SKF) in tandem to resist moments and radial loads (see Fig. 7.2). The inner case of the ball bearings sits on their shafts shoulders and becomes secure by snap rings from the other side. The outer case of the ball bearings is fixed by two end caps 8. The first link 9 of the pantographs is fixed on the input shafts 10 by miniature setscrews through parts 11. The position of each pantograph can be adjusted in the axial direction of the input shafts by those setscrews to compensate for the manufacturing errors. The input shafts of the pantographs can be coupled to its own actuator, which is basically a direct-drive electric motor with encoders to work as a haptic device with force feedback or with potentiometers 12 as a hand-controller. The input shaft 10 is connected to the actuator or potentiometer's shafts through a zero-backlash flexible helical coupling 13 (SDP/SI). The coupling is able to compensate for up to 5° angular misalignment, a parallel offset of 0.25 (mm) and an axial motion between $\pm$ 0.25 (mm). The actuators or potentiometers 12 are fixed to the base plate 14 by the L-shape assemblies 15. The two pantographs are jointed together by a deep groove ball bearing (SKF) at point P (see Fig. 7.3). The joint shows small compliance, which can be eliminated by having two deep-groove ball bearings in tandem. Two lock nuts 16 are used to adjust the relative height between two pantographs to allow one pantograph to be adjusted in the vertical direction with respect to the other one during assembly. One of them is shown in Fig. 7.3, and the other one is inside the joint.

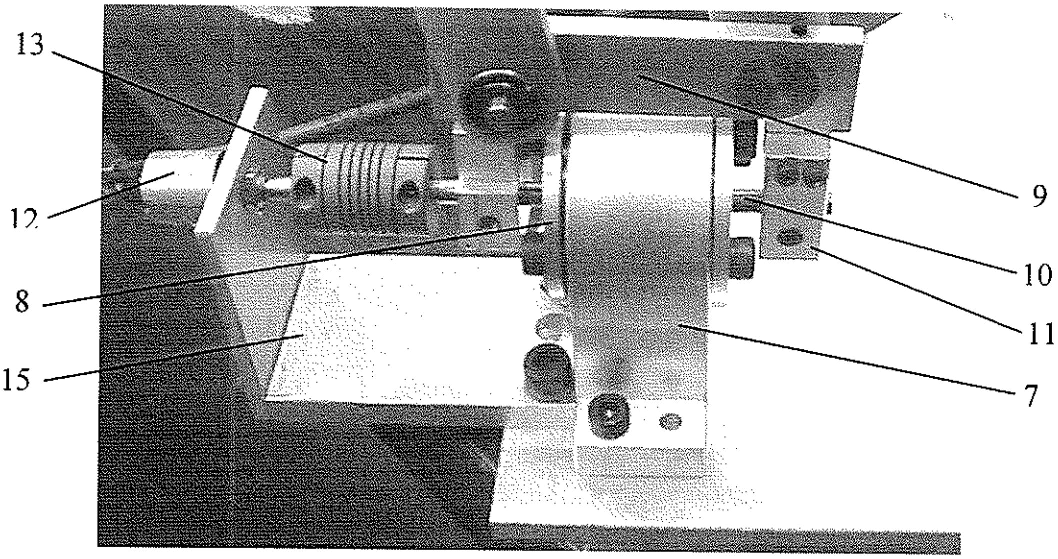

Fig. 7.2: Detailed view showing the connection between pantographs and their actuators.

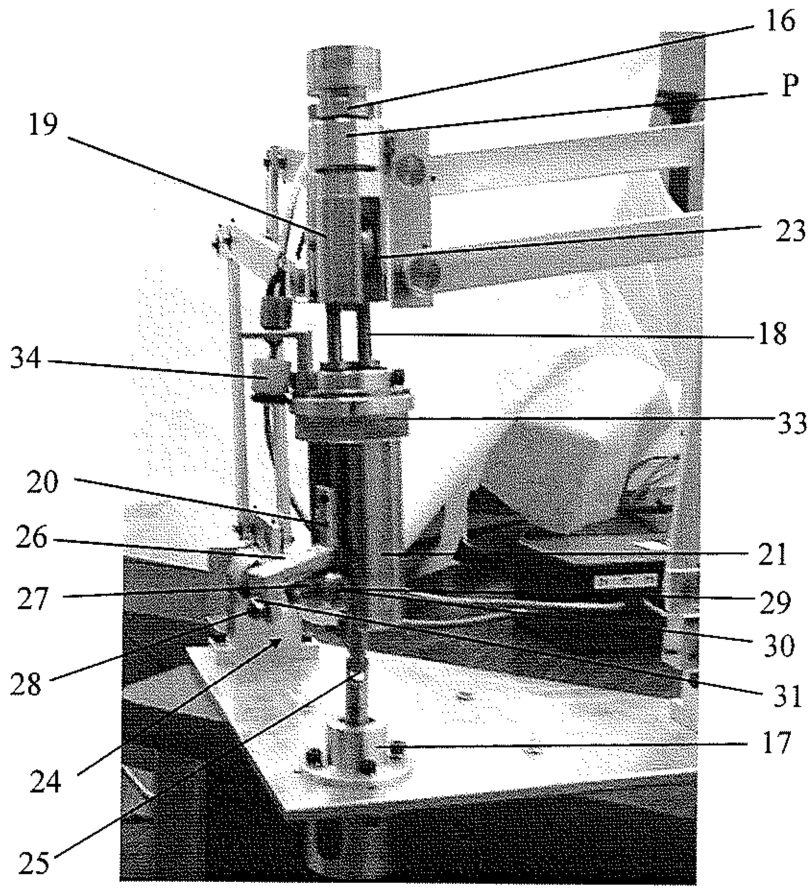

Fig. 7.3: General view of the third degree-of-freedom.

The whole assembly of the third degree-of-freedom is prototyped as a separate unit and is fixed to the first pantograph from the top through an intermediate part by hexagonal head screws and is joined to the base plate 14 by housing 17 including two deep-groove ball bearings (SKF) in tandem, which accommodate the input shaft of the third degree of freedom (not shown). The linear drive of the third degree of freedom consists of two standard precision steel shafts 18 (Warner) which are fixed by small set screws to the upper and lower housings 19 and 20 from the top and the button respectively. The centerline of shafts 18 is concentric with the radius of the created hemisphere by the two pantographs. The linear drive also contains the handle 21, which contains two standard linear ball bearings 22 (Warner) (see Fig. 7.1), which are able to precisely slide up and down on the precision shafts 18. The linear ball bearings 22 are secured in the handle 21 by snap rings. The upper housing 19 contains a turn-around pulley 23 (SDP/SI), which has a miniature ball bearing in its bore. This combination allows the internal ball bearing to only receive radial loads instead of a combination of radial forces and moments, which usually happens by having two ball bearings at the end of the pulley's shaft. This ball bearing arrangement reduces generated friction forces inside the ball bearing, which is vital in haptic applications. The lower housing contains two miniature guiding pulleys (not shown) (SDP/SI), which have small ball bearings in their bores, cable tensioning mechanism 24, which is different than the one explained in embodiment design (Chapter 4). It also accommodates two miniature decoupling deep-groove ball bearings (SDP/SI) with 0.005- 0.013 mm radial play. This ball bearing decouples the rotational motion of the universal joint 25 from the fixed structure composed of the upper and lower housings 19 and 20 and precision shafts 18 and consequently from the two pantographs.

The cable-tensioning mechanism has an L-shaped aluminum housing 26 and an aluminum slider 27. The housing 26 is fixed to the lower housing 20 by miniature head cap screws. The slider 27 can move in and out and is fixed to a long setscrew 28 by a locknut and spring washers. The slider 27 has a miniature shaft 29, which has two miniature pulleys 30 (SDP/SI) at its ends, which are fixed on shaft 29 by miniature snap rings. The long setscrew 28 goes through the housing 26 and its position can be adjusted by tightening and loosing the nuts 31. By changing the position of the setscrew 28, the internal tension of the cable can be adjusted. The arrangement of the cable-tensioning mechanism with respect to the handle 21 does not have any interference with the operator's hand during operation. Most of the cable drive is accommodated inside handle 21, which has an outside diameter = 38 (mm) and length = 90 (mm), which are quite ergonomic for the size of an average hand.

A closed loop miniature cable (SDP/SI) covered by nylon with an outside diameter = 0.024 (in) and a breaking strength = 40 (Lbs) has been used to transform the rotary motion of the input actuator through the universal joint 25 into a linear motion of the handle 21 between upper and lower housings 19 and 20, which is almost 45 (mm). The nylon reduces friction between the steel cable and steel pulleys, which is quite important in haptic applications.

In this prototype, the fourth degree-of-freedom is passive and is assembled over the handle 21; therefore this degree of freedom will be used only as hand-controller. It has a deep groove ball bearing 32 (SKF) (see Fig. 7.3) sited on the handle 21 and its outer case is connected to a knurled ring 33. Knurling enables the operator to effectively manipulate the ring 33 (see Fig. 7.3). Turning the ring 33 causes the friction wheel 34, its potentiometer, to rotate.

The overall dimensions of the hand controller are selected to satisfy the ergonomic requirements (Chapter 4). The operator is able to hold the handle 21 and moves it freely inside the hand controller without any interference.

Figures 7.4 to 7.8 show the hand-controller's mobility and its workspace at different configurations.

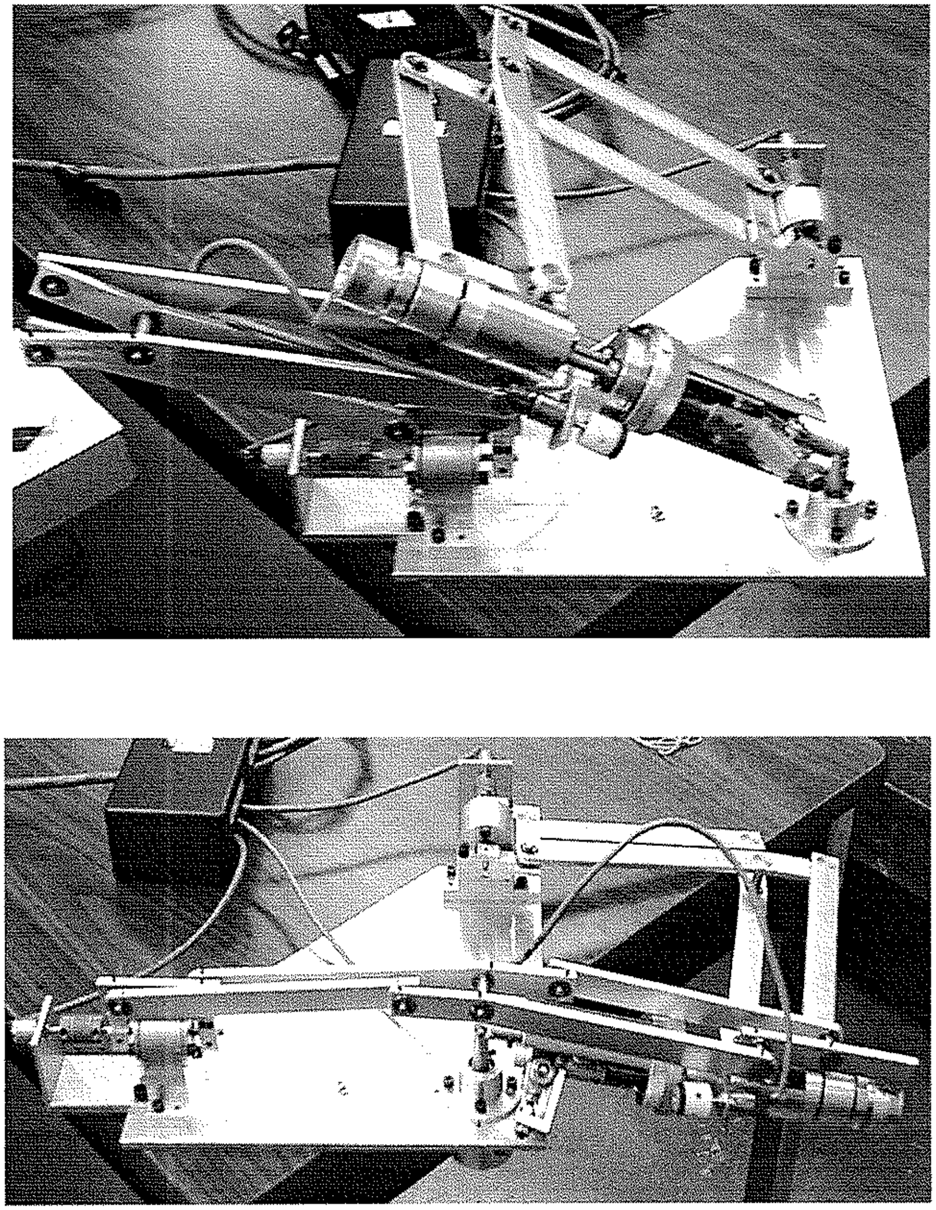

Fig. 7.4: Hand-controller at its yaw angles.

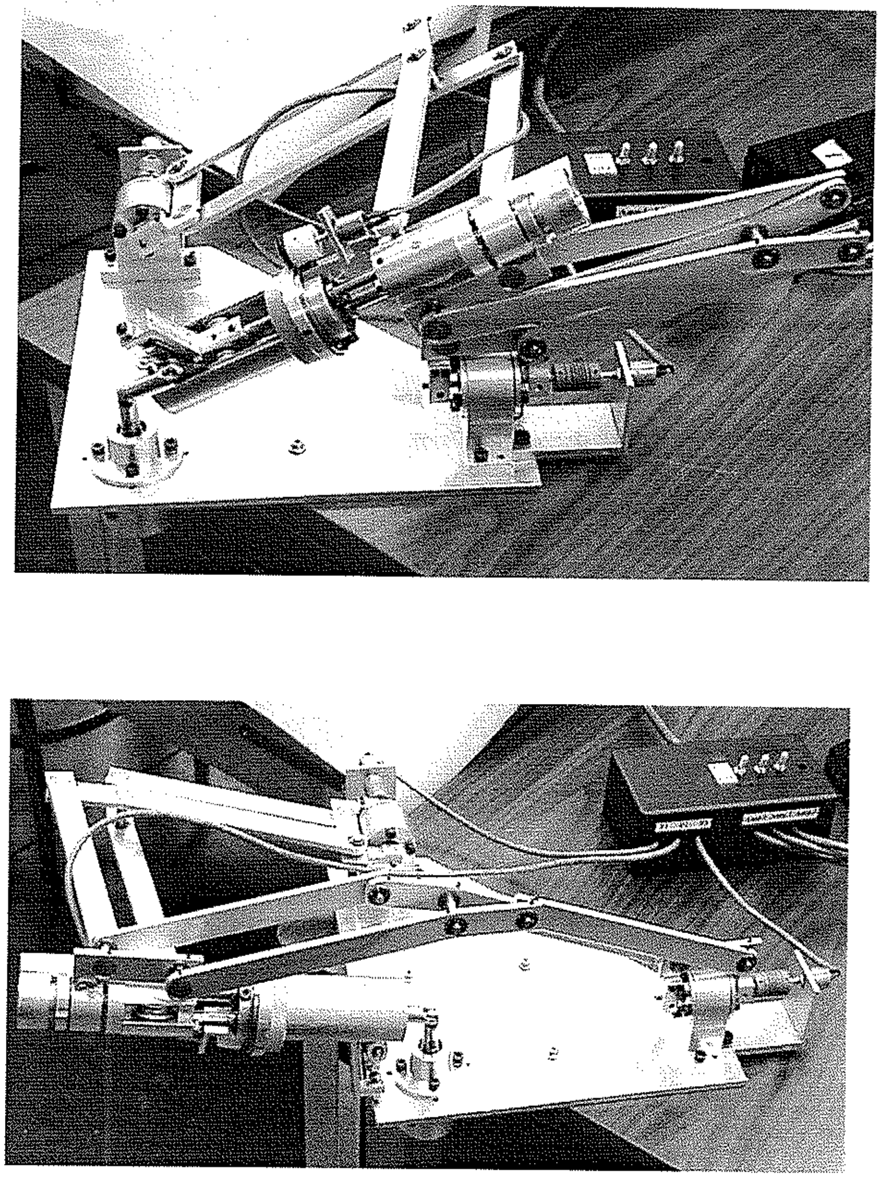

Fig. 7.5: Hand-controller at its pitch angles.

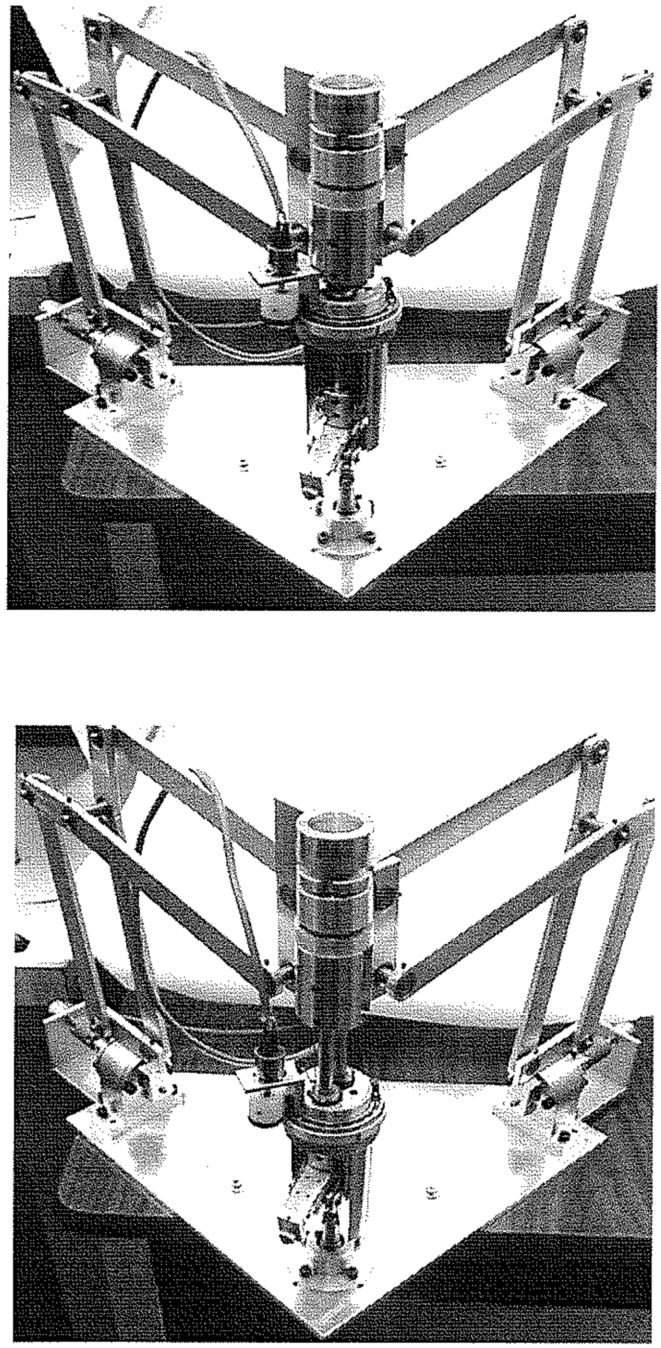

Fig. 7.6: Hand-controller at its radial motions.

7.2. Wrist's Mechanical Specifications

A simplified version of the four degrees- of-freedom wrist has been prototyped to verify the concepts developed during the embodiment design described in Chapter 5. The prototyped model has up to three degrees-of-freedom (see Figs. 7.7 to 7.10). It consists of two perpendicular pantographs 1 and 2, which are inclined with respect to the horizontal plane to provide a safe distance between the wrist components and patients during examinations. These two pantographs together generate a hemispherical motion around a fixed remote-center-of-motion FCM. The third degree-of-freedom 3 generates a rotary motion about the radius of the created hemisphere, which is the axis of the ultrasound probe 4. The power train of the fourth degree-of-freedom and the two modules of the designed wrist (see Chapter 5) have not been made in this prototype. Due to the types of its movements, the developed prototype is most suitable for performing ultrasound examinations.

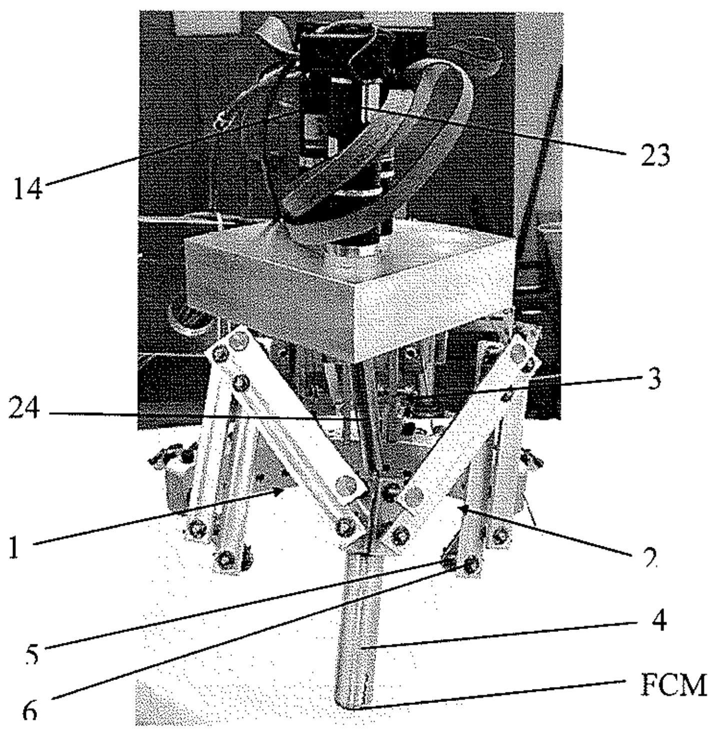

Fig. 7.7: A general view of the wrist.

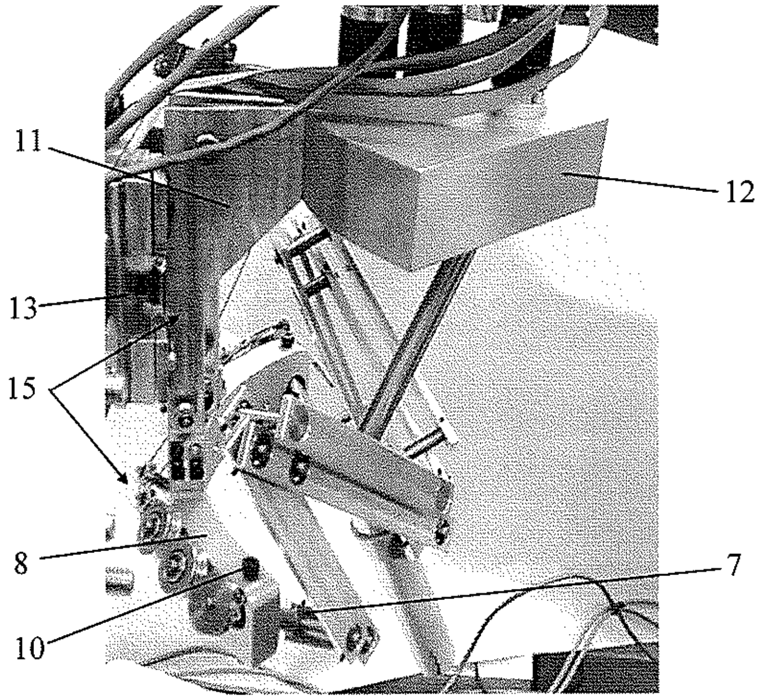

Fig. 7.8: A general side view of the wrist.

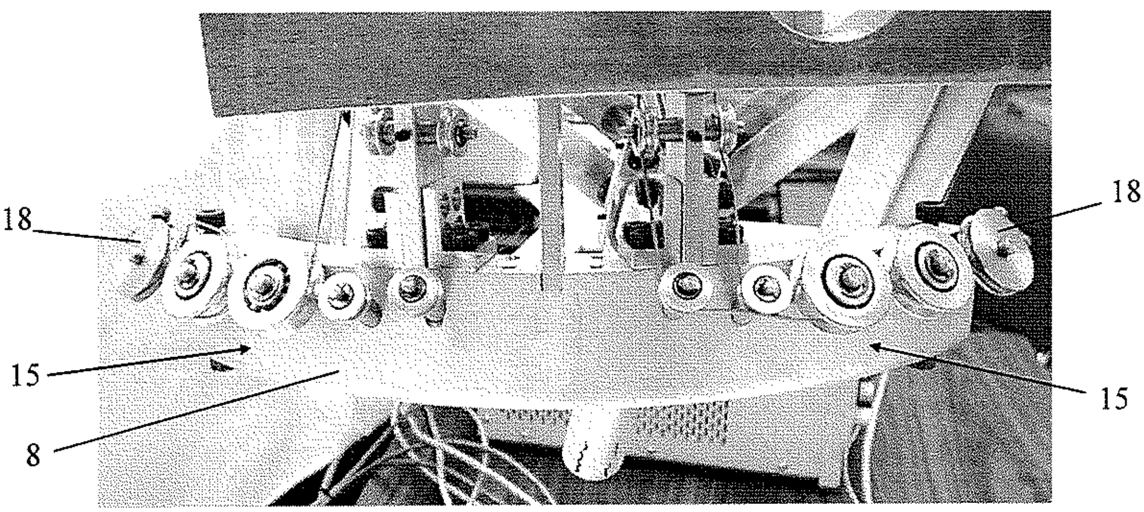

Fig. 7.9: A detailed view of the cable drive.

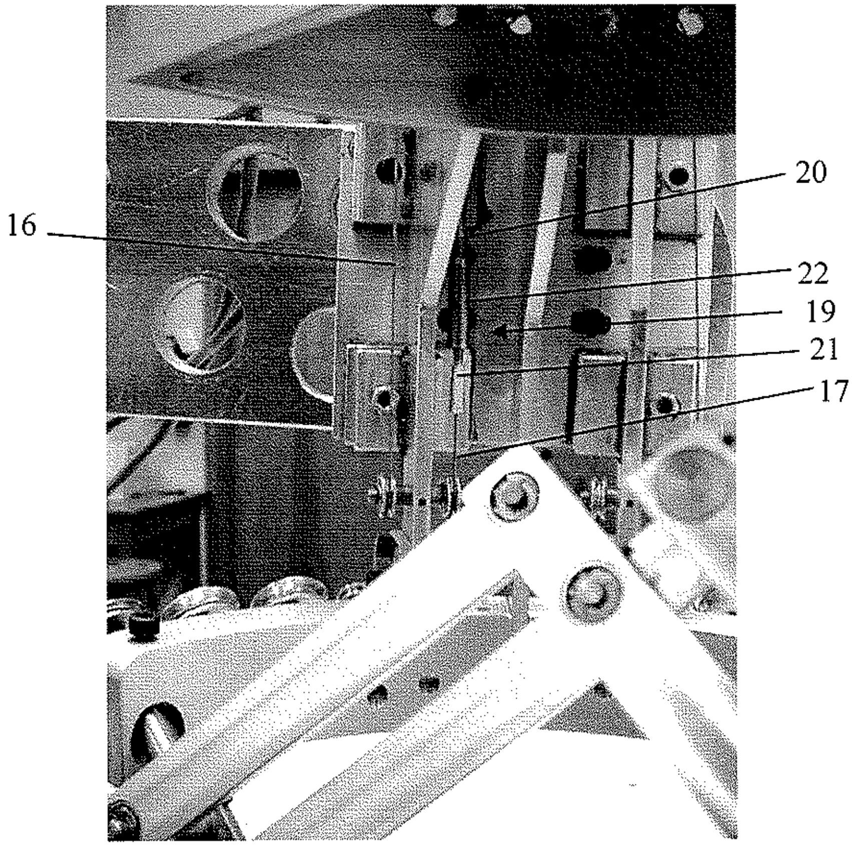

Fig. 7.10: Detailed view of the cable routes.

The structure of the pantograph's linkages has been made of ordinary aluminum, which was the most available light material for prototyping. The linkages are connected together by shafts and deep-groove ball bearings. One end of each shaft 5 is sited in the hole of the linkages and is secured by miniature setscrews and the other end of the shaft is joined to its counterpart hole by ordinary no-shielded deep groove ball bearings 6 (SDP/SI) (see Fig. 7.7). The friction force imposed by shielded ball bearings is high, however, it does not affect the wrist performance, since using no-shielded ball bearings increases the power train efficiency. This in turn decreases the size of the motor and gearboxes, which consequently reduces the cost and weight of the wrist. In practical applications, all the no-shielded ball bearings must be protected against contamination by using cups at both ends of the ball bearings.

The pantograph's input link 7 is jointed to the circular housing 8 by two deep groove ball bearings (SDP/SI) in tandem with 0.0002-0.0005 (in) radial play (see Fig. 7.8). The first link 7 and the input shaft are made of steel and manufactured as one piece to increase the integrity of the system while achieving more compactness. The inner case of the ball bearings sits on their input shaft's shoulders and becomes secured by snap rings 9 (see Figs. 7.7 and 7.10). The outer case of the two ball bearings is fixed by two head cap screws 10 from the top and bottom of the circular housings 8. The arrangement of the screws 10 allows the operator to adjust the position of each pantograph in the axial direction of their input shafts to compensate for the manufacturing errors during assembly. The input shafts 7 are jointed to the fixed aluminum-made structure, which consists of circular housing 8, ribs 11, upper housing 12 and back plate 13. The ribs 11 connect the circular and upper housings 8 and 12 together by small head cap screws through small brackets to satisfy structural integrity. The back plate 13 allows the wrist to be attached to any manipulator.

Each pantograph is driven by brushed DC motor 14 (Maxon) (shown in Fig. 7.7) equipped with planetary gearbox (Maxon) and digital encoder (Maxon) through the cable drive system 15 (see Fig. 7.8). The upper housing 12, ribs 11 and circular housing 8 accommodate drive, guiding and driven pulleys (see Figs. 7.8 and 7.9). The internal structure of the guiding pulleys is similar to ones discussed for the hand controller (see chapter 7). The guiding pulleys lead the cable routs through straight and circular patterns on the fixed structure, which generate a long and at the same time very compact power train that is a critical factor in wrist design (see Figs. 7.8 and 7.9). Each cable drive consists of two cable routs 16 and 17 (see Fig. 7.10). One end of the miniature cable (SDP/SI) is fixed on the rim of the drive pulley and the other end is fixed on the rim of the driven pulley 18 by means of head cap screws. The other cable route has the same type of fixation on the drive and driven pulleys. In addition, it also has a miniature turn-buckle system to adjust the cable tension. The cable routs work in the opposite direction of each other, which means that when the drive pulley rotates in the C.W. direction, the other route is idle and only follows the drive route and vice versa. The miniature turnbuckle system 19 has the brass-made right-and-left-hand threaded plugs 20 and 21, and left-and-right-hand nut 22, which is made of cold rolled steel (see Fig. 7.10). By using this type of cabling scheme, elimination of backlash due to presence of the slippage between the cable and the pulleys is guaranteed. This factor is quite important for safety purposes. The first two degrees of freedom generate the pitch and yaw motions for the ultrasound probe (see Chapter 2).

The third degree of freedom has the brushed DC motor 23 (Maxon), a ceramic version planetary gearbox (Maxon) and a digital encoder (Maxon), which drives a zero backlash, low inertia telescoping universal joint 24 (SDP/SI) with the operating angle = 60° to rotate the ultrasound probe (see Fig. 7.7). It consists of two universal joints and a ball spline, which are integrated together by the manufacturer. This power train provides the spinning motion of the ultrasound probe. Figures 7.11 and 7.12 show the wrist's mobility and its workspace at different configurations.

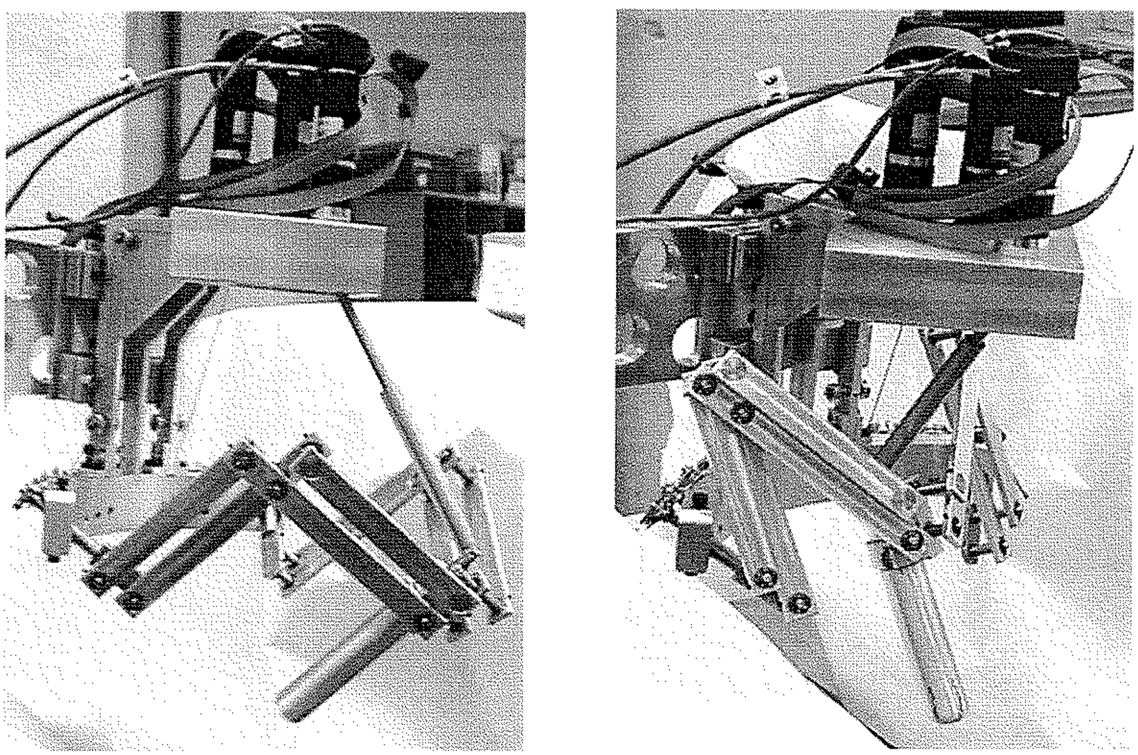

Fig. 7.11: Wrist at its fully extended and retracted positions.

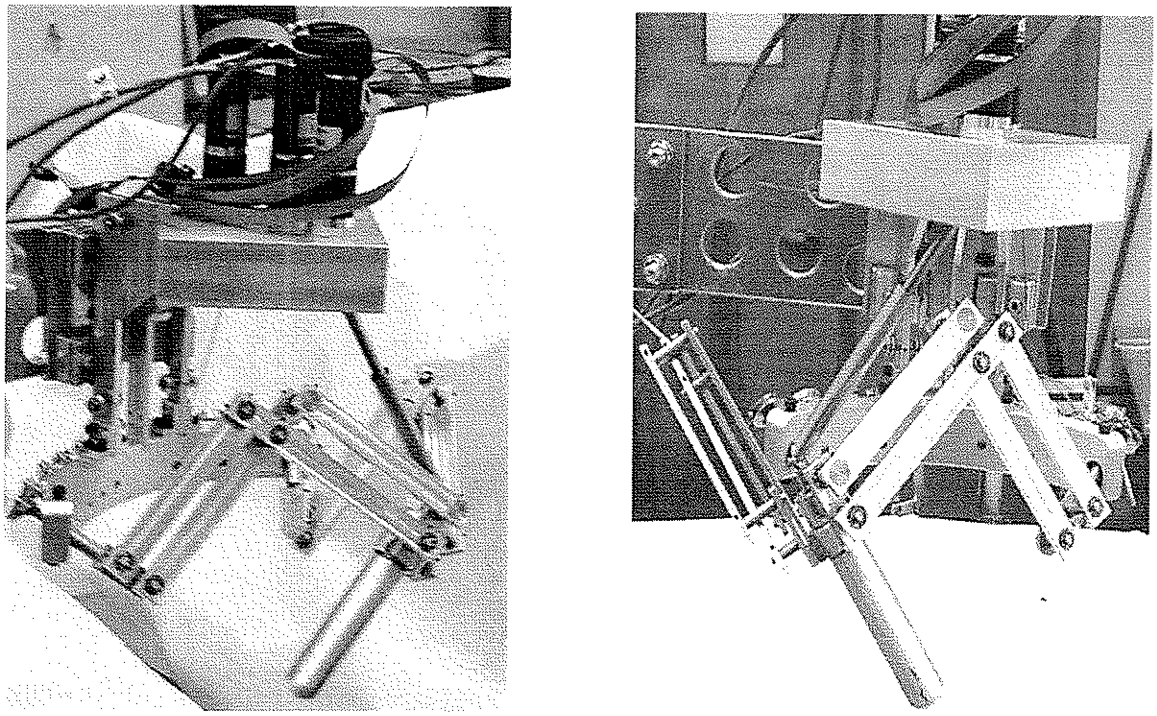

Fig. 7.12: Wrist at its maximum pitch and yaw angles.

Chapter 8

Computer Interfacing

In the present setup the pitch, yaw and spinning motions of the hand-controller are equipped with carbon potentiometers (Precision Electronic components Ltd) and its linear motion is equipped with a DC motor (Maxon) and planetary gearbox (Maxon), a digital encoder (Maxon), which is inactive in this setup. The corresponding degrees of freedom in the wrist have three DC motors (Maxon) with three planetary gearboxes (Maxon) and three digital encoders (Maxon). The developed hand-controller and the wrist have similar kinematic configuration. This novel feature simplifies the control algorithm and makes it more reliable. Each DC motor on the wrist has a separate controller, which receives its desired value directly from its correspondent degree of freedom in the hand-controller. Fig. 8.1 shows the control block diagram of present tele-operation system. The operator sets the desired position of the wrist by turning the hand-controller and its respective potentiometer, and the controller compares the actual position and the desired one and sends appropriate voltage to its DC motor through a servo amplifier. The prototyped hand-controller and the wrist are interfaced to a PC by various data acquisition and interfacing boards. The schematic of the interfacing diagram is shown in Fig. 8.2. The output voltages of the potentiometers are connected to a high-speed 16 channel input/output board (OMEGA), which is capable of reading 16 analog-to-digital input channels with 2 digital to analog channels. The digital rotary encoders are monitored by a quadrature incremental encoder board (Keithley). This board is able to read up to four axes. Each DC motor is controlled by a linear servo amplifier (Maxon), which is capable of controlling the current and speed of a DC motor. Each servo amplifier receives its set value (control voltage) from control software through an input/output expansion board (Keithley) providing 6 channels of analog output and 24 lines of digital I/O. It is also capable of sending bipolar voltages to each servo amplifier to reverse the direction of the rotation. Each servo amplifier sends the appropriate voltages to its DC motor according to the received set values from the control software.

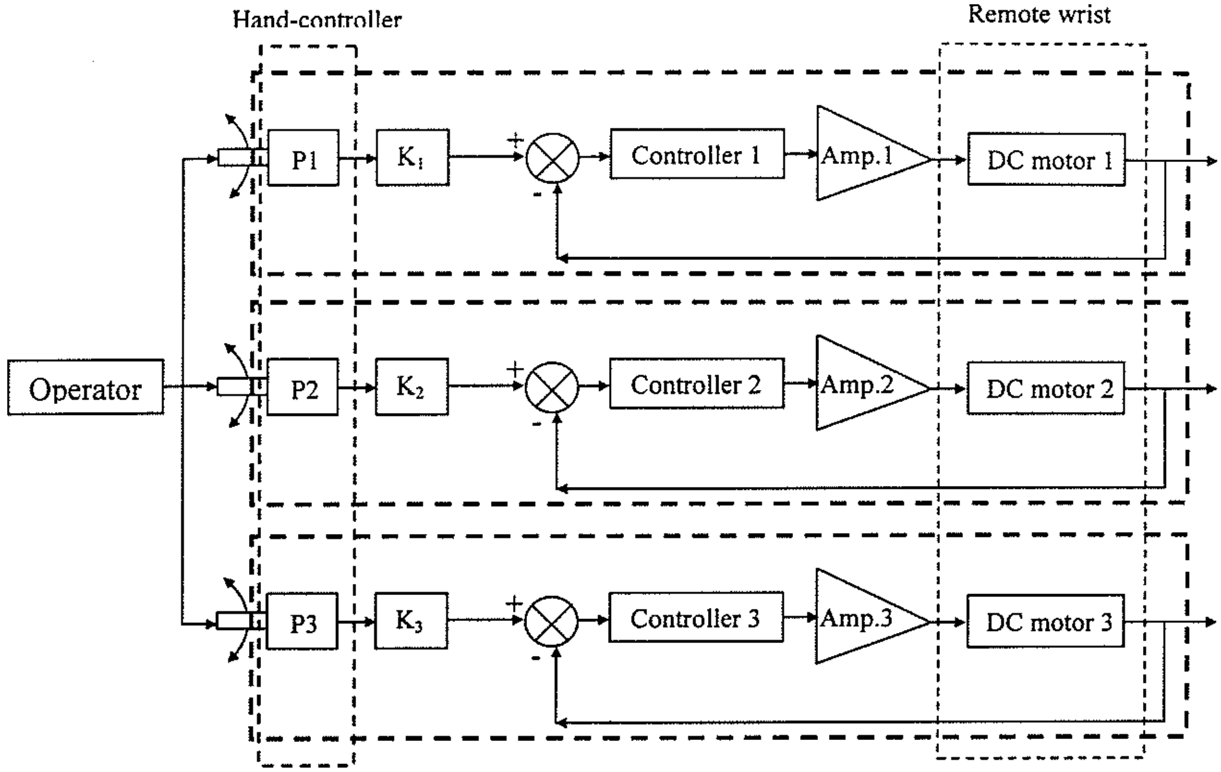

Fig. 8.1: Control block diagram of the present master-slave system.

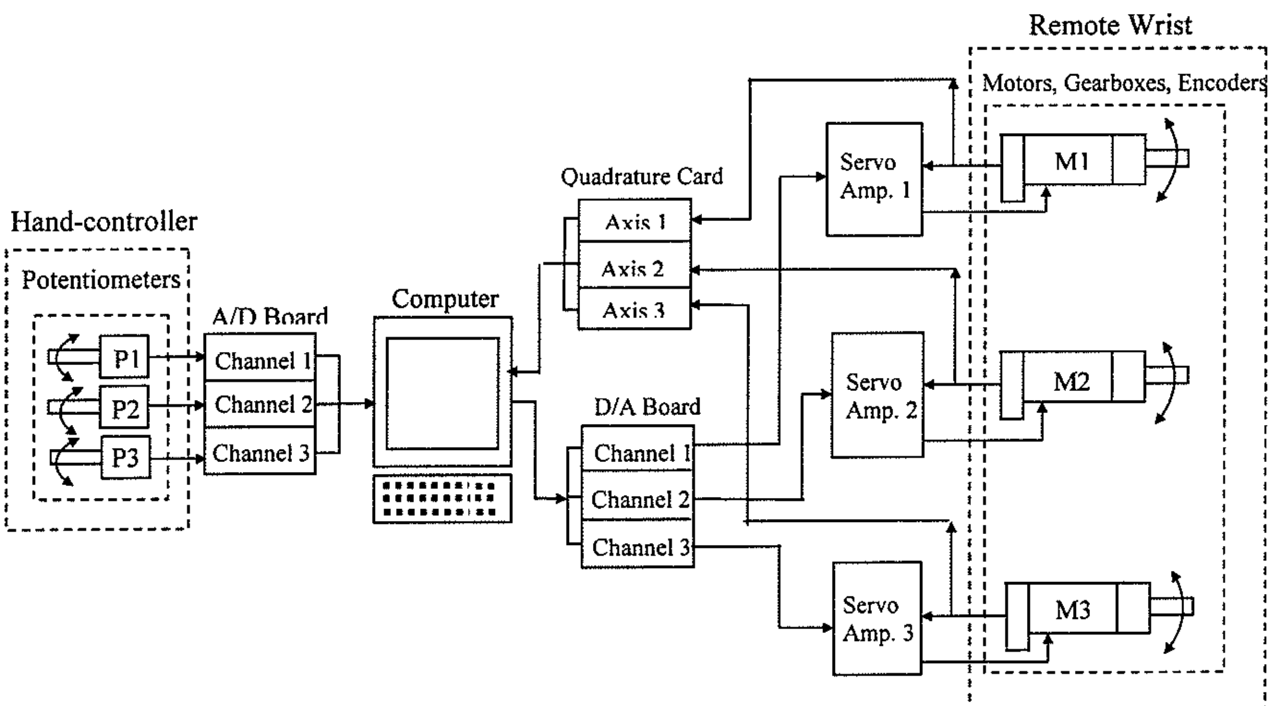

Fig. 8.2: Interfacing diagram of the present master-slave tele-robotic system.

In the first set of our experiments, an equal step input (10 degrees) has been applied to the wrist's actuators. Simple PD controllers with different gains have been applied to each degree-of-freedom. The results are shown in Figs. 8.3 to 8.5.

In the second set of experiments, an operator moved the hand-controller in an arbitrary manner and the wrist tracked the movements of the hand-controller. Simple controllers with different gains have been applied to each degree of freedom. The results are shown in Figs. 8.6 to 8.11.

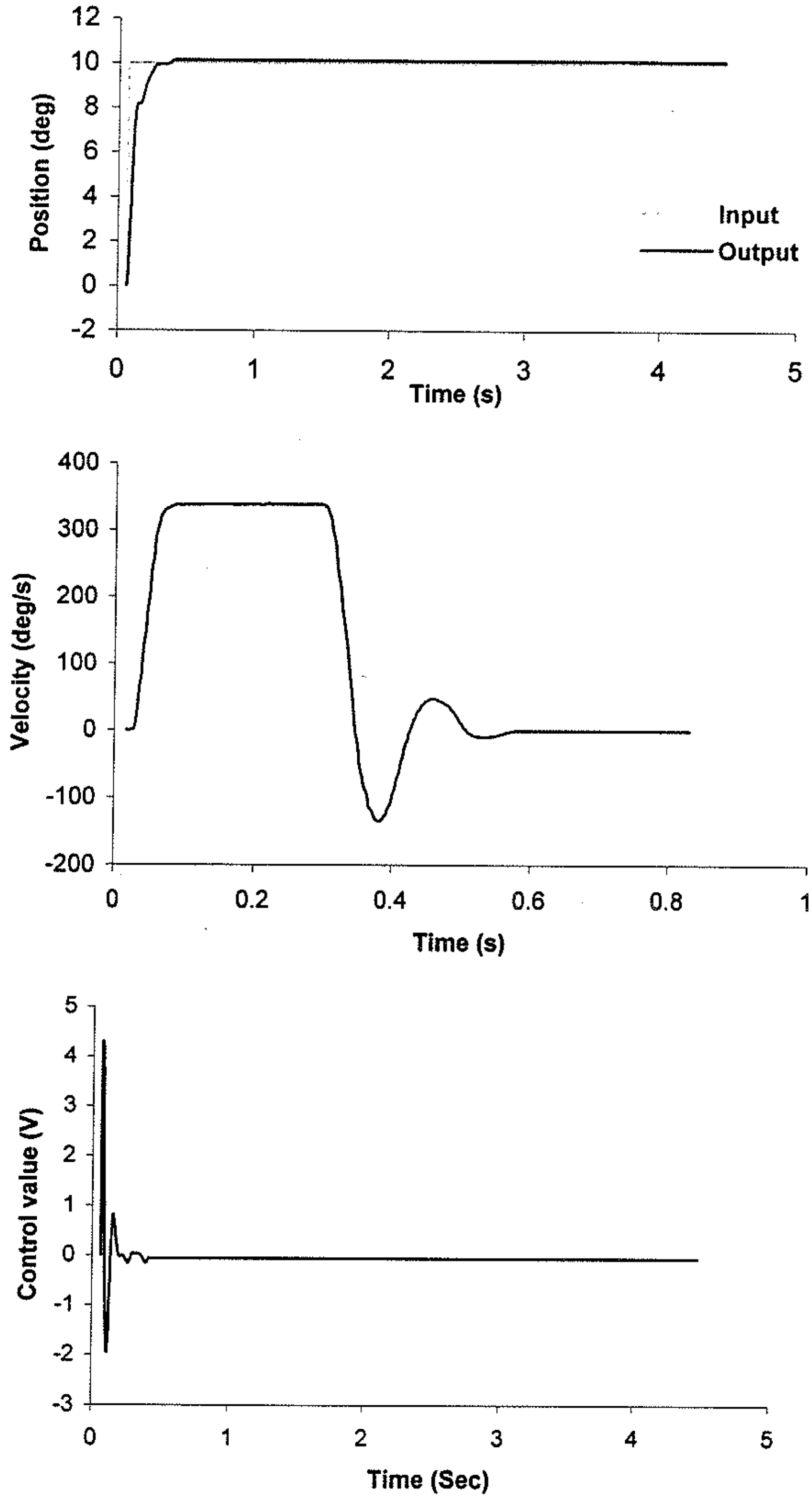

Fig. 8.3: Response of motor one (maxon RE 25 with gear ratio = 84) to step input for K_p= 0.43 (V/deg) and K_v =0.02 (Vs/deg).

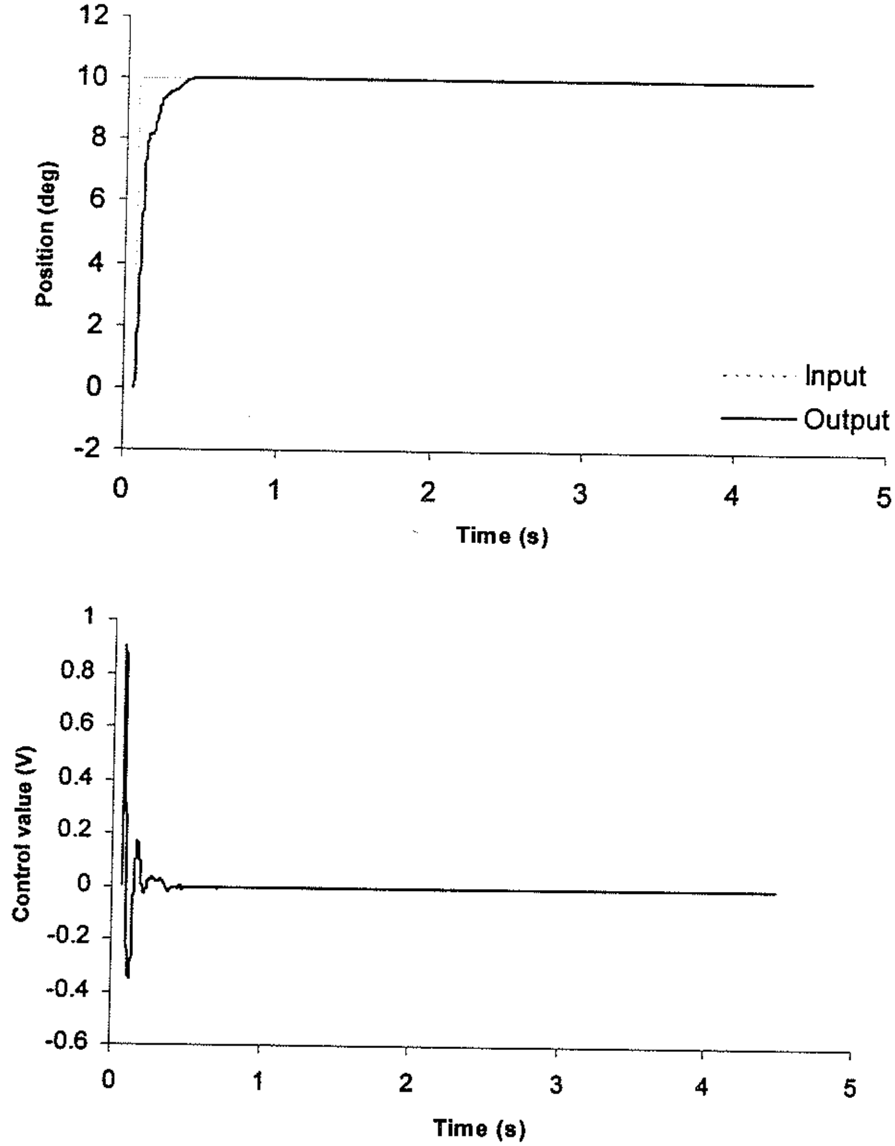

Fig. 8.4: The response of motor two (Maxon RE 25 with gear ratio = 19) to step input for $K_p = 0.09$ (V/deg) and $K_v = 0.005$ (Vs/deg).

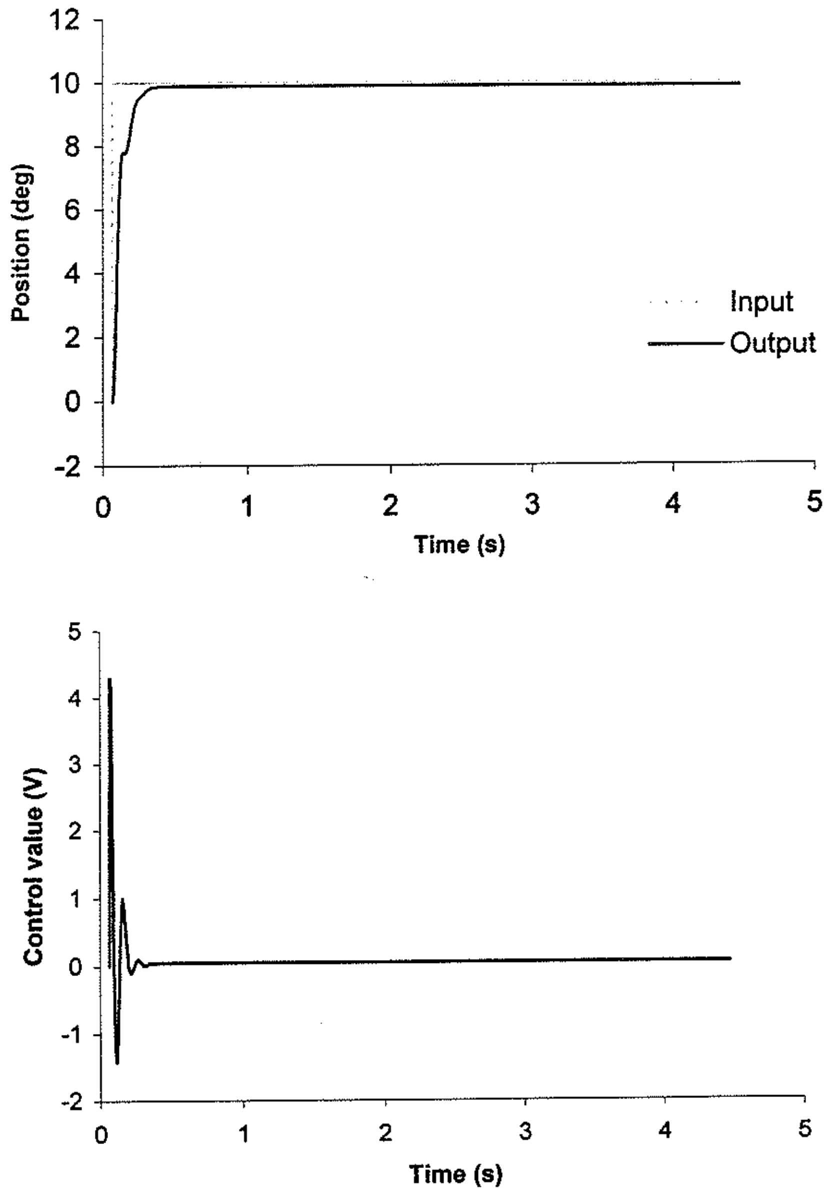

Fig. 8.5: The response of the third motor (Maxon RE 25 with gear ratio = 84) to step input for $K_p = 0.43$ (V/deg) and $K_v = 0.02$ (Vs/deg).

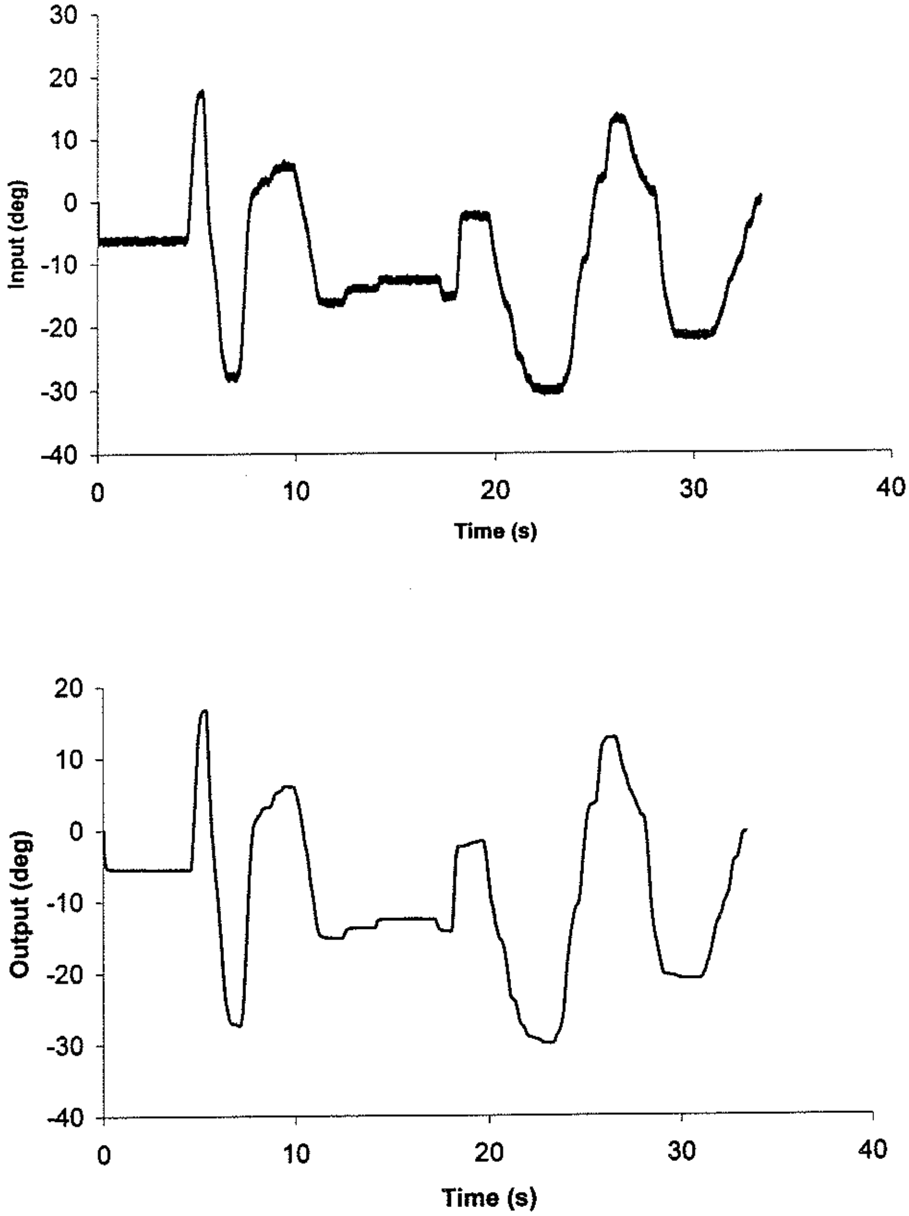

Fig. 8.6: Tracking response of the first motor (Maxon RE 25 with gear ratio = 84); K_p=0.6 (V/deg) and K_v = 0.02 (Vs/deg).

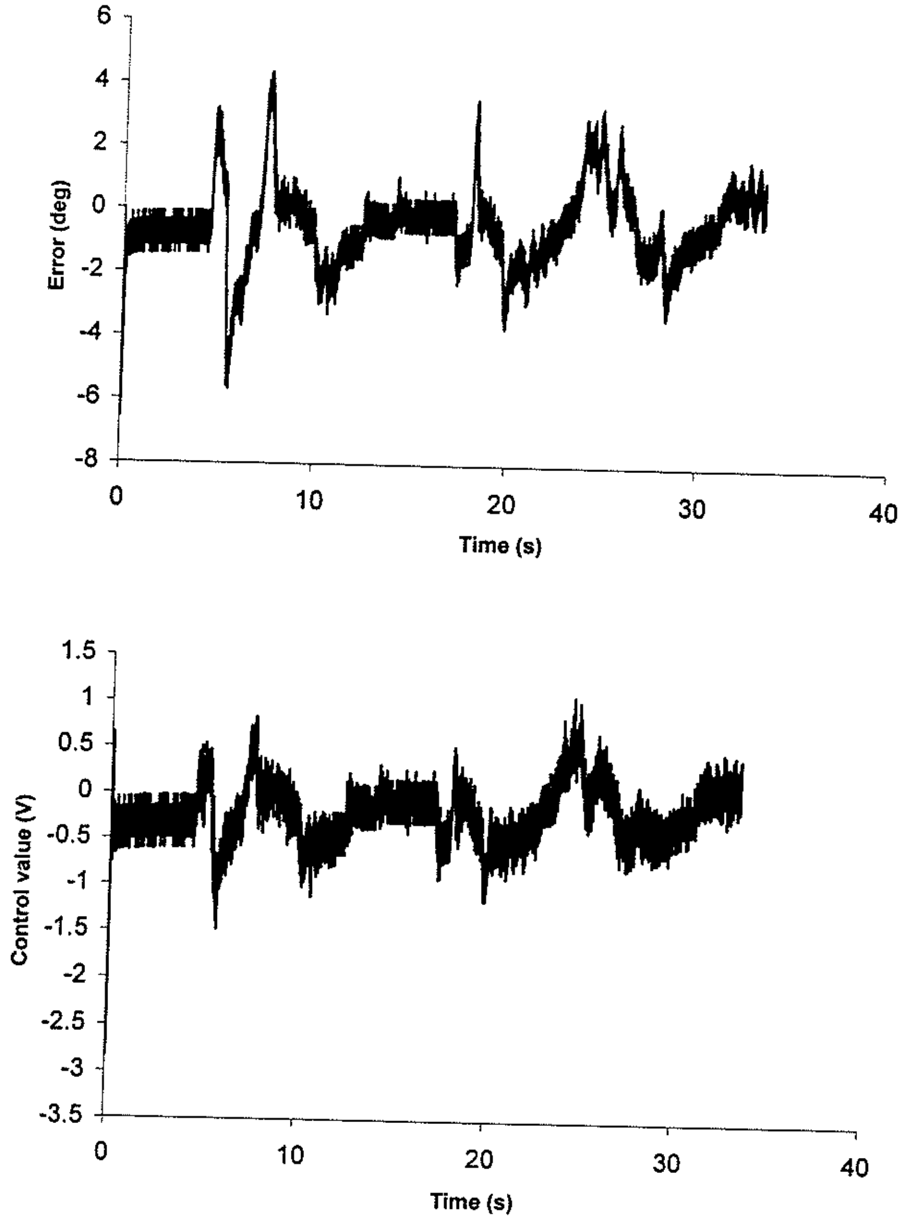

Fig. 8.7: The tracking response of the first motor (Maxon RE 25 with gear ratio = 84); $K_p = 0.6$ (V/deg) and $K_v = 0.02$ (Vs/deg).

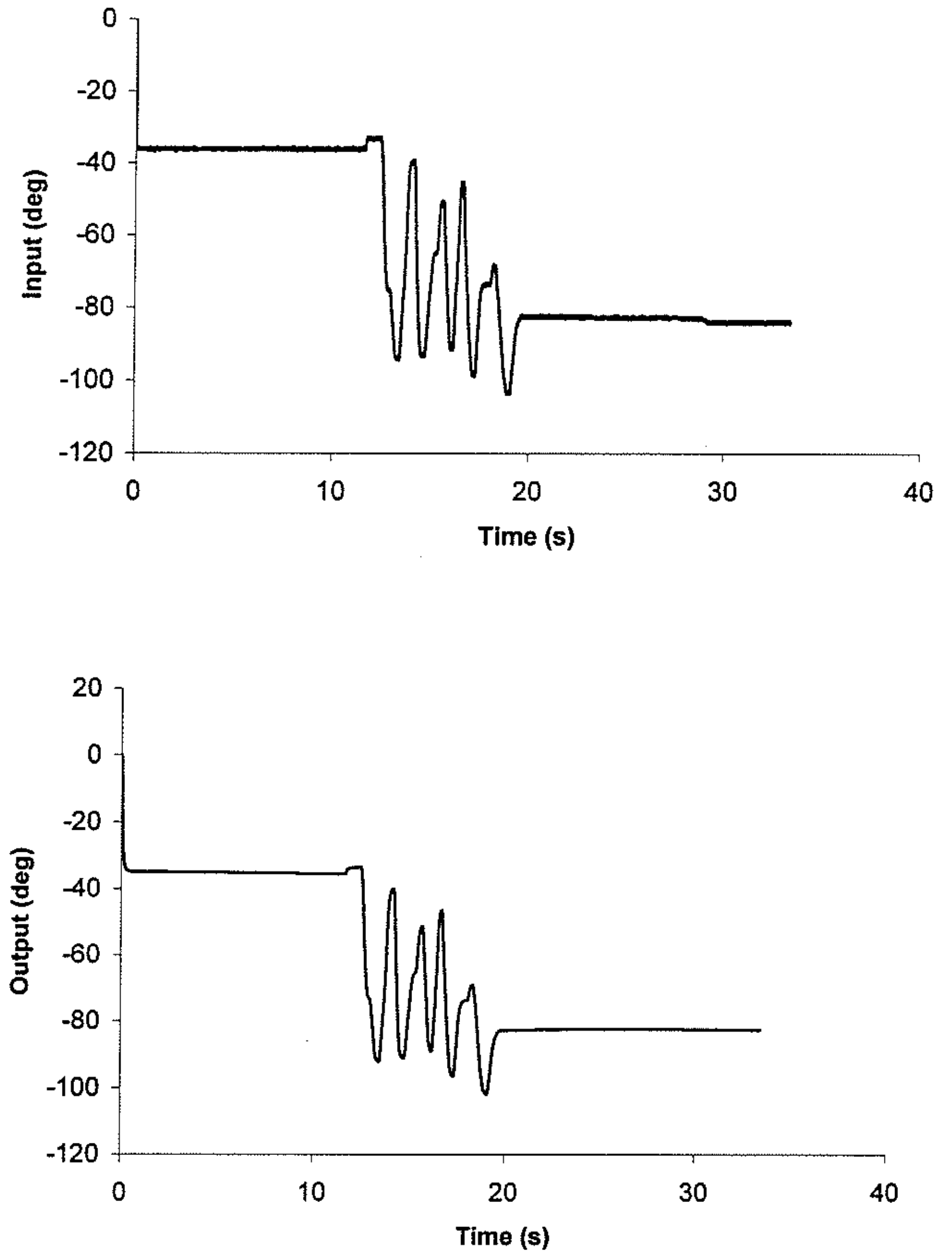

Fig. 8.8: Tracking response of the second actuator (Maxon RE 25 with gear ratio = 19); K_p = 0.04 (V/deg) and K_v = 0.005 (Vs/deg).

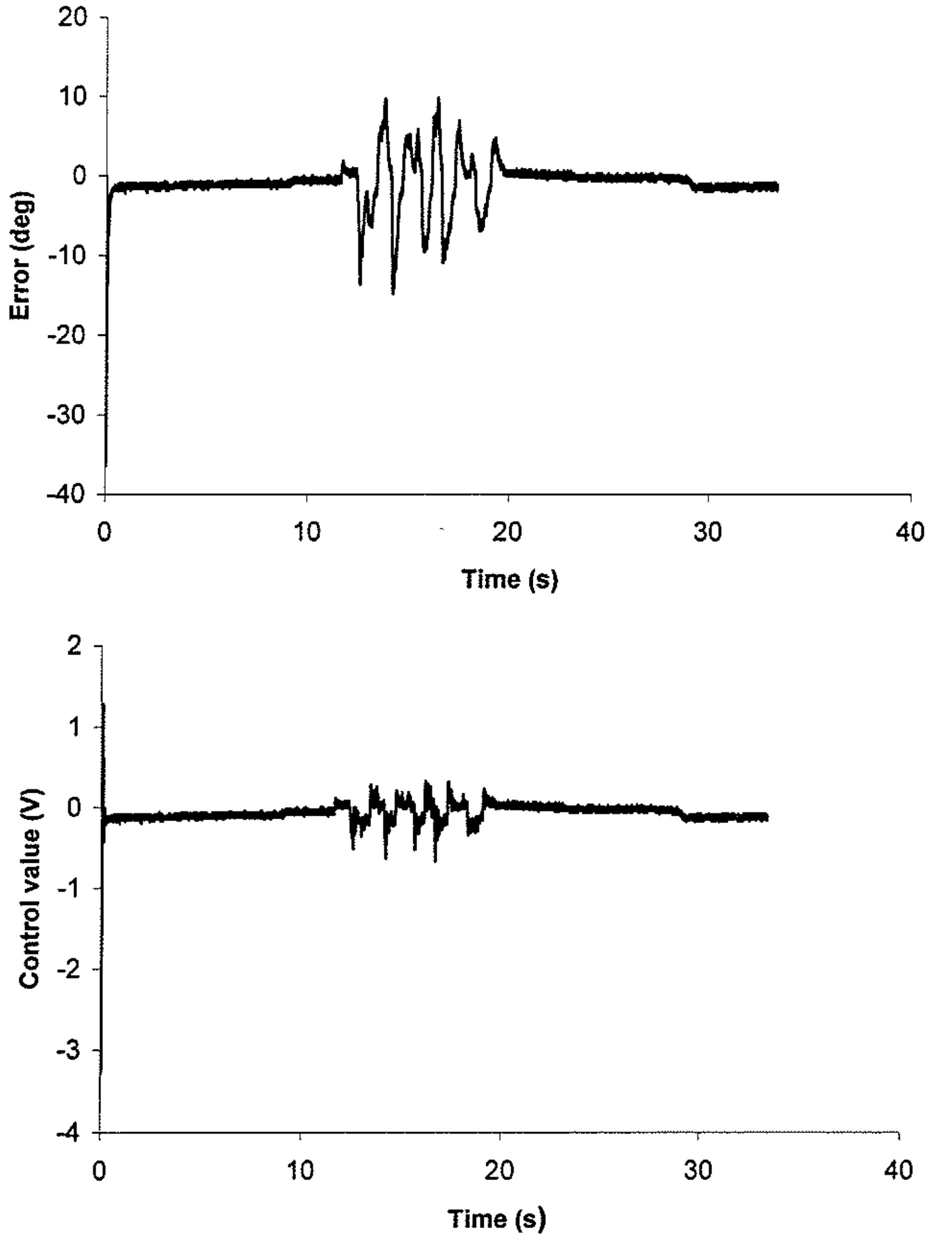

Fig. 8.9: Tracking response of the second actuator (Maxon RE 25 with gear ratio = 19); $K_p = 0.04$ (V/deg) and $K_v = 0.005$ (Vs/deg).

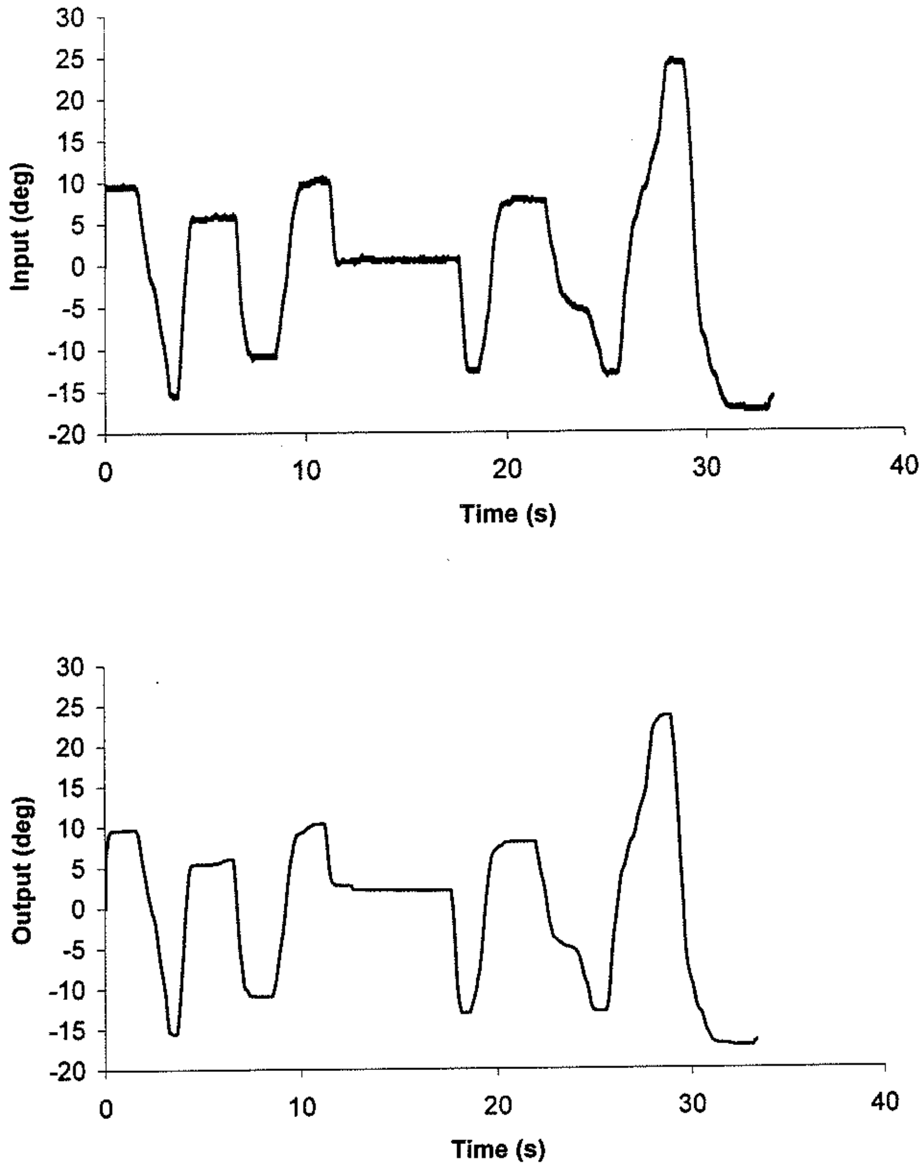

Fig. 8.10: Tracking response of the third actuator (Maxon RE 25 with gear ratio = 84); K_p = 0.6 (V/deg) and K_v = 0.02 (Vs/deg).

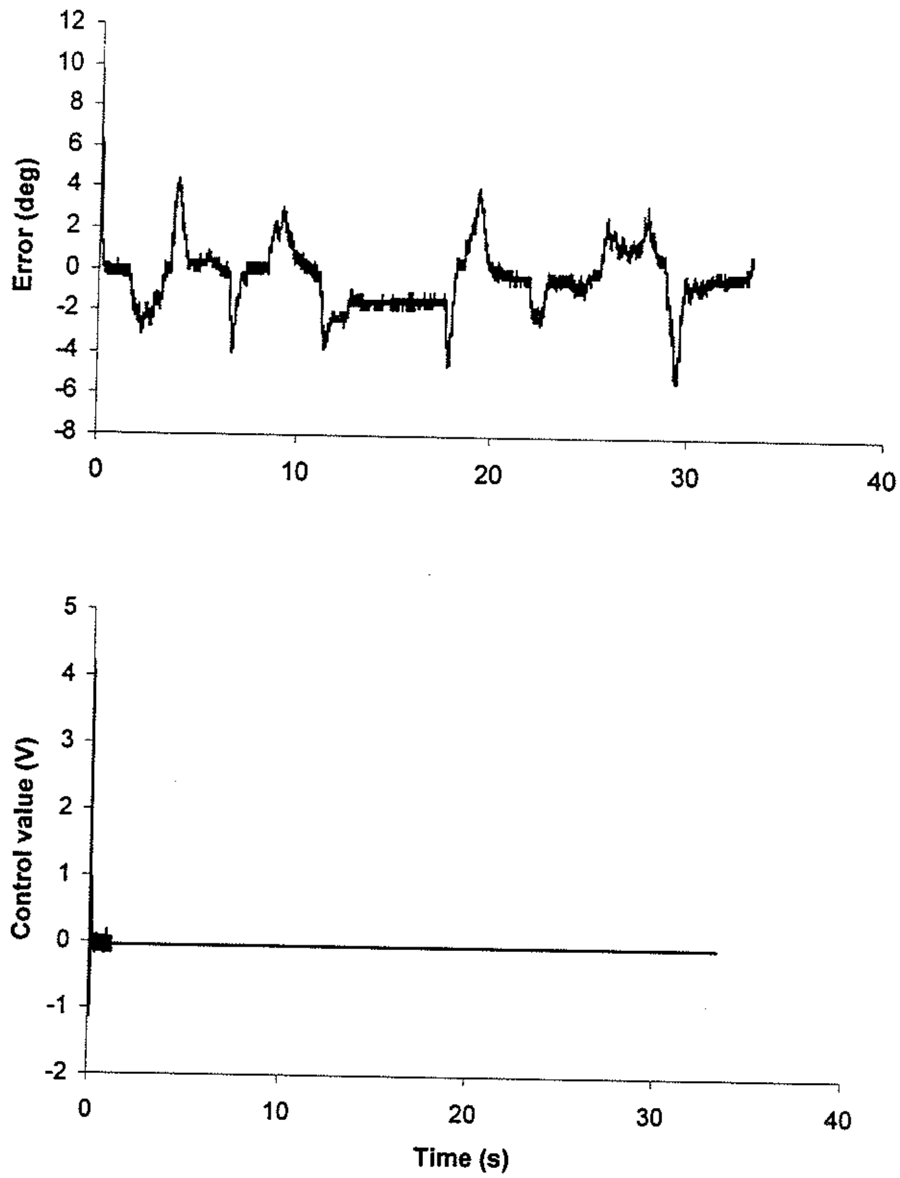

Fig. 8.11: The tracking response of the third actuator (Maxon RE 25 with gear ratio = 84); $K_p = 0.6$ (V/deg) and $K_v = 0.02$ (Vs/deg).

Chapter 9

Contributions of this Thesis

In this work, a novel master-slave mechanism was designed and prototyped to enable physicians to perform ultrasound diagnosis and palpation on patients at a remote site. The system consists of two major subsystems: a four degrees-of freedom hand-controller with force reflecting capability, and a wrist mechanism. The system also has the capability of accommodating different kinds of sensors such as force and ultrasound transducers to collect different kinds of information such as ultrasound pictures or muscle tenderness of the abdomen. The whole system has been interfaced to a computer through various interfacing boards to enable a computer to receive and send commands and information between hand-controller and the wrist.

The designed hand-controller has four degrees of freedom and has been designed based on parallel mechanisms. The use of parallel configurations is beneficial during palpating forces. Due to the nature of the ultrasound and palpation tasks, the hand-controller was designed to have four degrees of freedom with constrained spherical motion around an interior fixed point, which is not available in any existing haptic devices as described in [US patent, 5,805,140], [US patent, 5,816,105], [US patent 6,104,382], [Hayward, 1995], [Lee, et al., 2001], [Yoon, et al. 2001] and [Birglen, et al. 2002]. The combination of pantographs with revolute joints, cable drive, universal joints, ball spline and a series of decoupling systems were employed. The resulting hand-controller is backdrivable due to the use of direct-drive electric motors and low-friction power trains such as revolute joints and an open loop cable drive, which are necessary for any force reflecting hand-controllers or haptics. By using parallel structures, the resulting structure is light and rigid. On the other hand, using parallel structures allows all the actuators to be grounded. This leads to lighter moving parts, which are hard to reach in serial configurations. The main drawback of parallel manipulators, however, is their limited workspace [Hui, et al. 1995]. By combining two special pantographs with a large workspace, the present hand-controller has a large workspace, which makes it unique among parallel structures. Another drawback of using parallel structures is the existence of singular points inside their workspaces [Lee, et al. 2001] and [Tsai, 1999]. The present hand-controller theoretically provides a hemispherical-shape workspace, which is free of any singular point. Parallel structures have kinematically coupled degrees-of-freedom, which make their inverse/forward kinematic and control quite difficult [Hui, et al. 1995]. By using simple revolute and prismatic joints as decoupling components, all four degrees of freedom in the hand-controller are completely decoupled. Kinematic analysis revealed straightforward forward/inverse kinematic solutions. A simplified version of the hand-controller with three degrees of freedom was prototyped and was interfaced to a computer. The prototype covers all the abovementioned design specifications with low manufacturing cost and shows unique features.

The designed wrist has four degrees of freedom developed based on parallel mechanisms. Similar to the hand-controller, the design is based on parallel structures to allow high contact forces for applications such as palpation. The wrist's end-effector should have four degrees of freedom with constrained spherical motion around an exterior fixed point. Literature survey for finding any wrist or manipulator having all the required parameters for the required palpating/ultrasound tasks failed [US patent, 6,026,703], [US patent 4,686,866], [US patent 4,628,765], [US patent, 6,192,143], [Vischer, and Clavel, 2000] and [Gourdon, et al. 1998]. In addition to all the designed characteristics discussed for the hand-controller, the designed wrist has a very compact size, which makes it unique among the existing manipulators in this category. A remote drive capability based on using non-floating actuators has been devised to increase the wrist's maneuverability and safety for medical applications, which has never been considered among the wrists and manipulators previously developed by others [US patent, 6,425,865], [Masuda, et al. 2001] and [Delgore, et al. 2002]. The designed wrist also has several features, which make it potentially a safe medical wrist. Those features are low weight and inertia to reduce the impact forces, backdriveability, a minimum number of actuated joints for performing ultrasound and palpation, and reasonable access to the patient in emergency cases, which have not been considered by others [Degoulange, et al. 1998], [Gonzales, et al. 2000] and [Masuda, et al. 2001]. Moreover, it has a modular configuration, which enables the wrist to fulfill different functions through the combination of distinct building blocks or modules. This feature has never been considered in similar works [Gourdon, et al. 1998], [Zhu, et al. 2000], [Gonzales, et al. 2001] and [Delgore, et al. 2002]. A simplified version of the wrist with three degrees-of-freedom has been prototyped and interfaced to a computer. The prototype is most suitable for performing ultrasound imaging.

Both systems together have a similar kinematical configuration, which allows the whole system to be operated in master-slave mode. This is the most suitable platform for implementing bilateral techniques in tele-operation, which makes the whole system unique among the other existing platforms [US patent, 6,425,865], [Gonzales, et al. 2001] and [Guerin, et al. 2003].

References

Adelstein, B.D., US patent No. 5,816,105.

Baumann, R., Maeder, W., Glauser, D., Claval, R., "The PantoScope: a spherical remote-center-of-motion parallel manipulator for force reflection", Proceeding IEEE International Conference on Robotics and Automation, pp. 718-723, 1997.

Bevrit, J., Moore, D.F., Norwood, J.Q., Rosenberg, L.B., Levin, M.D., US patent No. 6,024,576.

Birglen, L., Gosselin, C., Pouliot, N., "ShaDe, a new 3 DOF haptic device", IEEE Transactions on Robotics and Automation, Vol.18, No.2, pp.166-175, 2002.

Cavusoglu, M.C., Tendick, M.C., Sastry, S.Sh., "A laparoscopic telesurgical workstation", IEEE Transaction on Robotics and Automation, Vol. 15, No.4, pp. 728-739, 1999.

Daniel, P.F., Siva, K.V., "Specification and design of input devices for tele-operation", Proceeding IEEE International Conference on Robotics and Automation, pp. 540-545, 1990.

Dario, P., Bergamasco, M., "An advanced robot system for automated diagnostic tasks through palpation", IEEE Transactions on Biomedical Engineering, Vol.35, No. 2, pp. 118-126, 1988.

Davis, B.L., "Computer integrated surgery: technology and clinical applications, `a discussion of safety issues for medical robots`" M.I.T. press, pp. 287-296, 2003.

Degoulange, E., Urbain, L., Caron, P., Boudet, S., Megnien, J.L., Pierrot, F., Dombre. E., "HIPROCRATE: an intrinsically safe robot for medical applications", Proceedings IEEE/RSJ, Internationall. Conference on Intelligent Robots and Systems, pp. 959-964, 1998.

Delgore, C., et al., "OTELO project: mobile tele-echography using ultra-light robot ", Telemed'02, 2002.

Dien, R. Y., Luce, E. C., US patent No. 4,628,765.

Duriez, Ch., Lamy, D., Chaillou, Ch., "A parallel manipulator as a haptic interface solution for amniocentesis simulation", IEEE International Workshop on Robot and Human Interactive Communication, pp. 176-181, 2001.

Faraz, A. Payandeh, Sh., "A robotic case study: Optimal design for laparoscopic positioning stands", The International Journal of Robotics Research, Vol.17, No.9, pp. 986-995, 1998.

Faraz, A. Payandeh, Sh., US patent No. 5,824,007.

Fenster, A., Downey, D.B., "3-D ultrasound imaging: a review", IEEE Engineering in Medicine and Biology, Vol. 15, Issue 6, pp. 41-51, 1996.

Funda, J., LaRose, D.A. Taylor, H.T., US patent No. 6,201,984.

Gonzales, A., et al., "TER: A system for robotic tele-echography", Proceeding International Conference of Medical Image Computing and Computer Assisted Intervention, pp. 326-334, 2001.

Gosselin, C.M., Wang, J., "Static balancing of spatial six-degree-of freedom parallel mechanisms with revolute actuators ", Journal of Robotic Systems, Vol.17, No.3, pp. 159-170, 2000.

Gourdon, A., Poignet, Ph., Poisson, G., Vieyres, P., Marche, P., "A new robotic mechanism for medical application", Proceeding IEEE/ASME International. Conference on Advanced Intelligent Mechatronics, pp. 33-38, 1998.

Guerin, N., Bassit, L., Poisson, G., Delgorge, C., Arbeille, Ph., Vieyres, P., "Clinical validation of mobile patient-expert tele-echography system using ISDN lines", Proceeding IEEE-EMBS Information Technology Applications in Biomedicine, pp. 24-26, 2003.

Hamlin, G.J., Sanderson, A.C., "A novel concentric multilink spherical joint with parallel robotics applications", Proceeding IEEE International, Conference on Robotics and Automation, pp.1267-1272, 1994.

Hayward, V., "Toward a seven axis haptic device", Proceeding IEEE International. Conference on Intelligent Robots and Systems 'Human Robot Interaction and Cooperative Robots', pp. 133-139, 1995.

Hong. B. Erdman, A. G., US patent No. 6,355,048.

Howe, R.D., Peine, W.J., "Remote palpation technology", IEEE Engineering in Medicine and Biology, pp. 318-323, 1995.

Hui, R., Ouellet, A., Wang, A., Williams, S., "Mechanisms for haptic feedback", Proceeding of International Conference on Robotics and Automation, pp. 2138-2143, 1995.

Ikta, k, Nokata, M., "General evaluation method of safety for human-care robots", Proceeding IEEE International Conference on Robotics and Automation, pp. 2065-2072, 1999.

Johnsen E. G., Corliss, W. R., " Human factors in applications in teleoperator design and operation", Wiley-Interscience, 1971.

Ikato, I, Koganezawa, K., Fujimoto, H, Hirata, M., "The automatic breast-cancer palpation robot: WAPRO-4R", IEEE International Workshop, pp. 73-78, 1988.

Khodabandehloo, K., Brett, P. N., Buckingham, R. O., "Computer integrated surgery: technology and clinical application, ` Special purpose actuators and architecture for surgery robots`", M.I.T press, pp. 263-275, 2003.

Kuleshov, V.S., Lakota, N.A., "Remotely controlled robots and manipulators", Mir Publishers Moscow, 1988.

Kyriacou, E., Pavlopoulos, S., Koutsouris, D., " Multri purpose health care tele medicine system ", Proceeding EMBS International Conference, pp. 3544-3547, 2001.

Lee, J.H., Eom, K.S., Yi, B.J., Suh, I.H., "Design of a new 6 DOF parallel haptic device", Proceeding IEEE International Conference on Robotics and Automation, pp. 886-891, 2001.

Madhani, A.J., Niemeyer, G., Salisbury, K. "The Black Falcon: A teleoperated surgical instrument for minimally invasive surgery", Proceeding IEEE/RSJ International Conference on Intelligent Robots and Systems, pp. 936-944, 1998.

Martin, K. M., Levin, M. D., Braun, A. C., US patent No. 6,104,382.

Masuda, K., Kimura, E., Tateishi, N., Ishihara, K., "Three dimensinal motion mechanism of ultrasound probe and its application for tele-echography system", Proceedings IEEE/RSJ, International Conference on Intelligent Robots and Systems, pp. 1112-1116, 2001.

McDougall, J., Lessard, L. B., Hayward, V., "Application of advanced materials to robotic design: the freedom –7 haptic hand controller", International. Conference on Composite Materials, pp. 806-815, 1997.

Mitsubishi M., Warisawa, Sh., Tsuda, T., Higuchi, T., Koizumi, N., Hashizume, H., Fujiwara, K, "Remote ultrasound diagnosis system", Proceeding IEEE International Conference on Robotics and Automation, pp. 1567-1574, 2001.

Mor, A. B., US patent No. 6,088,020.

Morita, T., Sugano, Sh., "Design and development of a new robot joint using a mechanical impedance adjuster ", Proceeding IEEE International Conference on Robotics and Automation, pp. 2469-2475, 1995.

Okada, M., Nakamura, Y., Ban, Sh., "Design of programmable passive compliance shoulder mechanism", Proceeding IEEE International Conference on Robotics and Automation, pp. 348-353, 2001.

Orlov, P., "Fundamentals of machine design", Mir Publishers Moscow, Vol. 1 and 2, 1979.

Ouerfelli, M., Kumar, V., "Optimization of a spherical five-bar parallel drive linkage", Transactions of The ASME Journal of Mechanical Design, Vol. 116, pp. 166-173, 1994.

Popov, E.P., Yurevich, E. I., " Robotics", Mir Publishers Moscow, 1987.

Rosenberg, L.B., Schena, B.M., US patent No. 5,805140.

Rosenberg, L.B., Braun, A. C., Schena, B. M., US patent No. 6,271,833.

Rosenberg, L.B., Schena, B. M., Gillespie, R.B., US patent No 5,721,566.

Rosenberg, L.B., US patent No. 6,154,198.

Rivin, E.I., " Mechanical design of robots", McGrawHill, 1988.

Rosheim, M.E., US patent No. 4.686,866.

Rosheim, M.E., US patent No. 4,723,460.

Rosheim, M.E., US patent No. 6,418,811.

Salcudean, S.E., Bell, G.S., Lawrence, P.D., Marko, A., Jameson, M., US patent No 6,425, 865.

Sanders, M.S., McCormick, E.J., "Human factors in engineering and design" McGraw-Hill, 1987.

Shelden, C.H., McCann, G.D., US patent No. 4,638,798.

Souluer, F., US patent No. 6,192,143.

Souluer, F., US patent No. 6,351,549.

Souluer, F., US patent No., 6,400,837.

Stanisic, M.M., Wiitala, J.M., Remis, S.J., US patent No. 6,026,703.

Sublett, J.W., Dempsey, B.J., Weaver, "Design and implementation of a digital tele-ultrasound system for real-time remote diagnosis", Proceeding IEEE Symposium on Computer-Based Medical System, pp. 292-298, 1995.

Taylor, R.H. Funda, J. Grossman, D.D. Karidis, J.P., Larose, D.A., US patent No. 5,397,323.

Taylor, H.T., Grossman, D.D., Karidis, J.P., LaRose, D.A., US patent No. 5,397,323.

Tidwell, P.H., Bandukwala, N., Reinholtz, C.F., Webb, G., "Synthesis of wrapping cams", Transactions of The ASME Journal of Mechanical Design, Vol.116, pp.634-638, 1994.

Tsai, l. W., " Robot analysis: the mechanics of serial and parallel manipulators", John Wiely and Sons, Inc., 1999.

Vischer, P., Clavel, R., "Argos: A novel 3-DoF parallel wrist mechanism", The International Journal of Robotics Research, Vol.19, No.1, pp. 5-11, 2000.

Wiitala, J., Stanisic, M. M., "Deisgn of an overconstrained and dextrous spherical wrist". Transactions of ASME Journal of Mechanical Design. Vol. 122, pp. 347-353, 2000.

Woodson, W.E., "Human factors reference guide for process plants", McGraw-Hill, 1987.

Yamada, Y., Hirasawa, Y., Huang, Sh., Umetani, Y., Suita, K., "Human-robot contact in the safeguarding space", IEEE/ASME Transactions on Mechatronics, Vol. 2, No. 4, pp. 230-236, 1997.

Yoon, J., Ryu, J., "Design, fabrication, and evaluation of a new haptic device using a parallel mechanism", IEEE/ASME Transactions on Mechatronics, Vol.6, No.3, pp. 221-230, 2001.

Zhu, W.H., Salcudean, S.E., Bachmann, S., Abolmaesumi, P., "Motion /force/image control of a diagnostic ultrasound robot", Proceeding IEEE International Conference on Robotics and Automation, pp. 1580-1585, 2000.